Structure-Function Studies of Integrin-Ligand Recognition

Thesis submitted for the degree
of Doctor of Philosophy at the University of Leicester

By

Clare McCleverty

Department of Biochemistry
University of Leicester

October 2001

ProQuest LLC
789 East Eisenhower Parkway
P.O. Box 1346
Ann Arbor, MI 48106-1346

STRUCTURE-FUNCTION STUDIES OF INTEGRIN-LIGAND RECOGNITION

Clare McCleverty

Department of Biochemistry, University of Leicester.

Integrins are a large family of αβ heterodimeric cell surface receptors that interact with the extracellular matrix and/or counter-receptors on other cells. These interactions control the adhesion and migration of cells as well as regulating numerous signal transduction pathways. Integrins exist in low and high affinity states, subject to allosteric regulation. Integrin-ligand recognition is divalent cation-dependent and mediated by the α subunit N-terminal repeats, the β subunit I domain and in certain integrins, the α subunit I domain.

Two competing models based upon structure predictions, the β-propeller and EF-hand-like models, were tested to determine which model represents the structural components of the ligand binding α subunit N-terminal repeats. Recombinant fragments of α4 repeats IV-V, VI-VII and IV-VII, corresponding to the EF-hand-like model, were insoluble, thus preventing further analysis. A recombinant fragment of all seven α4 repeats contains a predominant secondary structure content of anti-parallel β-sheet, compatible with the β-propeller model.

The interactions of the αM I domain with fragment D from fibrinogen and the extracellular domains of ICAM-1 were studied using surface plasmon resonance. Optimal binding conditions and equilibrium dissociation constants were established for these interactions. Co-crystallisation studies were pursued with the αM I domain and its ligands, fragment D and ICAM-1, but a co-crystal was not obtained due to the presence of a subpopulation of low affinity I domain molecules. Disulphide bonds were then introduced to lock the αM I domain in the open and closed conformations, corresponding to the high and low affinity states, respectively. Equilibrium dissociation constants for the open and closed mutants reveal a marked increase and decrease in ligand binding affinity, respectively. Stabilisation of the closed mutant via a disulphide bond is verified in the crystal structure. The affinity state of both mutants is fully reversible by reduction of the disulphide bond. These mutants provide useful tools for future studies to understand integrin allostery and will simplify ligand binding studies in the isolated I domain and intact receptor.

Acknowledgements

I am grateful to Bob Liddington for his supervision, which allowed much scientific freedom, and for showing me the sunnier side of science! In addition, thanks to Janette Thomas for her supervision and help during my visits to Glaxo Wellcome.

Thanks also goes to all the G5/G8 crowd in Leicester and the lab at the Burnham Institute for their everyday help, spirited friendship and amusing antics. In particular, Geoff Briggs and Jonas Emsley who provided much needed initial experimental support and humour during the early days and José de Pereda for his continued scientific input throughout the course of my PhD. Additionally, thanks to Chris Lombardo for advice with my surface resonance studies.

Thanks to my family and friends for putting up with me throughout this time and a special thanks to Neill for his constant loving support and encouragement.

Contents

List of Figures

Chapter 3: Ligand binding and crystallisation of the αM I domain

Chapter 4: Designing the open high affinity conformation of the αM I domain

List of Tables

Appendix

Abbreviations

BCA	Bicinchoninic acid
CHES	2-(N-cyclohexylamino)ethanesulphonic acid
CD	Circular dichroism
DMSO	Dimethylsulphoxide
DTNB	5, 5' dithio-bis (2-nitrobenzoic acid)
DTT	Dithiothreitol
ECM	Extracellular matrix
EDC	N-ethyl-N′-(3-dimethylaminopropyl)carbodiimide hydrochloride
EDTA	Ethylenediamine tetraacetic acid
EM	Electron microscopy
FPLC	Fast-protein liquid chromatography
GST	Glutathione-S-transferase
HEPES	N-2-hydroxyethylpiperazine-N-2-ethanesulphonic acid
I domain	Inserted domain
Ig	Immunoglobulin
IPTG	Isopropyl β-D-thiogalactopyranoside
K_D	Equilibrium dissociation constant
kDa	Kilodalton
kV	Kilovolt
LB	Luria broth
mAb	Monoclonal antibody
MIDAS	Metal ion-dependent adhesion site

NDSB	Non detergent sulphobetaine
NHS	N-hydroxysuccinimide
OD_{600}	Optical density at 600 nm
PBS	Phosphate buffered saline
PCR	Polymerase chain reaction
PDB	Protein data bank
PEG	Polyethylene glycol
PEGMME	Polyethylene glycol monomethyl ether
pI	Isoelectric point
PMSF	Phenylmethylsulphonylfluoride
rmsd	Root mean square deviation
rpm	Revolutions per minute
RU	Response unit
SDS	Sodium dodecyl sulphate
SDS-PAGE	Sodium dodecyl sulphate polyacrylamide gel electrophoresis
sICAM-1	Soluble intercellular adhesion molecule -1
TB	Terrific broth
Tris	Tris hydroxymethyl aminomethane
v/v	Volume to volume
WT	Wild type
w/v	Weight to volume
w/w	Weight to weight
X-gal	5-bromo-4-chloro-3-indolyl-β-D-galactoside

Media

TB media	Per litre: 12 g, tryptone, 24 g yeast extract, 4 ml glycerol, 0.17 M KH_2PO_4, 0.72 M K_2HPO_4
LB media	Per litre: 10 g bactotryptone, 5 g yeast extract, 10 g NaCl
2 xYT media	Per litre: 16 g bactotryptone, 10 g yeast extract, 5 g NaCl
LB plates	Per litre: 10 g bactotryptone, 5 g yeast extract, 10 g NaCl, 15 g agarose
X-gal plates	Per litre: 10 g bactotryptone, 5 g yeast extract, 10 g NaCl, 15 g agarose, 1 mM IPTG, 1 mM X-gal

Chapter 1: Introduction

1.1 The integrin family

Integrins are a large family of plasma membrane glycoproteins which mediate cell-cell and cell-extracellular matrix (ECM) adhesion (Hynes, 1992). They contain extracellular domains, which bind the extracellular matrix (ECM), and/or counter-receptors on other cells and cytoplasmic domains that associate with the intracellular cytoskeleton and affiliated proteins. The integrin transmembrane receptors are αβ heterodimers and to date, eight β subunits and eighteen α subunits have been identified (Humphries, 2000). The α subunit (~1000 residues) and β subunit (~750 residues) noncovalently interact to form a diverse range of receptors which bind many different ligands. Table 1.1 summarises the known extracellular ligands of integrins to date (Sugimori *et al.*, 1997; Camper *et al.*, 1998; Curley *et al.*, 1999; Velling *et al.*, 1999; Plow *et al.*, 2000).

1.2 Integrin function

Integrins are the central mediators of information transfer between cells and the ECM or counter-receptors on other cells. Not surprisingly, they are involved in numerous biological and pathological functions in nearly every cell type. As these functions are widespread, a brief summary will be given.

Integrins are crucial from the very first stages of embryogenesis when cells

Integrin		Extracellular ligand
β1	α1*	Collagens, laminin,
	α2*	Collagens, laminin, tenascin, fibronectin, vitronectin, E-cadherin, *echovirus 1, snake venom protein jararhagin*
	α3	Laminin, fibronectin, collagen I, epiligrin, entactin, thrombospondin, *invasin (Yersinia spp.)*
	α4	Fibronectin, VCAM-1, MAdCAM-1, thrombospondin, *invasin (Yersinia spp.)*
	α5	Fibronectin, denatured collagen, fibrinogen, *invasin (Yersinia spp.)*
	α6	Laminin, sperm fertilin, epiligrin, *invasin* (Yersinia spp.)
	α7	Laminin
	α8	Fibronectin, vitronectin, tenascin, osteopontin
	α9	Tenascin, collagen, VCAM-1, VCAM-2, osteopontin
	α10*	Collagen
	α11*	Collagen
	αV	Vitronectin, fibronectin, collagens, fibrinogen, von Willebrand factor
β2	αL*	ICAM-1,-2-3,-4,-5, *H. Capsulatum*
	αM*	Fibrinogen, ICAM-1,-2,-3, iC3b, factor X, heparin, kininogen, denatured proteins, lipopolysaccharides, *Candida albicans, neutrophil inhibitory factor (Ancylostoma C.) , gp63 (Leishmania C.), filamentous hemagglutinin (Bordetella pertussis), WI-1 antigen (Blastomyces dermatididis), H. Capsulatum*
	αX*	iC3b, fibrinogen, CD23, lipopolysaccharides, *H. Capsulatum*
	αD*	ICAM-3, VCAM-1
β3	αIIb	Fibrinogen, fibronectin, von Willebrand factor, vitronectin, thrombospondin, collagens, denatured collagen, plasminogen, PECAM-1, decorsin, *Borrelia burgdorferi, disintegrins*
	αV	Collagens, tenascin, bone sialoprotein, denatured collagen and laminin, fibronectin, fibrinogen, matrix metalloproteinase-2, osteopontin, prothrombin, thrombospondin, vitronectin, CD31, von Willebrand factor, *adenovirus penton base protein, disintegrins, HIV Tat protein*
β4	α6	Laminin, collagens, plectin
β5	αV	Vitronectin, bone sialoprotein, fibrinogen, fibronectin, *HIV Tat protein, adenovirus penton base protein*
β6	αV	Fibronectin, tenascin,
β7	α4	VCAM-1, fibronectin, MAdCAM-1, CD106
	αE*	E-cadherin
β8	αV	Vitronectin, fibronectin, laminin, collagens

Table 1.1 Integrin extracellular ligands. Italics indicates pathogenic ligands and * indicates integrins with an I domain.

establish interactions with the ECM. These interactions, as shown from knockout mutations in mice (De Arcangelis & Georges-Labouesse, 2000), are critical for the organisation of cells in organs and tissues during development as well as cell differentiation and proliferation. Depletion of some integrins, such as the β1 integrins, result in severe phenotypes where embryos die early in development. In some cases, the function of a deleted integrin can be replaced by an overlapping function of another integrin (Yang & Hynes, 1996).

Integrins contribute to cell growth by providing a physical linkage between cytoskeletal structures and the ECM, and by participating in various signal transduction pathways. Integrin-mediated adhesion can regulate the basal cell cycle apparatus by stimulation or inhibition of key cell cycle mediators, including cyclins and early-response genes (Howe *et al.*, 1998). When cells are completely deprived of integrin-mediated anchorage to the ECM, they undergo a form of apoptosis that has been termed anoikis (Frisch & Ruoslahti, 1997). The authors suggest that *in vivo* anoikis may prevent detached cells from re-attaching to new sites and growing dysplastically.

Cell motility is essential for many biological processes, including embryological morphogenesis, wound healing, immune surveillance and inflammation. Integrins play a major role during the cyclic process of cell migration by allowing the reversible attachment of the cell to the ECM (Holly *et al.*, 2000). Integrin-dependent signalling initiates multiple events which induce cell shape change and provide the contractile forces needed to spread the cell over the ECM. These processes occur at specific structures called focal contacts, which provide a structural framework for signalling proteins required for cell spreading.

Integrins, in particular the β2 integrins, are important mediators in the immune system (Berton & Lowell, 1999; Epler *et al.*, 2000; Smith, 2000; Tanaka, 2000). They are involved in functions, such as transmigration of leukocytes into the inflammatory

site, cytokine secretion, production of reactive oxygen intermediates, degranulation and phagocytosis. Lymphocytes can be non-adherent when circulating throughout the body and also adherent when they transmigrate across the vasculature, encounter antigen-presenting cells in the lymph nodes, or act as effector cells to lyse their target (Hogg & Leitinger, 2001; Woods & Shimizu, 2001). This adhesion and de-adhesion behaviour is controlled by the activity of integrin receptors on the cell surface of lymphocytes. Some integrins have multifunctional roles in the immune system. For example, αMβ2 functions as an adhesion molecule mediating the diapedesis of leukocytes across the endothelium, and as a receptor for iC3b, which is responsible for phagocytic and/or degranulation responses to microorganisms (Ross, 2000). As integrins play a central role in cell migration and invasion they are therefore essential to tissue healing following injury (Tailor & Granger, 2000). When exposed to a damaged vessel wall, platelets adhere and efficiently seal the wound. Key integrins involved are α2β1, which binds to the collagen exposed following injury, and αIIbβ3, which brings about platelet aggregation through fibrinogen binding, plugging the ruptured endothelial surface.

Integrins are crucial for promoting and maintaining the neuronal networks during brain development. During maturity, they also play an important role in regulating synaptic plasticity (Benson *et al.*, 2000) and influencing neural crest migration, axonal outgrowth, Schwann cell differentiation and maintaining the peripheral nervous system (Previtali *et al.*, 2001).

Integrins can also have major downstream effects on specific gene expression and differentiation. The various signalling pathways involved in these processes will be discussed later.

1.3 Integrins in health and disease

The progression of a number of disease states is dependent on aberrant cellular adhesion. Integrins are the major class of cellular adhesion receptors, so they often play major roles in disease pathogenesis.

Several human genetic diseases that affect integrin function demonstrate their critical importance in biological processes (Kuijpers *et al.*, 1997; Clemetson & Clemetson, 1994; Pulkkinen & Uitto, 1999). Examples are shown in table 1.2. Hematopoietic stem cell transplantation is the main treatment for leukocyte adhesion deficiency (LAD) but this is complicated by transplant-related toxicities and graft-versus-host disease. An alternative approach of retroviral-mediated gene transfer of the β2 subunit is proving effective in correcting the structural and functional defects in LAD leukocytes (Bauer & Hickstein, 2000).

Integrin subunit absent or with mutation	**Disease**	**Physiological outcome**	**Symptoms**
β2	Leukocyte adhesion deficiency-1	Impaired leukocyte migration to sites of inflammation. Neutrophilia	Recurrent bacterial infections Impaired healing
β3 & αIIb	Glanzmann thrombasthenia	Reduced platelet adhesion and aggregation	Bleeding disorders
β4 & α6	Epidermolysis bullosa	Inabiltiy to bind collagen	Skin blistering - detachment of epidermis from epithelial basement membranes Pyloric atresia
β4	Osteogenesis imperfecta	Inabiltiy to bind collagen	Bone malformations and fragility

Table 1.2 Disease states caused by mutations found in integrin subunits

Thrombosis of coronary arteries is a major cause of death in heart attack and stroke. The platelet integrin αIIbβ3 plays a crucial role in this process since its activation and adhesion to fibrinogen leads to platelet aggregation and adherence (Curley *et al.*, 1999). This is the first step in thrombosis development, which can block blood vessels at sites of injury or atherosclerotic plaques. αIIbβ3 has been the target for therapeutic intervention to control platelet aggregation in conditions, such as arterial thrombosis, unstable angina, myocardial infarction and stroke (Curley *et al.*, 1999). Therapeutic agents have also been developed that beneficially inhibit the normal function of αIIbβ3 under certain conditions. For example, the anti-αIIbβ3 monoclonal antibody-based antagonist, abciximab, has been designed to inhibit blood clotting in patients undergoing angioplasty who are at a high risk of the treated coronary vessel suddenly closing (Coller, 1997).

Uncontrolled or excessive leukocyte migration has been implicated in a number of inflammation disorders, including multiple sclerosis, rheumatoid arthritis, asthma, inflammatory bowel disorder and reperfusion injury following myocardial infarcation or stroke (Lobb & Hemler, 1994). Integrins implicated in these disease states include αLβ2, α4β1 and α4β7 and several antagonists have been designed to target these integrins in order to treat the disorders (Curley *et al.*, 1999).

Cancer formation is profoundly influenced by the altered regulation of integrin activity states. This was demonstrated using αVβ3 in a melanoma cell line which supported cell migration on vitronectin *in vitro* and metastasis *in vivo* (Filardo *et al.*, 1995). Mutation of a conserved motif in the β3 cytoplasmic tail, which is required for activation, resulted in an inhibition of cell migration and a decrease in metastatic behaviour. Different aspects of integrin function have been shown to be important in tumour progression.

Reduced sensitivity to anoikis appears to be an important hallmark for

oncogenic transformation, particularly in the process of metastasis. The breakdown of normal integrin-mediated cell-cell interactions might contribute to neoplasia by conferring anoikis resistance (Frisch & Francis, 1994). Protection of cells from anoikis transformed their phenotype to anchorage-independent and tumourigenic as is commonly found in human carcinoma cells (Frisch *et al.*, 1996).

Tumour progression is aided by integrin-guided cell motility and degradation of the extracellular matrix via matrix metalloproteinases (MMPs), endopeptidases that degrade most extracellular components. Integrins regulate MMP gene expression as well as MMP release and activation enabling them to remodel the ECM (Ivaska & Heino, 2000). Highly invasive melanoma cells are able to switch integrin expression to elevate the production levels of MMP-2, which degrades collagen (Seftor *et al.* 1993).

The ongoing formation of new tumour vasculature, angiogenesis, is also a key part of tumour progression. αVβ3 has been shown to play an important role in angiogensis as it is expressed on several malignant tumour cells and is upregulated in the newly formed blood vessels to the tumour (Seftor *et al.* 1992; Clezardin, 1998). Antagonists of αVβ3 have been shown to block tumour-associated angiogenesis presenting αVβ3 as an interesting target for cancer therapy (Curley *et al.*, 1999).

Although antagonists are being developed to inhibit integrin activity in disease states, more information is requires to elucidate the exact nature of integrin-ligand recognition. Identification of the structural determinants utilised by ligands within the integrin receptor and an understanding of the mechanisms involved in integrin activation would offer further opportunities for therapeutic intervention in the diseases and disorders described.

1.4 Integrin structure

Electron microscopy images of the αIIbβ3 integrin revealed an extracellular globular head (~70-100 Å in diameter) which comprised the N-terminal portions of the α and β subunits, followed by two long stalks (~100 Å) between the head and the membrane-spanning helices, and short C-terminal cytoplasmic tails (Erb *et al.*, 1997). Recently, the crystal structure of the extracellular segment of αVβ3 has been published (Xiong *et al.*, 2001). This structure is reported to be the active, ligand-competent state of the integrin as truncation of the transmembrane and cytoplasmic regions is known to produce the high affinity integrin. The structure, as shown in figure 1.1, is composed of an ovoid headpiece, assembled from the N-terminal sections of the α and β subunits, followed by two nearly parallel tails. The headpiece consists of a β-propeller domain from αV and an I domain from the β3 subunit. These two domains will be described in more detail in the following sections. The αV tail is made up of three immunoglobulin-like β-sandwich domains termed the thigh and calf domains. The β3 tail begins with an immunoglobulin-like hybrid domain followed by a plexins, semaphorins and integrins (PSI) domain, four epidermal growth factor (EGF) domains and a β-tail domain (βTD). The overall structure has a bent conformation, as shown in figure 1.1a, with the integrin tails folding at ~135° at the "genu" between the thigh and first calf domain of αV.

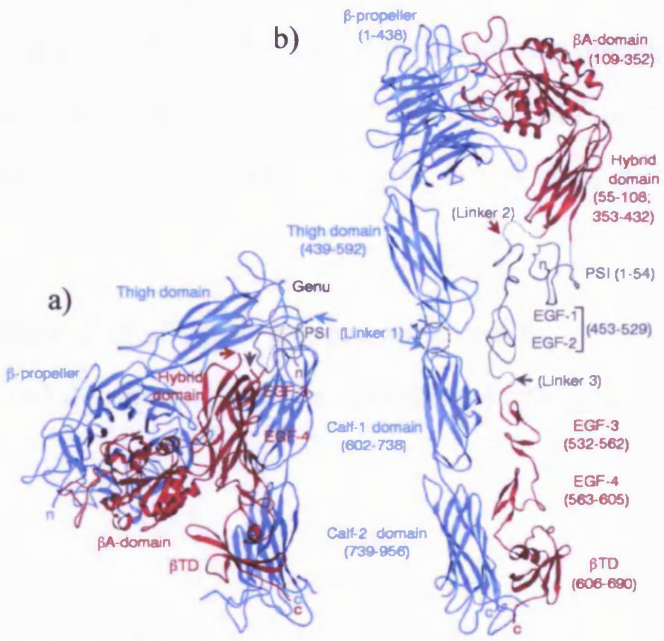

Figure 1.1 (a) Ribbon diagram of the αVβ3 extracellular domains with the α subunit is shown in blue with the β subunit in red. (b) shows the straightened αVβ3 structure. Taken from Xiong *et al.* (2001).

1.4.1 Integrin-ligand interactions

The first integrin recognition site identified in molecular detail was the arginine-glycine-aspartic acid (RGD) found in fibronectin (Pierschbacher & Ruoslahti, 1984). However, not all integrins recognise this motif and not all integrin ligand contain a functional RGD site. A common theme for integrin recognition sites seems to be short peptide sequences with an acidic residue (Ruoslahti, 1996; Plow *et al.*, 2000). The collagens are an exception as the recognition site involves triple-helical motifs (Knight *et al.*, 1998). Some ligands, such as fibrinogen, which does not possess an RGD motif, contain multiple recognition sites. Another feature of integrin-ligand binding is the involvement of cations. Different cations were found to have different effects on ligand

recognition by α5β1 (Mould *et al.*, 1995; Hu *et al.*, 1996). Both Mn^{2+} and Mg^{2+} supported binding although Mn^{2+} facilitated higher affinity binding. Ca^{2+} mediated very poor ligand binding and was a non-competitive inhibitor of ligand binding supported by Mn^{2+}. The roles of divalent cations in integrin ligand binding and activation will be discussed later.

Three major sites of ligand recognition have been identified in integrins. These are the α subunit I domain, the α subunit N-terminal repeats and the I domain of the β subunit.

1.4.1.1 The α subunit I domain

Nine integrin α subunits contain a ~190 residue sequence near the N-terminus, called the I domain. The isolated recombinant I domains have been shown to recapitulate many of the ligand-binding properties of the intact integrin (Michishita *et al.*, 1993; Zhou *et al.*, 1994; Tuckwell *et al.*, 1995; Calderwood *et al.*, 1997; Stanley & Hogg, 1998). Removal of I domains from αMβ2 and αLβ2 completely inhibits binding to certain ligands (Leitinger & Hogg, 2000; Yalamanchili *et al.*, 2000) and the isolated αLβ2 I domain locked in its active state binds ligands as well as the intact activated αLβ2 receptor (Lu *et al.*, 2001a; Lu *et al.*, 2001b).

The ligands for I domain-containing integrins are diverse as shown in table 1.1. They include cell surface transmembrane proteins that are members of the immunoglobulin family, such as ICAM-1, -2, and –3, and extracellular matrix proteins, such as collagen or laminin. Several pathogens utilise the I domain as a ligand to gain entry into human cells or to counter a potential immune response. For example, the αM I domain has been shown to bind neutrophil inhibitory factor from canine hookworm

(Rieu *et al.*, 1994) and the fungal pathogen *Candida albicans* (Forsyth *et al.*, 1998).

The crystal structures of the I domains from αM, αL, α2 and α1 have been determined (Lee *et al.*, 1995b; Qu & Leahy, 1995; Emsley *et al.*, 1997; Nolte *et al.*, 1999). They all adopt a very similar conformation of a dinucleotide-binding fold with a central parallel β sheet surrounded on both sides by α helices as shown in figure 1.2.

Figure 1.2 Ribbon diagram of the αM subunit I domain. β strands are labelled A-F and α helices are labelled 1-7 and the Mg^{2+} ion is represented by the blue sphere. Taken from Lee *et al.* (1995b)

Binding of the I domain to protein ligands has been found to be dependent on divalent cations. At the C-terminal end of the β sheet, a divalent cation coordination sphere has been located, which is termed the metal ion-dependent adhesion site (MIDAS). It contains the conserved sequence DxSxS (single letter code and x is any amino acid) where highly conserved oxygenated residues directly coordinate the metal.

Point mutations in this MIDAS motif disrupt cation and ligand binding (Michishita *et al.*, 1993; Kern *et al.*, 1994; Edwards *et al.*, 1995; McQuire & Bajt, 1995; Kamata *et al.*, 1999). The upper surface of the domain surrounding the MIDAS motif is highly variable and has also been shown to be involved in ligand binding (Huang & Springer, 1995; Zhang & Plow, 1999). This region may provide specificity in integrin-ligand interactions.

The αM I domain has been crystallised in two significantly different conformations with Mg^{2+} and Mn^{2+} bound, as illustrated in figures 1.3 and 1.4 (Lee *et al.*, 1995a).

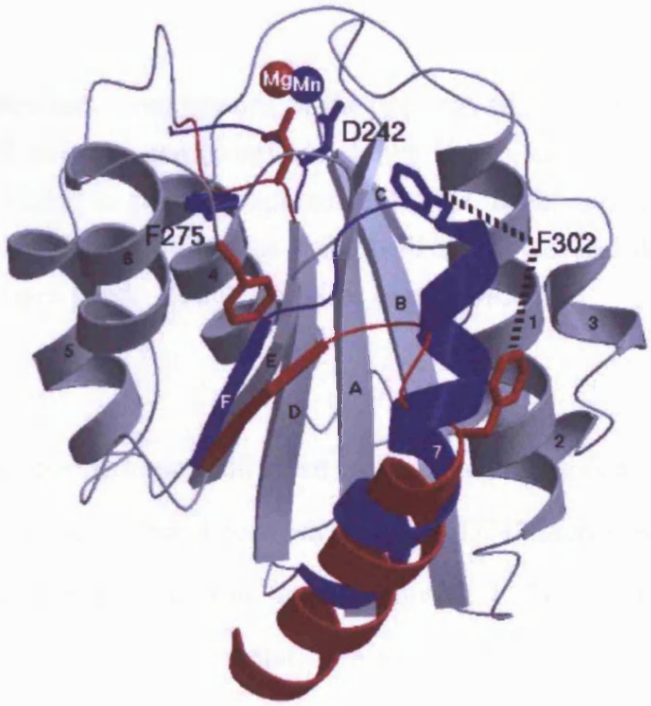

Figure 1.3 Ribbon diagram showing the major conformational differences between the open and closed states of the αM I domain. Red illustrates the Mg^{2+}-bound open conformation and blue illustrates the Mn^{2+}-bound closed conformation. β strands are labelled A-F and α helices are labelled 1-7. The remainder of the I domain which does not undergo any significant conformational changes is coloured grey. Taken from Lee *et al.* (1995a)

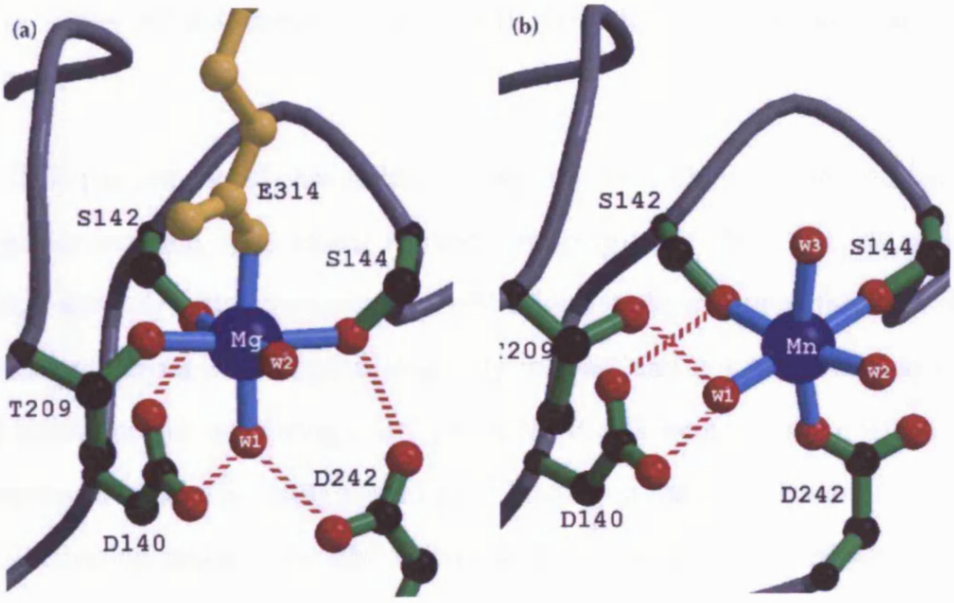

Figure 1.4 Structural comparisons of the open (a) and closed (b) αM I domain at the MIDAS site. Oxygen atoms are shown in red, carbon in black, and the schematic backbone in grey. The glutamate from a neighbouring molecule (a) is shown in yellow, water molecules are labelled W1-W3 and dashed red lines illustrate hydrogen bonds. Taken from Lee *et al.* (1995a)

The metal coordination is different in the two structures as illustrated in figure 1.4. The absence of a direct bond between Mg^{2+} and D242 increases the electrophilicity of the metal and a glutamate from a neighbouring I domain in the crystal lattice completes the coordination of the metal. The change in metal coordination is linked to structural changes, as shown in figure 1.3. In the Mn^{2+} form, the C-terminal helix moves 10 Å up the side of the domain and two phenylalanine residues are buried into the hydrophobic core. Burial of these phenylalanine residues causes shifts in the loops surrounding the MIDAS, rearranging the metal-coordinating residues. It was hypothesized that the glutamate at the MIDAS of the Mg^{2+} form mimics a natural integrin-ligand interaction as integrin ligands contain a critical acidic residue in their

binding motif. The two conformations are proposed to represent the adhesive and non-adhesive states of the domain, which shall be referred to as open and closed respectively.

This conformational change has subsequently been shown to occur upon ligand binding. For example, monoclonal antibody mapping with CBRM1/5, an activation-dependent antibody which recognises the αM I domain, demonstrated that the I domain conformational changes were physiologically relevant and not just a consequence of crystal lattice interactions (Oxvig *et al.*, 1999). NMR data were consistent with a similar conformational change occuring upon ligand binding in the αL I domain (Huth *et al.*, 2000). Activating mutants for αM I domain, based on the open and closed crystal structures, have been designed giving varying degrees of increased ligand binding (Li *et al.*, 1998; Shimaoka *et al.*, 2000; Xiong *et al.*, 2000). A high affinity mutant of αL I domain has also been formed by locking the C-terminal helix in the open position, preventing the domain from adopting the closed conformation (Shimaoka *et al.*, 2001). Recently, the structure of α2 I domain complexed with a collagen peptide has been determined (Emsley *et al.*, 2000) This provides the most convincing evidence for the conformational change in the I domain which accompanies ligand binding. An alteration in metal coordination at the MIDAS motif that allowed bond formation between the divalent cation and a glutamate from the collagen was linked to a 10 Å downward shift of the C-terminal helix. These structural changes were very similar to those observed in the two crystal forms of αM I domain demonstrating a common mechanism for activation.

1.4.1.2 The α subunit N-terminal repeats

The N-terminal region of all integrin α subunits is composed of seven repeats, of about 60 amino acids each, which contain FG-GAP consensus repeats. A large body of evidence suggests that these repeats contain residues involved in ligand binding. For example, mutation of residues in predicted β-turn structures of the third N-terminal repeat in α4 and α5 disrupted ligand recognition (Irie *et al.*, 1995). Mutations in the third N-terminal repeat of αIIb also blocked binding to fibrinogen (Kamata *et al.*, 1996). Exchanging the N-terminal third of αV with the corresponding residues of αIIb altered the specificity of the chimearic receptor (Loftus *et al.*, 1996). In addition, Ca^{2+} binding sites have been identified in repeat 4 in some integrins and in repeats 5 through 7 in all integrins (Tuckwell *et al.*, 1992).

Prior to the crystal structure of the extracellular domains of αVβ3, the structural composition of the α subunit N-terminal repeats was the subject of much discussion with two alternate models presented. The repeats had been predicted to fold as EF-hand-like domains or as a β-propeller domain. The evidence for both models is presented later in section 2.1. The crystal structure of αVβ3 has however clarified this issue as the α subunit N-terminal repeats form a β-propeller structure, as shown in figure 1.5 (Xiong *et al.*, 2001). The seven blades of the propeller are arranged radially about a central pseudo symmetry axis with each blade composed of a four-stranded antiparallel β-sheet. Four Ca^{2+} binding sites were found in β-hairpin loops of blades four through seven on the lower face of the propeller. Integrin ligands are predicted to bind to the upper surface loops of the β-propeller (Mould *et al.*, 1998a; Tozer *et al.*, 1999; Zhang *et al.*, 1999; Irie *et al.*, 1997; Munoz *et al.*, 1997; Mould *et al.*, 2000).

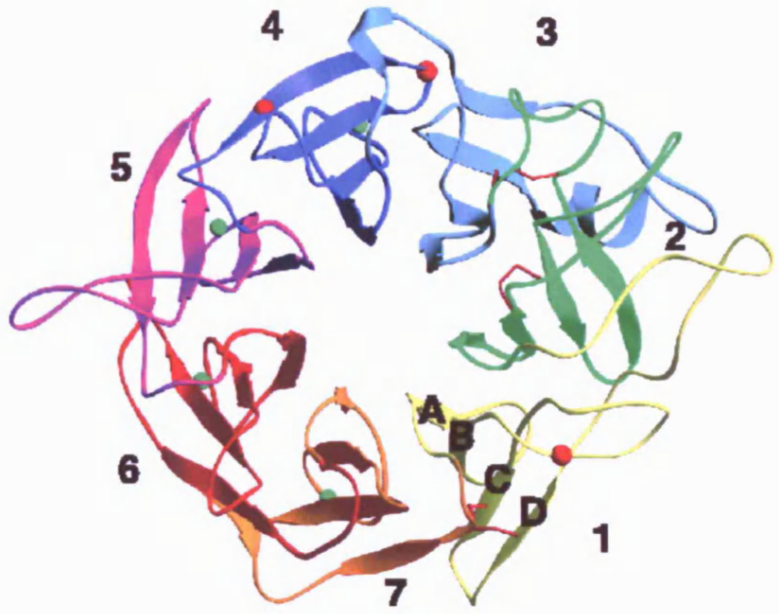

Figure 1.5 Ribbon diagram of the β-propeller domain from αVβ3. The disulphides are shown as red sticks, glycans as red spheres and Ca^{2+} ions as green spheres. Taken from Xiong *et al.* (2001).

1.4.1.3 The β subunit I domain

A third region important for ligand binding by integrins is present in the N-terminal half of the β subunit. Numerous studies demonstrate that this region is important in ligand binding and specificity (Loftus *et al.*, 1990; Takada & Puzon, 1993; Shih *et al.*, 1993; Loftus *et al.*, 1994; Lin *et al.*, 1997a)

The most highly conserved region of the β subunit is a ~250 residue stretch located near the N-terminus which was proposed to have an I domain-like fold similar to that of the α subunit (Lee *et al.*, 1995b; Tozer *et al.*, 1996; Tuckwell & Humphries, 1997; Huang *et al.*, 2000). Mutation of residues predicted to be involved in cation coordination at the proposed MIDAS motif disrupted ligand binding (Bajt *et al.*, 1995; Goodman & Bajt, 1996; Puzon-McLaughlin & Takada, 1996; Lin *et al.*, 1997b).

Naturally occuring β subunit mutations which disrupt integrin function such as those observed in leukocyte adhesion deficiency-1 patients correspond to the β I domain (Loftus *et al.*, 1990; Hogg *et al.*, 1999).

The crystal structure of the αVβ3 extracellular domains has confirmed the presence of a β subunit I domain (Xiong *et al.*, 2001). The structure of the β3 I domain, which is shown in figure 1.6, adopts a nucleotide-binding fold with a central six-stranded β-sheet surrounded by eight helices. The MIDAS is located in the same position as previously described for the α subunit I domain, although a metal ion did not occupy this site in the crystal structure. An additional metal binding site termed ADMIDAS is present, adjacent to the MIDAS. This site was occupied by calcium in the crystal structure and was proposed to have a potential regulatory function.

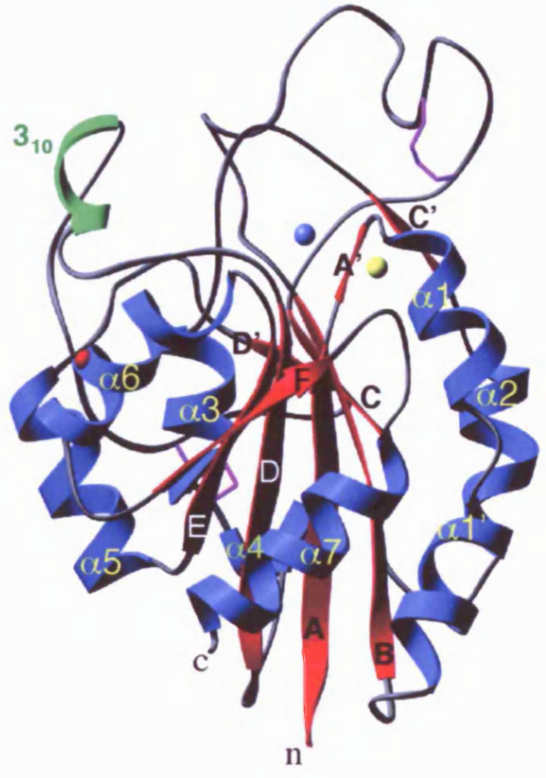

Figure 1.6 Ribbon diagram of the β subunit I domain from αVβ3. Disulphides are shown in purple with a glycan as a red sphere. The Ca^{2+} ion at the ADMIDAS is represented as a yellow sphere and the blue sphere represents the proposed position of the metal ion at the MIDAS. Taken from Xiong *et al.* (2001).

1.4.2 Spatial arrangement of ligand binding domains

As shown in figure 1.1, the α-subunit β-propeller and β-subunit I domain interface is large with six of the seven blades of the propeller in contact with the I domain. The most important contact point is mediated by the residues from the 3_{10} helix of the I domain protruding into the channel of the propeller where they interact with two concentric rings of predominantly aromatic propeller residues. The α subunit I domain also connects to the β-propeller through its C-and N-terminal helices and is predicted to be inserted between β-sheets 2 and 3 of the β-propeller domain (Springer, 1997). The α subunit and β subunit I domains are proposed to be next to one another on the same side of the β-propeller domain with the bottom of the α-subunit I domain in close proximity to the β-subunit I domain (Puzon-McLaughlin *et al.*, 2000). The putative interactions of these ligand binding domains during adhesion events shall be presented later.

1.5 Integrin signalling and activation

Integrins are versatile receptors that can exist in various activation states and interact with the both the exterior and interior of the cell. Binding of extracellular ligands can trigger a conformational change within the integrin that is transmitted across the plasma membrane. This 'outside-in' signalling can then activate various intracellular signalling pathways. Alternatively, binding events in the cytoplasmic tails that trigger conformational changes across the membrane can control the adhesiveness of the integrins extracellular domains. This is termed 'inside-out' signalling.

1.5.1 Outside-in signalling

Integrins transduce signals from the outside of the cell to control cell movement, cell morphology, cell growth and gene expression. Activated integrins can mobilise a diverse complex of molecules at the cell-substratum interface to generate a variety of intracellular signals. Integrin engagement can cause the elevation of intracellular calcium, activation of Na/H antiporters, phosphorylation (serine/threonine and tyrosine) of cytoplasmic proteins, phosphatidylinositol turnover and accumulation of GTP-bound $p21^{ras}$ (Schwartz *et al.*, 1995). A good example of outside-in signalling can be observed in anoikis, where integrin-dependent interaction with the ECM suppresses apoptosis (Frisch & Ruoslahti, 1997). Gene expression is also regulated by this type of signalling, as demonstrated by the laminin receptor integrins (Roskelley *et al.*, 1995). Outside-in signalling through these integrins can lead to AP-1 and STAT5-induced transcription of β-casein in murine mammary epithelial cells. Upon ligand binding, integrins initiate intracellular signalling cascades at specialised sites called focal adhesions.

1.5.1.1 Focal adhesion sites

Integrins that are not bound to ECM ligands are generally diffusely distributed over the cell surface and appear not to be linked to the actin cytoskeleton. Upon ligand binding, integrins move laterally in the plane of the membrane to form clusters at focal adhesion sites (Sastry & Burridge, 2000). These sites are large integrin aggregates found at the ends of prominent bundles of actin filaments. They connect the ventral plasma membrane to the ECM and recruit a complex mixture of cytoskeletal proteins, including vinculin, talin, paxillin, α-actinin, filamin, tensin and signalling molecules (Critchley, 2000). Cytoskeletal proteins, such as α-actinin, talin and paxillin, have been

shown to interact with integrin cytoplasmic tails (Otey *et al.*, 1993; Calderwood *et al.*, 1999; Liu & Ginsberg, 2000). Focal complexes are smaller integrin clusters that occur at the tips of filopodia and lamellipodia, which represent structures important for cell motility.

Focal adhesions are highly dynamic structures that are constantly remodelled in shape, size and molecular assembly. Coordinating regulation of integrin-binding affinity and actin filament dynamics is fundamentally important to cell adhesion, cellular architecture, cell motility and integrin signalling. Organisation of the integrin-associated actin structures, as well as binding of integrins to the ECM ligands, is regulated by members of the Rho and Ras families (Schoenwaelder & Burridge, 1999). The signalling pathways implicated in this regulation by small GTPases are summarised in figure 1.7.

1.5.1.2 Intracellular signalling pathways

Integrins do not contain intrinsic enzymatic activity so they are probably unable alone to transmit signals from their cytoplasmic tails to the intracellular mediators of signal transduction. Several proteins have been identified which can directly bind integrins and modulate their functions. These include integrin-associated protein, transmembrane-4 superfamily, focal adhesion kinase, integrin-linked kinase, integrin cytoplasmic domain-associated protein-1, cytohesin-1, β3-endonexin, calcium- and integrin-binding protein and calreticulin (Coppolino & Dedhar, 2000).

Early studies on integrin-dependent cell adhesion and signalling demonstrated that cell ligation to the ECM was accompanied by integrin clustering, and this could trigger increased tyrosine phosphorylation of a number of intracellular proteins

(Schlaepfer & Hunter, 1998). Focal adhesion kinase (FAK) was one of the first proteins demonstrated to be activated by phosphorylation during cell adhesion via integrins and has since been the most widely studied (Cary & Guan, 1999). FAK is a tyrosine kinase and has been shown to bind directly to the cytoplasmic domains of β1, β2 and β3 *in vitro* (Liu *et al.*, 2000). Engagement of integrins induces auto-phosphorylation of FAK and activation of FAK tyrosine kinase activity. This allows FAK to interact with docking or adaptor proteins such as paxillin, tensin and Grb2/Son of Sevenless (SOS) and the Src family of nonreceptor kinases. Src interaction with FAK causes the phosphorylation of other tyrosine residues, that results in maximal activation of FAK.

Activation of FAK by integrins is thought to play a central role in cell growth control. Mutation of residues critical to FAK autophosphorylation prevented integrin-mediated proliferation (Schlaepfer *et al.*, 1994). Also, introduction of constitutively active FAK led to cell transformation, anchorage-independent growth and suppression of anoikis (Guan & Shalloway, 1992). The role of FAK and other effectors in anoikis is summarised in figure 1.8. The phosphorylation of FAK and other cytoskeletal proteins at the focal adhesion site triggers an accumulation and activation of signal transduction molecules, such as Src-type kinases, Src substrates, Ras, mitogen-activated protein kinases (MAPKs) i.e. ERK, JNK and p38 (Cary & Guan, 1999). Integrin mediated activation of the MAPK signal-transduction pathway provides a common route leading to transcriptional regulation of genes that are crucial for cell growth and differentiation (Chang & Karin, 2001). Family members that are sequentially activated following transient activation of Ras GTP-binding proteins via receptor tyrosine kinases include MAPK, MAPK kinase or MEK, Raf and extracellular signal-regulated kinase (ERK) 1 and 2. The adaptor protein, Shc, has also been implicated in integrin signalling to MAPKs independent of FAK. MEK-dependent phosphorylation of ERK1 and ERK2 results in their translocation to the nucleus, where they phosphorylate and activate a number of transcription factors associated with early-response genes (Hill & Treisman,

1995). Integrins also appear to cooperate with growth factor receptors in a synergistic fashion to activate FAK and MAPK (Miyamoto *et al.*, 1996).

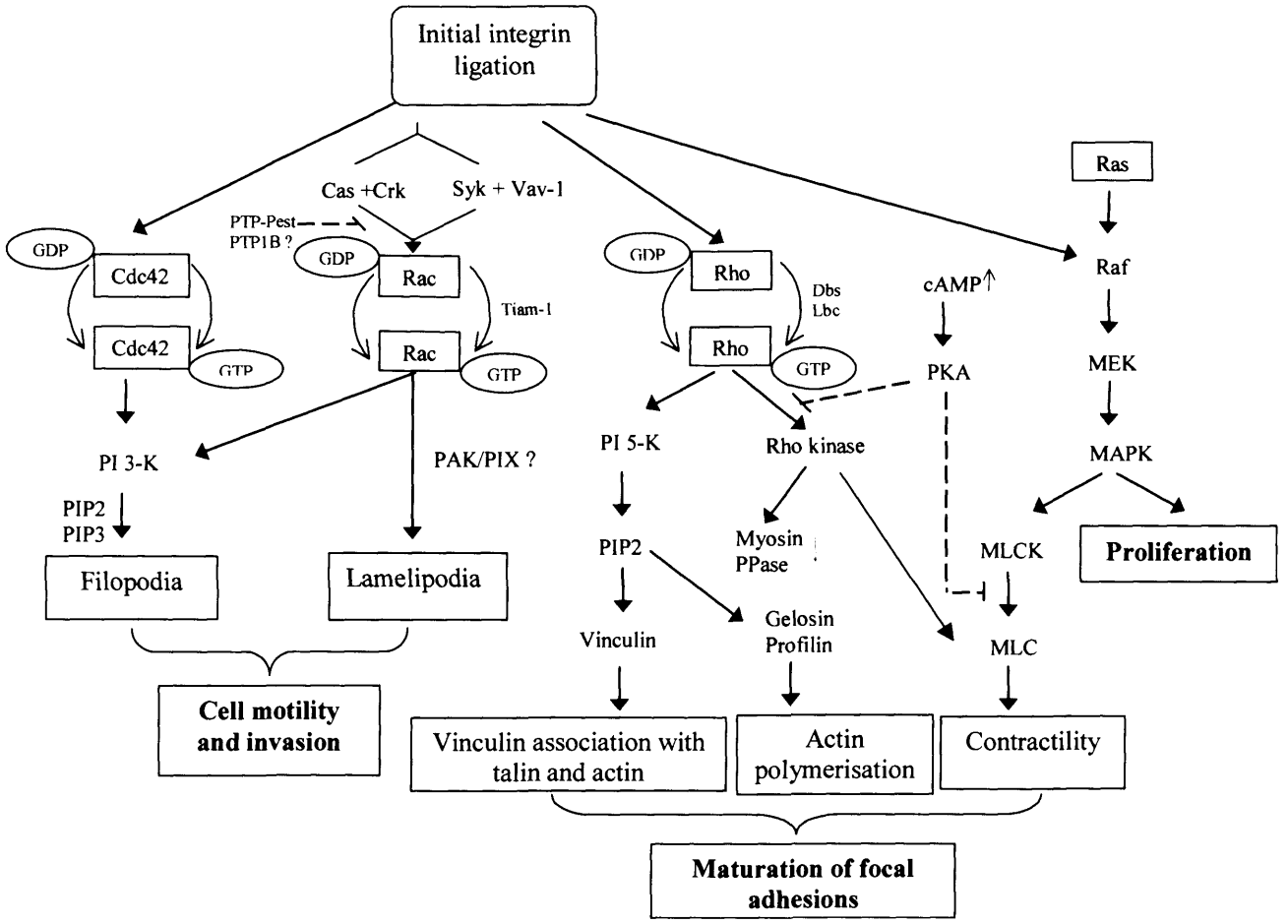

Figure 1.7 Signalling pathways involving small GTPases in integrin-mediated cell motility, invasion and assembly of focal complexes.

Abbreviations: MAPK, mitogen-activated protein kinase; MEK, MAPK kinase; MLC, myosin light chain; MLCK, myosin light chain kinase; PI 3-K, phosphoinositide 3-kinase; PI 5-K, phosphatidylinositol 4-phosphate 5-kinase; PIP2, phosphatidylinositol (4,5)-bisphosphate; PIP3, phosphatidylinositol (3,4,5)-trisphosphate; myosin PPase, myosin phosphatase; PAK, p21-activated kinase; PIX, PAK interacting exchange factor; PTP, protein tyrosine phosphatase; PKA, protein kinase A; cAMP, cyclic adenosine monophosphate; GDP, guanosine diphosphate; GTP, guanosine triphosphate Dotted lines indicate inhibition pathways. Adapted from Keely *et al.* (1998)

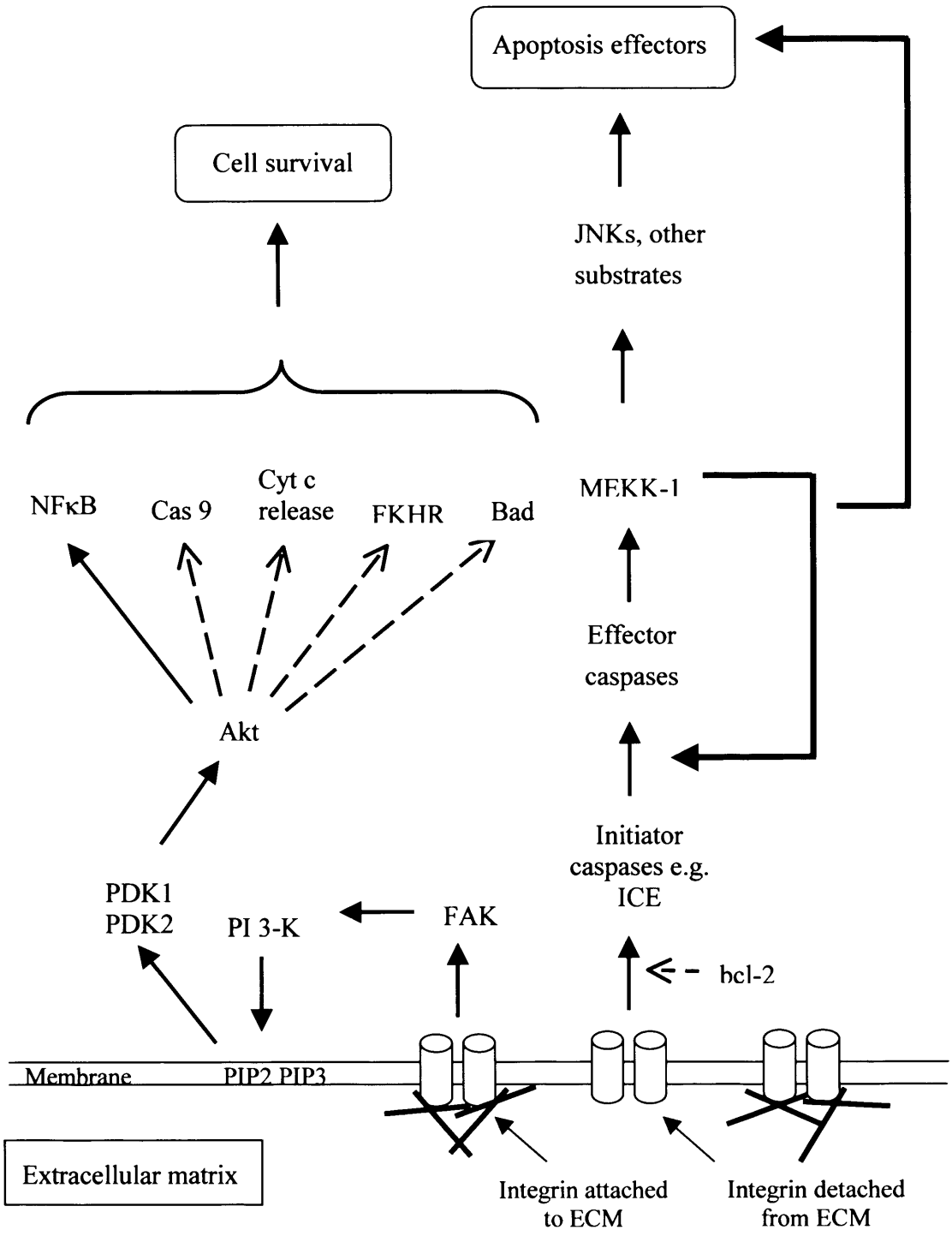

Figure 1.8 Pathways implicated in anoikis. Dotted lines indicate inhibition of a pathway or resulting mediator. Abbreviations: ICE, interleukin-1-converting enzyme; MEKK-1, MAPkinase/ERK kinase kinase-1; JNK, Jun amino-terminal kinases; PI 3-K, phosphoinositide 3-kinase; FAK, focal adhesion kinase; PIP2, phosphatidylinositol (4,5)-bisphosphate; PIP3, phosphatidylinositol (3,4,5)-trisphosphate; NFκB, nuclear factor κB; Cas 9, caspase 9; Cyt c, cytochrome c; FKHR, Forkhead transcription factor; ECM, extracellular matrix. Adapted from Frisch & Ruoslahti (1997).

As integrins have distinct functions, they must be able to activate subunit-specific pathways in addition to the common pathways. This was first demonstrated with a subset of integrins (α1β1, α5β1, α6β4, αVβ3) which promoted cell proliferation via recruiting Shc and activating the Ras-ERK pathway using caveolin as an adaptor (Wary *et al.*, 1996). Transmembrane-4 superfamily proteins interact with integrins, such as α3β1 and α6β1, to activate phosphatidylinositol 4-kinase and possibly other signalling molecules (Yauch *et al.*, 1998). Association with transmembrane adaptor proteins may not be the only activation mechanism for subunit-specific pathways. An alternative may involve the cytoplasmic tails of the α subunit (Wei *et al.*, 1998).

A redox site in the extracellular domain has been proposed as an additional form of regulation in integrin activation (Yan & Smith, 2000). Changes to the redox site prevent the inter-conversion between the resting and active integrin. The two pathways to activation, inside-out and redox, could serve different purposes with the redox site regulating rapid and transient changes in activation state without the requirement of communicating factors in the cytoplasm.

1.5.2 Inside-out signalling

Integrins can be controlled from the inside of the cell, modulating their ligand binding affinities (Crowe *et al.*, 1994; Shimizu *et al.*, 1990). This is accomplished by unidentified cytoplasmic signals that switch the receptor from a low affinity binding state to a high affinity state (Lollo *et al.*, 1993). These changes in integrin activity can be explained by two mechanisms; changes in avidity and changes in affinity, which are not mutually exclusive.

1.5.2.1 Avidity modulation

Changes in integrin avidity are most likely to result from their redistribution in the plane of the plasma membrane, resulting in integrin clusters at sites of ligand binding. For example, evidence suggests that β1 integrin oligomerisation facilitates fibronectin binding in the absence of increases in receptor affinities (Yauch *et al.*, 1997). The membrane proximal residues of the β1 cytoplasmic domain were shown to be required for oligomerisation using chimeras and deletion analysis (Zage & Marcantonio, 1998). Recently, a cytoplasmic region of the β2 subunit was shown to be crucial for activation and clustering of αLβ2 is considered to be a prerequisite for its activation and ligand binding (Bleijs *et al.*, 2001). This mechanism would allow for multivalent interactions with ligands to facilitate rebinding events.

Integrin clustering can be regulated by intracellular signalling events that remodel the cytoskeletal linkages or alter receptor diffusion rates within the cell membrane (van Kooyk & Figdor, 2000). Experiments with α4β1 and αLβ2 demonstrated that linkage to the cytoskeleton restricted integrin lateral diffusion and clustering (Lub *et al.*, 1997; Yaunch *et al.*, 1997). Release from this constraint allowed the integrin motility so it could cluster, promoting outside-in integrin-mediated adhesion. Additional molecular mechanisms of this regulation may include phosphorylation events, GTP-GDP exchange and phospholipid metabolism (Coppolino & Dedhar, 2000).

1.5.2.2 Affinity modulation

Many integrins are expressed in an inactive form and can be activated to bind ligands by intracellular signals. Changes in integrin activity are thought to involve the propagation of conformational changes from the integrin cytoplasmic domains to the extracellular ligand binding domains. Substantial evidence indicates that integrins change their conformation during ligand binding and activation. In the case of αIIbβ3, a relatively large conformational change in quaternary structure can occur upon ligand binding (Hantgan *et al.*, 1999). Several studies, using chimeras and truncations, have demonstrated that the α and β cytoplasmic domains can mediate affinity modulation via inside-out signalling (O'Toole *et al.*, 1991; O'Toole *et al.*, 1994; Hughes *et al.*, 1995). Conserved sequences in the α and β cytoplasmic tails have been shown to be a requirement for integrin activation, for example the NPXY motif in the β tail (Hughes & Pfaff, 1998).

Affinity modulation may be controlled by two mechanisms; by "unmasking" of the ligand binding site by domain movement or by "shape shifting", tertiary conformation changes that alter the shape and charge properties of the ligand binding domain surface (Loftus & Liddington, 1997). Shape shifting has been demonstrated in the α subunit I domain, as previously described, and a model for unmasking will now be discussed.

An initial model of integrin conformational activation was proposed using the αIIbβ3 integrin (Hughes *et al.*, 1996). A salt bridge between the membrane-proximal regions of the α and β subunit cytoplasmic domains suggested that the integrin was held in the inactive conformation by this bond. Mutation of the charged residues involved in the salt bridge resulted in a constitutively active integrin that could induce bidirectional transmembrane signalling.

A system analogous to the heterotrimeric G-proteins was initially proposed due to the structural similarities between the α subunit GTPase domain and the integrin α subunit I domain, and the GTPase βγ propeller and putative integrin α subunit β-propeller (Loftus & Liddington, 1997). In the heterotrimeric G-protein system, the βγ subunits form a propeller with ligand binding sites masked in the inactive state by the α subunit GTPase domain. Upon hydrolysis of GTP, the GTPase domain changes its conformation and ligand binding properties, detaches from the βγ propeller, and unmasks ligand binding sites on the propeller (Lambright *et al.*, 1996). Similarly, for an integrin allosteric model, it was proposed that the β subunit I domain would sit on top of the α subunit propeller in the low affinity quaternary state so that the propeller ligand binding sites would be sterically blocked (Loftus & Liddington, 1997). Upon activation, the β subunit I domain would be released from its contacts with the propeller, leading to shape shifting in the β subunit I domain and unmasking of the propeller ligand binding sites. In the case of integrins that contain an α subunit I domain, this I domain sits on top of the propeller, between the second and third blades, where it would sterically block potential binding sites. The shape shifting within the I domain that is required for high affinity could lead to a hinge motion of the I domain, unmasking the ligand binding sites on the β-propeller.

A "two state" scissor model was proposed for this integrin allosteric model where the closed conformation, with low affinity for ligand, would be more stable in the absence of ligand and stabilised by bonds between the α and β subunits (Loftus & Liddington, 1997). The open conformation would be able to form high affinity bonds with the ligand because the stabilising bonds between the subunits would be broken. Thus, during activation, the membrane proximal regions of the α and β cytoplasmic tails were proposed to act like a hinge during the scissor-like motion of the αβ complex, as shown in figure 1.9. The integrin would be in equilibrium between these conformational states and ligand binding to the cytoplasmic tails may shift this balance

to the high affinity ligand binding state. The mechanisms of such a quaternary conformation change that is linked to activation are still unclear and the subject of much investigation.

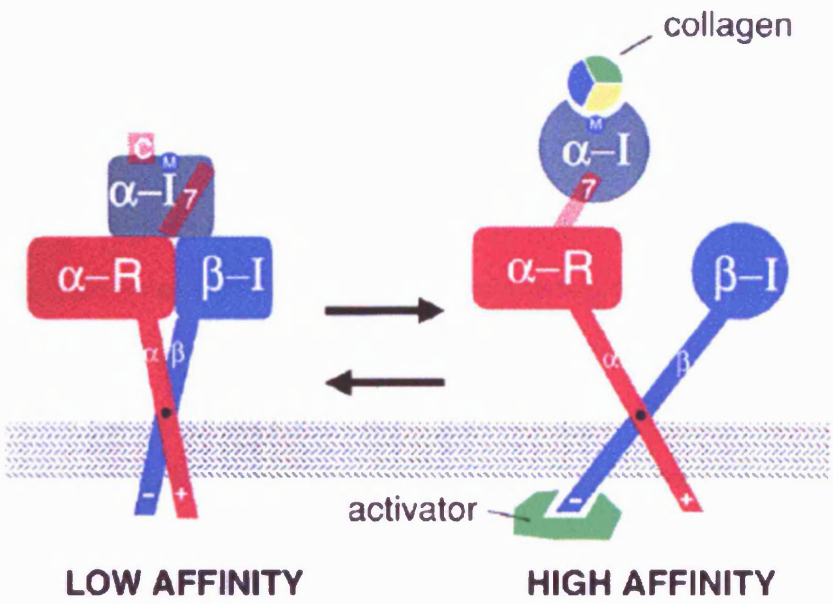

Figure 1.9 Model for integrin allostery demonstrating the two quaternary conformations, the low affinity and high affinity states, in equilibrium. The α subunit is coloured red and the β subunit is blue. The α subunit I domain (α-I) is attached to the β-propeller (α-R) by the C-terminal helix (α7) depicted by a red rectangle. The high affinity state is shown with an intracellular activator illustrating inside-out signalling. Outside-in signalling could occur by an extracellular ligand, such as collagen binding the α I domain via the MIDAS metal, labeled M in a blue sphere.

A growing body of evidence supports this allosteric control of integrin activation. The separation between the α and β extracellular stalk-like domains of αIIbβ3 was increased upon fibrinogen binding (Weisel *et al.*, 1992). Cleavage of αIIb on platelets at the membrane-proximal region converts αIIbβ3 from a resting to a ligand binding receptor in the absence of any signalling events (Si-Tahar *et al.*, 1997). Many activating antibodies map to the stalk region of the β subunit and are proposed to act as

a wedge that loosens the association of the α and β subunits at the membrane proximal region (Huang *et al.*, 2000). Substitution of heterodimer-forming α-helical coiled coils in the cytoplasmic domains of αL and β2 maintained αLβ2 in an inactive state (Lu *et al.*, 2001c). Finally, a construct was made of the α5β1 extracellular fragments with the interaction between the α and β subunit cytoplasmic domains replaced by an artificial clasp (Takagi *et al.*, 2001). Release of the clasp resulted in increased binding to fibronectin and an ~14 nm seperation of the extracellular stalks. This data along with the other evidence suggests an overall mechanism for affinity modulation involving the spatial seperation of the cytoplasmic and/or transmembrane domains. This last piece of data also suggested a slightly different model, where the hinge is located in the N-terminal binding region rather than at the junction of the transmembrane and cytoplasmic domains. In this model, the cytoplasmic domains would function to keep the stalks closed rather than acting as a hinge.

Evidence also supports the involvement of the α subunit I domain in this model of activation. Data shows that if the conformational changes within the I domain, such as the large C-terminal helix shift, can be prevented then the I domain and integrin can be trapped in the open or closed conformation. This may prevent quaternary changes from occuring, leaving the ligand binding sites in the β-propeller permanently unmasked or masked. For example, substitution of residues at the bottom of the αM I domain, in a region that would connect the I domain to the β-propeller, produced a constitutively active receptor even though ligand binding is located at the top of this domain (Zhang & Plow, 1996). Another study found that soluble αL I domain inhibited Mg^{2+}-induced αLβ2 adhesion and prevented a conformational change that is required for transition to the high affinity form of the integrin (McDowall *et al.*, 1998). The I domain regions involved in this inhibition were located to its lower face which would potentially contact the β-propeller. The authors suggested that the soluble I domain was competing with the cellular I domain in the intact integrin for binding to the β-propeller.

This was preventing an interdomain movement between the I domain and β-propeller domain that would be necessary for activation. Recently, the I domain from αLβ2 has been locked via its C-terminal helix in the open and closed conformation (Lu *et al.*, 2001a). The locked-open I domain in αLβ2 produced an integrin which was constitutively active, whereas the locked-closed I domain abolished the integrins constitutive and activatible adhesion. A small molecule inhibitor, lovastatin, binds in a pocket at the bottom of the αL I domain, under the conformationally mobile C-terminal helix, which would be at the interface with the β-propeller (Kallen *et al.*, 1999). Its presence was predicted to inhibit αLβ2 ligand binding by blocking movement of the I domains C-terminal helix, which would prevent unmasking of the ligand binding sites. This hypothesis was supported by experiments using the αL I domain conformational mutants in αLβ2 which showed that lovastatin could inhibit the wild type integrin, but not the integrin with the locked-open I domain (Lu *et al.*, 2001a).

The α subunit I domain and β subunit I domain appear to be near one another on the same side of the β-propeller domain (Puzon-McLaughlin *et al.*, 2000). The authors predicted that the bottom of the α subunit I domain would be in close proximity to the top of the β subunit I-like domain. Using αLβ2, a linkage between the α I domain and the β subunit I domain has been demonstrated and the β subunit I domain has been proposed to have a regulatory rather than a direct role in ligand binding, as previously suggested (Lu *et al.*, 2001c). The authors suggested that the αL I domain and the β2 I domain were allosterically linked with the β2 I domain regulating ligand binding by the αL I domain. It had previously been hypothesised that mutation of β subunit residues that disrupt ligand binding in integrins containing α subunit I domains may block the β subunit I domain in the inactive conformer rather than directly disrupt ligand binding (Loftus & Liddington, 1997). In integrins that lack an α subunit I domain, the β subunit I domain may either have a direct role in ligand binding, or may regulate the conformation of adjacent loops in the β-propeller (Puzon-McLaughlin *et al.*, 2000).

The exact intracellular mechanisms that regulate inside-out signalling are unclear. The phosphorylation state of the integrin subunits may be important in their regulation (Blystone *et al.*, 1997). In the cell, the affinity state switch may also be regulated by calreticulin (Coppolino *et al.*, 1997), serine/threonine kinases and the Ras family of small GTP-binding proteins. Activated H-Ras and its kinase effector Raf-1 inhibit integrin activation (Hughes *et al.*, 1997) whereas R-Ras stimulates integrin ligand binding affinity (Zhang *et al.*, 1996).

1.5.3 The role of divalent cations in integrin ligand binding and allosteric regulation

The recent structure of the extracellular segment of αVβ3 revealed six divalent cation binding sites (Xiong *et al.*, 2001). Four Ca^{2+} were bound to the lower face of the β-propeller, a Ca^{2+} was bound to the ADMIDAS in the β subunit I domain and a Ca^{2+} was bound at the genu between the α subunit thigh and calf 1 interface (see figures 1.1, 1.5 and 1.6). The authors proposed that the cation bound at the genu and the β-propeller-thigh interface may help to make these interfaces more rigid thereby regulating integrin-ligand interactions in an allosteric manner. Integrin-bound cations may therefore act allosterically or play a direct role in ligand binding, as demonstrated in the α subunit I domain.

A displacement model has been proposed where ligands form a ternary complex with the integrin-bound cation. The cation is then displaced when the interactions between the ligand and integrin stabilise and the integrin undergoes a conformational change to its activated state (D'Souza *et al.*, 1994; Dickeson *et al.*, 1998). Cation occupancy of α5β1 leads to a conformational change in the integrin where the α and β subunits are seen to move apart, unmasking sites involved in ligand binding (Mould *et al.*, 1998b). Different cations have distinct effects on the conformation of the integrin.

Mn^{2+} and Mg^{2+} were both able to induce the conformational change necessary to expose ligand binding sites, although Mn^{2+} was more effective than Mg^{2+}. Ca^{2+} has been found to competitively displace Mg^{2+} and decrease ligand binding (Labadia *et al.*, 1998). It also appeared to cause a conformational change, but exposure of a β subunit activation epitope was found to be suppressed. Consequently, occupancy of the integrin by Ca^{2+} may allow the α subunit to adopt an active conformation while maintaining the β subunit in an inactive conformation. Again this would be consistent with the hypothesis of the β I domain allosterically regulating ligand binding.

An example of how cations can regulate integrins *in vivo* is maybe demonstrated in the adhesion of bone-resorbing osteoclasts. The osteoclast adheres to the bone surface mainly through αVβ3 (Ross *et al.*, 1993). As mineralised bone is resorbed, the concentration of Ca^{2+} beneath the osteoclast increases and induces osteoclast detachment and resorption is halted. The allosteric inhibitory Ca^{2+} site within the integrin may mediate this effect. Another example is during the initial healing process, when the levels of Mg^{2+} increase, elevating the Mg^{2+}/Ca^{2+} ratio in the plasma (Grzesiak & Pierschbacher, 1995). Since Mg^{2+} generally promotes integrin activation and Ca^{2+} inhibits, this ratio change may facilitate wound closure.

1.6 Study aims

An understanding of how integrins become activated and function is beginning to emerge. However, further work is needed to clarify all of the ligand binding sites within the integrin receptor and how these sites cooperate with one another. Two of the potential three integrin ligand binding sites were the subject of this research, namely the α subunit N-terminal repeats and the α subunit I domain.

As the structure of the extracellular segment of αVβ3 was only recently published, the structure of the α subunit N-terminal repeats was unknown at the time of this study, although two models had been proposed. Consequently, both models were investigated using all seven N-terminal repeats and the proposed EF-hand-like repeats from α4. The main aim of this research was to determine the true structural components of the ligand binding sites within the α subunit.

The crystal structure of the I domain from the αM subunit has been previously solved, making it a good candidate for further co-crystallisation studies with ligands. The objective of this study was to determine the crystal structure of an αM I domain-ligand complex. This would identify the structural determinants of the interacting surfaces and aid in the design of antagonists to the I domain. The structure would also reveal any conformational changes which occur upon ligand binding. A knowledge of ligand-induced conformational change within the whole integrin receptor will be necessary to understand allosteric control of integrin activation.

Chapter 2: The ligand binding α4 N-terminal repeats

2.1 Introduction

Ca^{2+} and ligand binding sites are present within the conserved seven N-terminal repeats of the integrin α subunits, as discussed in section 1.4.1.1. These repeats have been found to be particularly important for ligand binding by integrins that lack the α subunit I domain. At the time of designing and performing the experiments in this chapter, the structure of these binding sites was unknown. Based upon structural predictions, the N-terminal repeats had been alternatively modelled to form EF-hand-like motifs or a β-propeller. There was no direct structural data for either model, although data had been presented to support the competing models.

2.1.1 Two competing models for the ligand binding α subunit N-terminal repeats

The ligand binding regions of the N-terminal repeats were initially predicted to be EF-hand-like motifs, similar to those found in troponins, calmodulin and parvalbumin (Ikura, 1996). This putative calcium binding motif was present in repeat IV in some integrins and in repeats V, VI and VII in all integrins (Tuckwell *et al.*, 1992). The EF-hand motif is composed of 13 residues, with co-ordination to Ca^{2+} typically supplied by residues 1, 3, 5, 7 and 12 and by a solvent molecule hydrogen bonded to residue 9 (Strynadka & James, 1989). The integrin sequences differed from classical EF-hands due to the lack of a co-ordinating residue at position 12. This residue in integrins is typically a small hydrophobic residue, rather than the aspartate or

glutamate found in classical EF-hands. It was proposed that an acidic residue from the integrin ligand would provide the missing cation co-ordinating group, thus facilitating integrin-ligand binding (Tuckwell *et al.*, 1992). Other proteins with EF-hand-like sequences were also defective in position 12, as identified in the galactose-binding protein from *Escherichia coli* (Edwards *et al.*, 1988). This sequence was shown to bind Ca^{2+} with a distant glutamate completing the Ca^{2+} coordination sphere. Homology modelling of integrin EF-hand-like motifs, using the crystal structure of calmodulin as a template, revealed that the integrin sequences were able to retain cations (Tuckwell *et al.*, 1992). Repeats V and VI of αL, which contain calcium binding sites and a proposed ICAM-1 binding site were also modelled as adjacent EF-hand-like domains (Stanley *et al.*, 1994). Recombinant fragments of the putative EF-hand-like domains have demonstrated their Ca^{2+} and ligand binding functionalities. For example, a fragment containing the four EF-hand sites within the αIIb subunit was shown to bind its physiological ligand, fibrinogen, and contained two affinity sites for Ca^{2+}. (Gulino *et al.*, 1992). Also, a recombinant fragment containing repeats IV through VII of α5 was shown to adopt a fold with 30-35% α helix and 20-25% β strand, consistent with four EF-hands (Banères *et al.*, 1998). The binding of Mg^{2+} or Ca^{2+} to these repeats resulted in a biphasic rearrangement compatible with the existence of two classes of divalent cation-binding sites with different affinities located in two conformationally independent lobes. The data further showed that these cation binding EF-hand-like domains represented an essential component of the ligand binding site. All four EF-hands were required to bind an RGD-containing fibronectin ligand, even though each pair of EF-hands was able to bind divalent cation. A conformational change was observed upon ligand binding suggesting an induced fit process whereby both interacting components undergo adaptive conformational changes to afford the ligand-integrin complex.

The N-terminal repeats were alternatively predicted to fold into a β-propeller

domain composed of seven four-stranded β sheets arranged in a torus around a pseudosymmetry axis (Springer, 1997). Each blade of the propeller would contain four β-strands connected by loops of varying lengths. These loops would be tilted so that the connecting β-hairpin loops were either on the lower or upper surfaces of the propeller. The calcium binding motifs were predicted to be located on the lower surface loops of the β-propeller (Oxvig & Springer, 1998) with the ligand binding sites on the upper surface loops (Mould *et al.*, 1998a; Tozer *et al.*, 1999; Zhang *et al.*, 1999; Irie *et al.*, 1997; Muñoz *et al.*, 1997; Mould *et al.*, 2000). The interaction of α5β1 with fibronectin requires two recognition sequences within fibronectin which are located 3 to 4 nm apart (Leahy *et al.*, 1996). Consistent with the β-propeller model, loops containing epitopes that recognise these sequences were mapped about 3 nm apart on the upper face of the propeller (Burrows *et al.*, 1999). The β-propeller model places the Ca^{2+} and ligand binding sites on opposite faces of the domain and data has supported a regulatory role for Ca^{2+} rather than a direct role in ligand binding (Pujades *et al.*, 1997; Cao *et al.*, 1998; Oxvig & Springer, 1998; Mould *et al.*, 2000). Due to the differences between the sequence characteristics of classical EF-hand motifs and the calcium binding motifs of integrins as previously described, a novel calcium binding β-hairpin loop was proposed which would better resemble the calcium binding site of integrins and would be compatible with the β-propeller model (Springer, 2000).

Folding of the ligand binding α repeats into EF-hand-like motifs, as shown by the structures of EF-hand proteins such as parvalbumin and calmodulin (Ikura, 1996), would result in a predominantly α helical structure. This would be completely incompatible with the alternative model where a β-propeller fold encompassing all 7 N-terminal repeats, analogous to that of the G proteins (Wall *et al.*, 1995), would result in a ligand binding domain of only β-strand and coil. Another conflicting difference between the two models is the role that Ca^{2+} would play in ligand binding by the α subunit N-terminal repeats. The EF-hand model postulates that Ca^{2+} plays a direct role

in binding ligand with an acidic ligand residue completing the Ca^{2+} coordination sphere (Tuckwell *et al.*, 1992), whereas the Ca^{2+} in the β-propeller model would play a regulatory role.

2.1.2 Study aims

Elucidation of the tertiary organisation of these α repeats, in their free states and complexed to ligand, will be necessary to determine the true components of the α subunit which are responsible for ligand binding. The competing models were tested in this chapter using the N-terminal repeats from the α4 subunit.

Constructs were designed which coded for α4 repeats IV-V, VI-VII and IV-VII, encompassing all of the proposed EF-hand-like motifs and the predicted ligand binding motif within repeat IV (Irie *et al.*, 1997). These constructs were based upon the recombinant fragments containing the EF-hand-like motifs of α5, which had previously been expressed (Banères *et al.* 1998). In addition to the previously discussed functional and secondary structure data of the proposed α5 EF-hand-like domains, crystals of these domains were reported to diffract to high resolution (Parello *et al*, meeting abstract, 1997). This information in particular provided the impetus for studying the proposed EF-hand-like domains of α4. The aims of these studies were to produce soluble recombinant protein for α4 repeats IV-V, VI-VII and IV-VII and to determine their structures and ligand binding properties. Secondary structure elements would be characterised by circular dichroism spectroscopy and three-dimensional structures determined by x-ray crystallography. Ligand binding properties would be analysed by surface plasmon resonance using the α4 ligand, VCAM-1. Ultimately, the crystal structure of the α4 repeats bound to VCAM-1 would be sought.

To study the β-propeller model, recombinant protein encoding all seven repeats of α4 was used. The secondary structure elements would be assessed by circular dichroism studies and crystallisation trials set up in order to determine the structure.

The crystal structure of the extracellular fragment of αVβ3 (Xiong *et al.*, 2001), containing the structure of the α subunit N-terminal repeats, was solved during the preparation of this thesis manuscript. However, this chapter is written based upon the data and the models available when the work was in progress. Correlations will be made between the data presented and the recent αVβ3 structure.

2.2 Materials and methods

2.2.1 Materials

Restriction and modification enzymes were purchased from Promega (Southampton, U.K.) and used as per the manufacturers' instructions. All PCR reactions were carried out in a Perkin-Elmer thermal cycler (Perkin-Elmer, Beaconsfield, U.K.). Protein concentrations were calculated using the BCA protein assay reagent (Pierce, Rockford, IL). All other chemicals unless otherwise stated were purchased from Sigma (Poole, U.K.).

The α4 synthesised oligonucleotides were provided by Glaxo Wellcome, U.K. and the α4 repeats I-VII (residues 1-430) recombinant protein was provided by Dr. Y. Takada, Scripps Research Institute, La Jolla, U.S.A.

2.2.2 Cloning α4 N-terminal repeats IV-V, VI-VII and IV-VII

2.2.2.1 DNA preparation for the α4 repeats

DNA for α4 repeats IV-V (residues 215-305), VI-VII (residues 334-430) and IV-VII (residues 215-430) were generated from a series of synthesised oligonucleotides based on *Escherichia Coli* codons. The 'oligo-assembly' PCR reaction was carried out using *Taq* polymerase and *Pfu* polymerase in a PCR reaction mixture as per the

manufacturers' instructions. Three sequential PCR cycles were used to generate the α4 cDNA, as shown in figure 2.1. The first cycle used 100 µl of the PCR reaction mixture and 25 µl of the subsequent PCR product was diluted to 100 µl with PCR reaction buffer and used in cycle 2. 25 µl of the second PCR product was diluted to 100 µl with PCR reaction buffer and used in cycle 3. The final PCR products were purified on a QIAPrep spin column (Qiagen, Crawley, U.K.) and visualised on a 1.5% agarose gel stained with ethidium bromide.

Cycle 1	94°C	15s	× 40
	40°C	30s	
	72°C	10s + 1s/cycle	
Cycle 2	94°C	15s	× 25
	40°C	30s	
	72°C	45s + 1s/cycle	
Cycle 3	94°C	15s	× 20
	40°C	30s	
	72°C	70s + 1s/cycle	

Figure 2.1 PCR reactions for the 'oligo assembly'

The 'oligo-assembly' PCR product was used in a subsequent PCR to introduce *EcoRV* sites for cloning into pBluescript SK(-) (Stratagene, Amsterdam, The Netherlands) and *NdeI* and *BamHI* sites for subcloning into pET-15b (Novagen, Madison, WI). The primers used are shown in figure 2.2.

Forward primer for repeats VI-VII;

EcoR *NdeI*

5' TGA GAT ATC CAT ATG CGT TTC GGC GAA AGC ATC 3'

Forward primer for repeats IV-V and IV-VII;

5' TGA GAT ATC CAT ATG TGT TAC CTG GGC TAC TCC 3'

Reverse primer for repeats IV-V;

EcoRV *BamH* Stop

5' GCC CTA TAG GGA TCC TCA CGC TGG AAG AAG CGC CTA 3'

Reverse primer for repeats VI-VII and IV-VII;

5' GCC CTA TAG GGA TCC TCA AGT GCG CAG CAG AAC TGC 3'

Figure 2.2 Primers used to introduce restriction sites for cloning into pBluescript SK(-) and subcloning into pET-15b. As examples, the forward primer for repeats VI-VII and the reverse primer for repeats IV-V are labelled with the restriction sites to be incorporated.

Amplification was performed using *Taq* and *Pfu* polymerase and proceeded through a cycle of denaturation at 94°C (30 seconds), annealing at 65°C (30 seconds) for repeats IV-V and IV-VII and at 60°C for repeats IV-VII, and extension at 72°C (30 seconds) for a total of 35 cycles. The PCR products were purified on QIAprep spin columns (Qiagen) and visualised on a 1.5% agarose gel stained with ethidium bromide.

2.2.2.2 Cloning the α4 repeats into pBluescript SK(-)

The α4 repeats cDNA were first cloned into pBluescript SK(-) to ensure high DNA yields for DNA sequencing. The PCR products and pBluescript SK(-) were digested with *EcoRV* for 2 hours at 37°C. The digested vector was dephosphorylated with calf intestinal phosphatase, to prevent re-ligation, and once more purified. 15 μl ligation reactions were set up using T4 DNA ligase and 1:1, 1:3 and 1:5 molar ratios of vector to insert. A control with vector only was used and the reactions were allowed to proceed at room temperature overnight. The ligated mixtures were then transformed into competent *Escherichia Coli* DH5α cells (Novagen), along with a control of cells only and a control containing undigested vector, and plated onto X-gal plates. After a 37°C overnight incubation, colonies containing insert could be selected by their colour. The vector *lacZ* gene produces β-galactosidase, which utilises IPTG to cleave X-gal, forming a blue colony. DNA insertion into the vector disrupts the *lacZ* gene, preventing cleavage of X-gal, producing a white colony. After picking single colonies and isolating the plasmids using the Qiagen miniprep kit, *EcoRV* digestions were performed with each plasmid to analyse for insertion of the α4 repeat PCR products. The digested fragments were run out on a 1.5% agarose gel and potential positive clones were sent for DNA sequencing.

2.2.2.3 Sub-cloning the α4 repeats into pET-15b

pBluescript SK(-) containing the correct PCR products for the α4 repeats along with the pET15b vector were digested with *NdeI* and then *BamHI.* The digestion products were run out on a 1.3% agarose gel, extracted and purified with the QIAquick gel extraction kit (Qiagen). Ligation of the α4 repeat PCR product into pET-15b was

carried out, as previously described in section 2.2.2.2. The ligation products were then transformed into *Escherichia Coli* DH5α cells, plated onto LB plates and incubated at 37°C overnight. Colonies were picked and the plasmids were isolated using the QIAquick spin columns. An *EcoRV* digest was used to select for clones containing the correct size insert. After further screening by DNA sequencing, positive clones were transformed into *Escherichia Coli* BL21 (DE3) cells (Amersham Pharmacia Biotech, Chalfont, U.K.) for expression tests. PET-15b allows expression of the corresponding sequence fused to a His tag N-terminal segment that includes a hexahistinyl sequence and a thrombin cleavage site.

2.2.3 Expression of α4 repeats IV-V, VI-VII and IV-VII

25 ml 2 x YT media with 0.1 mg/ml ampicillin were innoculated with a single colony of *Escherichia Coli* BL21 (DE3) cells transformed with the recombinant pET-15b plasmids containing the α4 repeats, IV-V, VI-VII and IV-VII. After overnight growth at 37°C, the cells were diluted into 1 L of fresh 2 xYT/ampicillin media and grown to OD_{600} = 0.4-0.5 at 37°C. The culture was then induced with 0.3 mM IPTG and grown at either 37°C, 30°C or room temperature. Cells were harvested after 3 hours of induction by centrifugation at 7500 rpm, in a GS3 Sorvall rotor, for 20 minutes at 4°C. The cell pellets were resuspended in 0.1% Triton X-100, 1 mM DTT and 1 mM PMSF in binding buffer (500 mM NaCl, 5 mM imidazole, 20 mM Tris-HCl, pH 8.0) and stored at –80°C.

Cells were thawed at 37°C and lysed by sonication on ice with 5 second on/off pulses for 1 minute. The lysate was then centriuged for 1 hour at 18000 rpm in an SS34 Sorvall rotor at 4°C.

2.2.4 Refolding the α4 repeats

α4 repeats IV-VII, IV-V, and VI-VII were expressed in the insoluble fraction of the bacterial lysate and therefore refolding was necessary. Repeat V contained one cysteine so for all of the purification and refolding steps involving repeats IV-V and IV-VII, 1 mM DTT was added to the buffers to prevent the formation of intermolecular disulphide bonds.

Prior to refolding attempts, the pellets containing the insoluble protein were subject to the following wash steps with a 15 minute 18000 rpm centrifugation step (SS34 Sorvall rotor) after each wash;

1) 20 ml binding buffer

2) 20 ml binding buffer + 0.05% Triton X-100

3) 20 ml binding buffer

4) 20 ml H_2O

5) 20 ml binding buffer + 1 M urea

6) 20 ml binding buffer + 6 M urea

The resolubilised protein was centrifuged at 32000 rpm, in a Beckman 60Ti ultracentrifuge rotor, to remove existing aggregates that could act as nuclei to trigger aggregation during refolding. The protein was then purified on a 5 ml Ni^{2+} chelating column (Amersham Pharmacia Biotech). The column was first washed with 3 column volumes (CV) of H_2O, 5CV of 0.1 M $NiSO_4$ and 3CV of 6 M urea in binding buffer. The protein was filtered and loaded onto the column at a flow rate of 1 ml/min and the column was washed with 10CV 6 M urea in binding buffer and 6CV wash buffer (6 M

urea, 60 mM imidazole, 0.5 M NaCl, 20 mM Tris-HCl, pH 8.0). The protein was eluted with a 60 to 400 mM imidazole gradient in 6 M urea, 0.5 M NaCl, 20 mM Tris-HCl, pH 8.0 over 10CV at 2 ml/min. The Ni^{2+} chelating column was regenerated with 3 CV of strip buffer (100 mM EDTA, 0.5 M NaCl, 20 mM Tris-HCl, pH 8.0) and stored in 20% ethanol.

After purification, the protein was dialysed into 6 M urea, 0.5 M NaCl, 20 mM Tris pH 8.0 to remove imidazole. Various refolding strategies were used as summarised below.

2.2.4.1 Dilution

1 ml resolubilised protein at 1 mg/ml was rapidly added every 2 hours to 1 L of cold buffer (50 mM Tris-HCl, 0.5 M NaCl, pH 8.0) with constant stirring at 4°C. A total of 10 ml protein were diluted and left for 3 days to refold, with stirring at 4°C.

2.2.4.2 Dialysis

10 ml resolubilised protein was dialysed against 1 L 50 mM Tris-HCl , 0.5 M NaCl, pH 8.0, overnight at 4°C.

2.2.4.3 Affinity chromatography

Protein was added to a slurry of Ni^{2+}-NTA agarose (Amersham Biotech Pharmacia), pre-equilibriated with 6 M urea in binding buffer, to achieve a capacity of 0.5 mg protein/ml packed wet resin. The suspension was incubated at 4°C with gentle

rocking for 1 hour. The resin was then loaded onto an empty column and washed with 6 M urea in binding buffer. The refolding step was carried out using a linear gradient of 6 to 0 M urea in binding buffer at 1 ml/min. The protein was eluted with 400 mM imidazole, 0.5 M NaCl, 20 mM Tris-HCl, pH 8.0.

After each refolding experiment, the protein was concentrated in an Amicon ultrafiltration stirred cell with a YM3 membrane (Millipore, Watford, U.K.). In addition, various parameters were altered in all of the above protocols to optimise refolding. A large pH range, pH 4, 7 and 10, was used, and 10 mM $CaCl_2$, 550 mM arginine, 10% (v/v) glycerol and 1 M non-detergent sulphobetaine (NDSB)-201 (Calbiochem, La Jolla, CA) were tested as refolding additives.

2.2.5 Circular dichroism studies with α4 repeats I-VII

α4 repeats I-VII were diluted to 15 μM and dialysed into 20 mM Tris, 1 mM EDTA, 0.5 mM DTT, pH 7.0. EDTA and DTT were present to prevent the formation of aggregates (personal communication, Dr. Y. Takada). Data were collected with a Jasco-700 dichrograph using a 0.1 cm cell at 20°C. Five scans between 190 and 260 nm with a bandwidth of 1nm were averaged. In addition, the protein buffer was scanned and substrated from the sample spectra in SigmaPlot to eliminate any background signals produced by the buffer. Molar ellipicities, [Θ], are given in degrees $\cdot$ cm^2 per dmol of mean amino acid residue. A mean residue weight of 109 was used.

The secondary structure average content from the α4 repeats I-VII was estimated from the circular dichroism (CD) spectra by two methods. Using the convex constraint analysis (CCA) (Perczel *et al.*, 1991; Perczel *et al.*, 1992a), the CD spectra between 195 and 240 nm were deconvoluted in 5 singular pure components by the

simultaneous analysis of 25 proteins plus the α4 repeats I-VII. The pure components obtained were assigned to 5 secondary structure components: α helix, antiparallel β sheet, β turn and/or parallel β sheet, chiral and disordered as described in Perczel *et al.*, 1992a. Alternatively, the α4 repeats I-VII CD spectrum was analysed as a linear combination of the 5-reference curve set obtained by the convex constraint analysis of the 25 reference spectra, employing the program LINCOMB (Perczel *et al.*, 1992b). Spectra were generated from the analysis with CCA and LINCOMB and overlayed with the experimental specta to assess the quality of fit.

To assess the accuracy of this technique, the secondary structure average content was estimated for the αM I domain, a protein of known structure, using the same analysis.

2.2.6 Electron microscopy studies of α4 repeats I-VII

α4 repeats I-VII were diluted to 10 μM in 50 mM Tris, 1 mM EDTA, 1 mM DTT, pH 7.0. Samples were prepared for viewing under the electron microscope by two techniques: negative staining and metal shadowing.

For negative staining, the protein sample was adsorbed onto a carbon-coated grid. After vapour fixation over glutaraldehyde for 2 minutes and washing with distilled water, a droplet of 1% (w/w) uranyl acetate solution was applied. Excess uranyl acetate was removed and the sample was left to dry. For metal shadowing, 50% (v/v) glycerol was added to the protein solution and sprayed onto freshly cleaved mica. The samples were placed in a high vacuum coating unit directly beneath the carbon evaporation source and at a distance of 130 mm and an angle of 5° from the platinum evapouration source. The unit was then evacuated to a pressure of 1×10^{-6} torr and samples were left

to dry. Samples were shadowed by evaporation of the platinum source and then carbon-backed by evaporation of the carbon source. After carbon-backing, the vacuum was released and replicas were floated onto a distilled water surface and lifted onto the surface of copper electron microscope grids. Electron micrographs were recorded by a Jeol 100 CX operated at 120 kV at a magnification of 60000.

2.2.7 Crystallisation trials

The α4 repeats I-VII were dialysed into 20 mM Tris-HCl, 150 mM NaCl, 1 mM EDTA, 1 mM DTT, pH 8.0 and concentrated in an Amicon ultrafiltration stirred cell using a YM10 membrane (Millipore) to 8 mg/ml. Crystallisation trials of the α4 repeats I-VII were set up using the commercial screens I and II (Hampton, Laguna Niguel, CA), Wizard I and II and Cryo I and II (Emerald Biostructures, Bainbridge Island, WA) at room temperature and 4°C. All trials were set up using vapour diffusion with sitting drop strips (Hampton). 100 µl of mother liquor was placed in the reservoir and 1 µl mother liquor was added to 1 µl protein in the drop.

2.3 Results

2.3.1 Expression of α4 repeats IV-V, VI-VII and IV-VII

Repeats IV-V, VI-VII and IV-VII of α4 were all expressed in the insoluble fraction of the bacterial lysate at 37°C, 30°C and room temperature. As an example, the soluble and insoluble fractions of α4 repeats IV-VII after lysis are shown in figure 2.3.

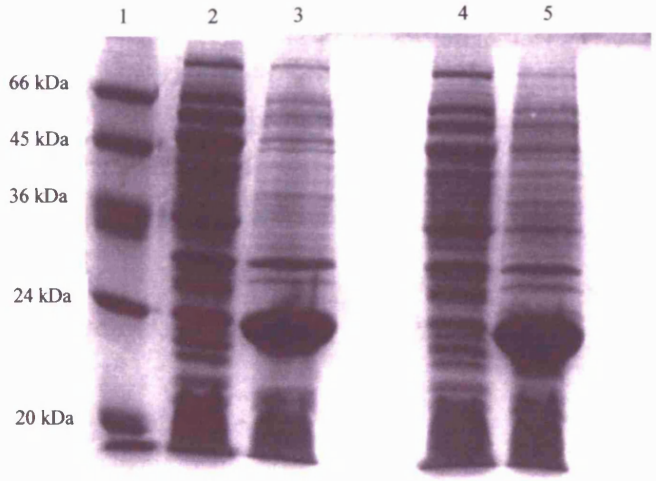

Figure 2.3 15% SDS PAGE gel of α4 repeats IV-VII expression at 37°C (lanes 2 and 3) and room temperature (lanes 4 and 5). Lane 1 shows the molecular weight markers, lanes 2 and 4 the soluble fractions after cell lysis and lanes 3 and 5 the insoluble fractions after lysis. α4 repeats IV-VII are 23 kDa.

2.3.2 Purification and refolding of α4 repeats IV-V, VI-VII and IV-VII

Figure 2.4 shows the α4 repeats purification procedure after re-solubilisation, using α4 repeats VI-VII as an example.

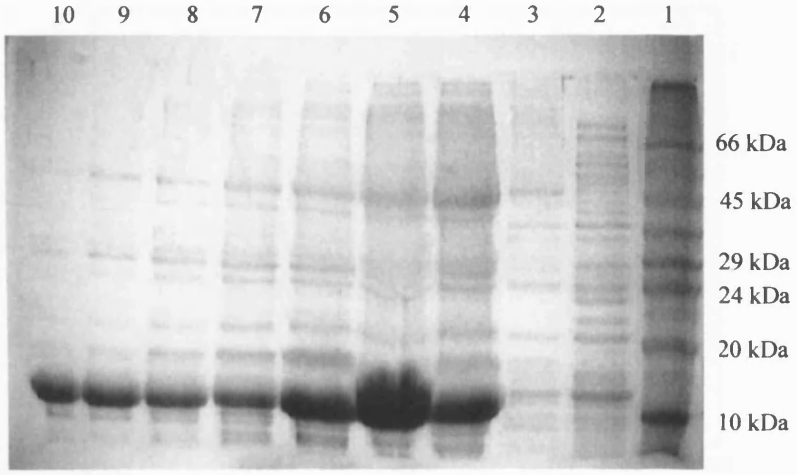

Figure 2.4 15% SDS PAGE gel of α4 repeats VI-VII purification (Ni^{2+} affinity column). Lane 1 -molecular weight markers, lane 2 -flow through from the column, lane 3 -flow through from the column wash with wash buffer, lanes 4-7 -fractions collected from elution with 250-400 mM imidazole in binding buffer + 6 M urea. α4 repeats VI-VII are 12 kDa.

Refolding experiments were not successful due to precipitation of >90% of the protein upon removal of the denaturant. Addition of 10 mM $CaCl_2$ and 550 mM arginine using the dilution method at pH 8.0 decreased the amount of precipitation but insufficient soluble protein was produced for further analysis.

2.3.3 Circular dichroism studies of the α4 repeats I-VII

The CD spectrum of the α4 repeats I-VII is shown in figure 2.5. The analysis of the secondary structure contents with CCA and LINCOMB is presented in table 2.1. Figures 2.6 and 2.7 show the superimposed spectra of the experimental data and the model spectrums generated with the CD analysis method CCA and LINCOMB respectively.

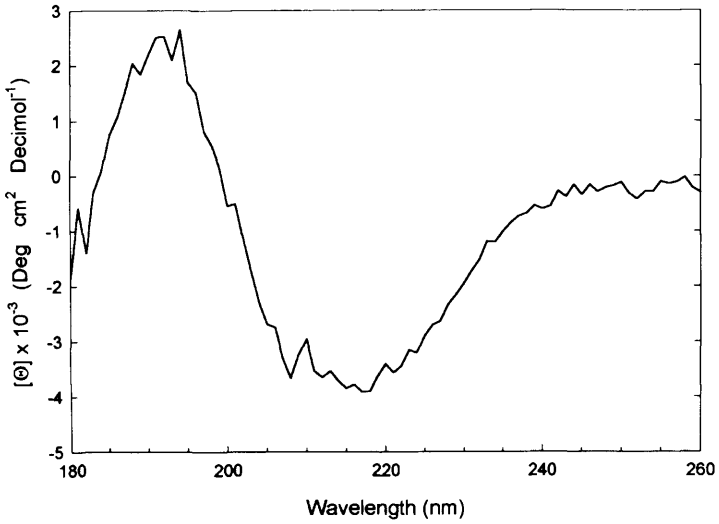

Figure 2.5 Circular dichroism spectrum of the α4 repeats I-VII. The spectrum shows the actual unsmoothed average of the five scans which has been blanked against buffer.

a)

	α-helix (%)	Antiparallel β-sheet (%)	β-turn and/or parallel β-sheet (%)	Chiral (%)	Random coil (%)
CCA	11	36	5	15	33

b)

	α-helix (%)	Antiparallel β-sheet (%)	β-turn and/or parallel β-sheet (%)	Aromatic and disulphide contribution (%)	Random coil (%)
LINCOMB	5	28	0	31	36

Table 2.1 Secondary structure content of the α4 repeats I-VII as estimated by circular dichroism analysis by CCA (a) and LINCOMB (b)

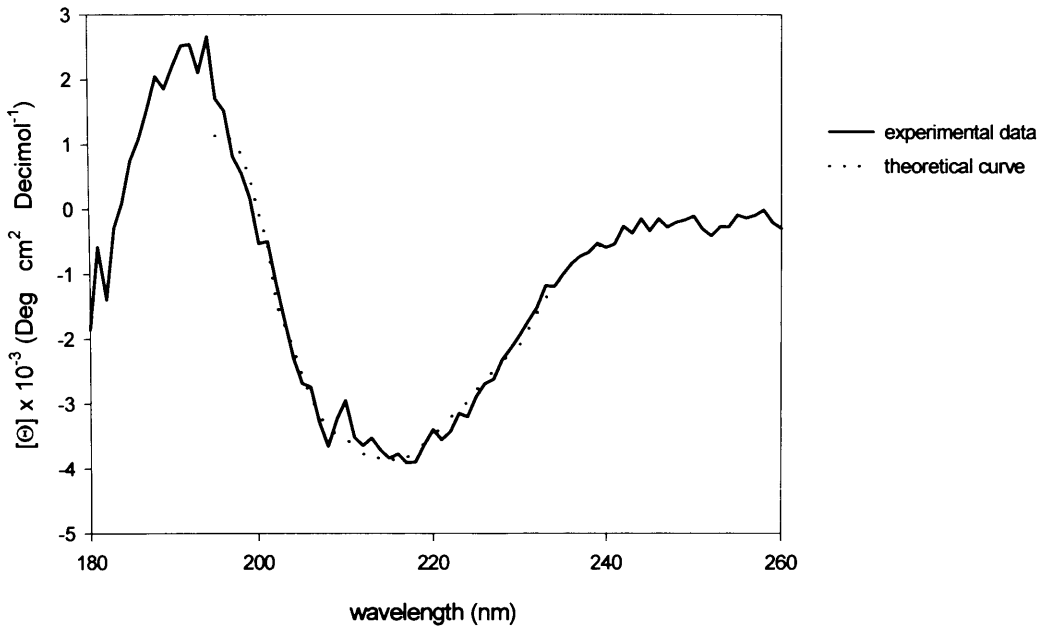

Figure 2.6 Circular dichroism spectrum of the experimental data of the α4 repeats I-VII overlayed with the model spectrum (dashed line) generated with the CD analysis method CCA.

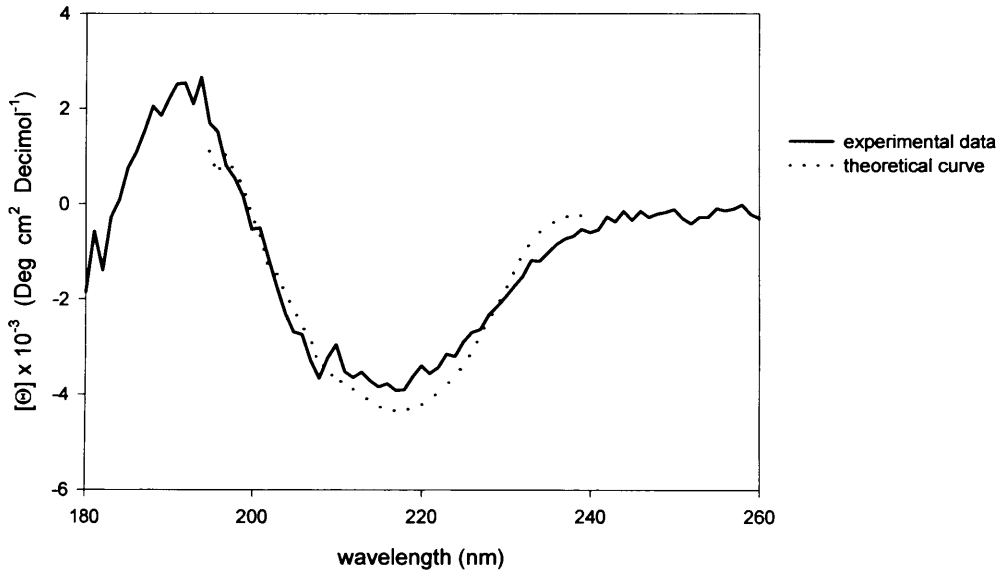

Figure 2.7 Circular dichroism spectrum of the experimental data of the α4 repeats I-VII overlayed with the model spectrum (dashed line) generated with the CD analysis method LINCOMB.

2.3.4 Electron microscopy of α4 repeats I-VII

Electron micrographs from the α4 repeats I-VII are shown in figure 2.8.

a)

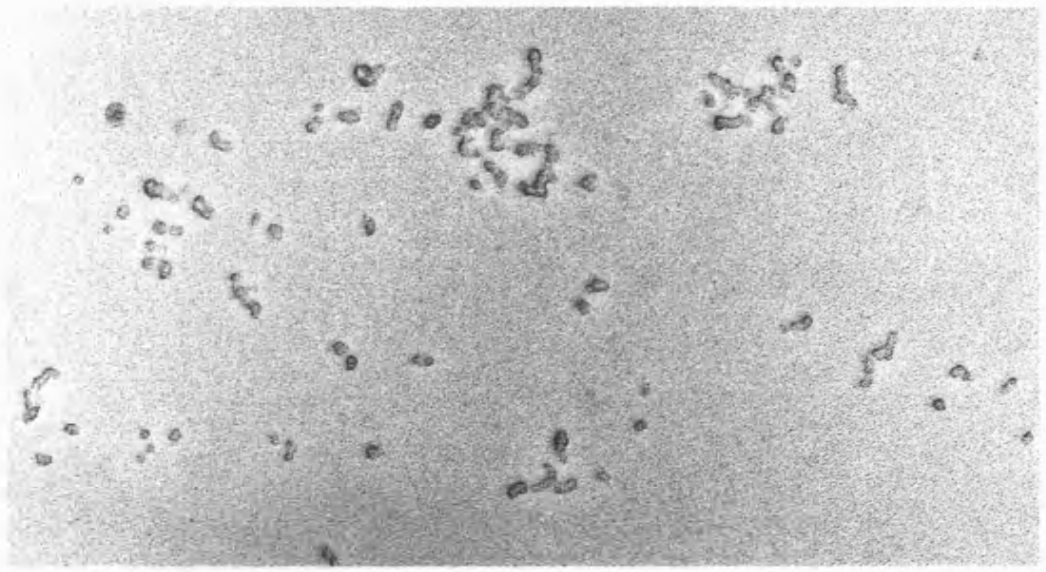

b)

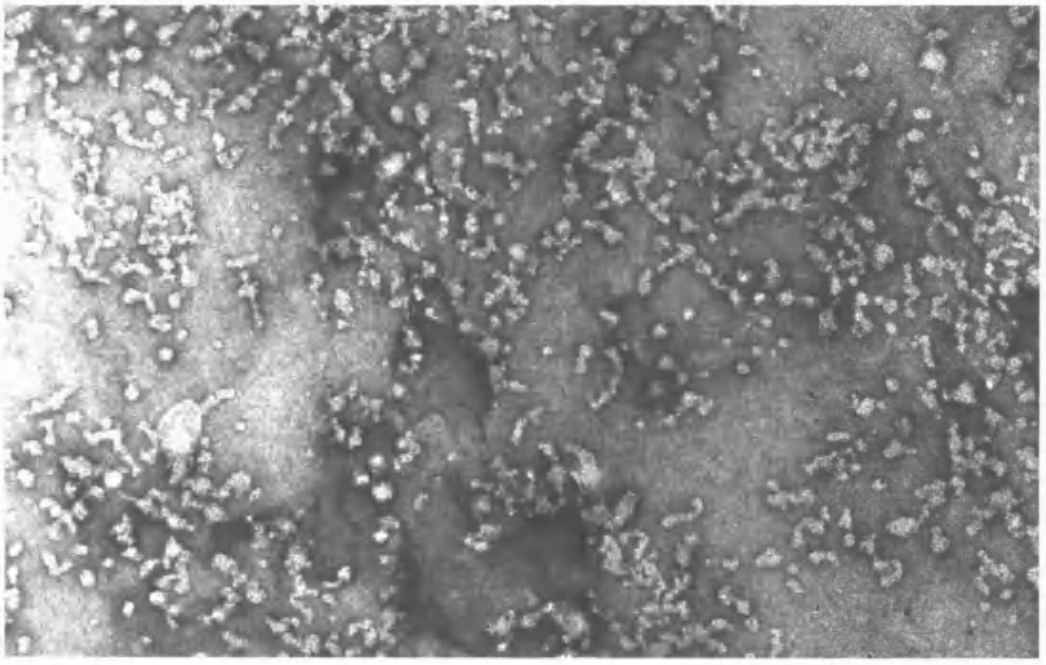

Figure 2.8 Electron micrographs of α4 repeats I-VII (60000 × magnification). (a) was prepared by metal shadowing and (b) by negative stain.

2.3.5 Crystallisation trials of α4 repeats I-VII

Crystals did not grow from the crystallisation trials with the α4 repeats I-VII.

2.4 Discussion

The α4 repeats IV-V, VI-VII and IV-VII were expressed in the insoluble fraction of the bacterial lysate and refolding protocols were unsuccessful. This was an unexpected result as the analogous α5 repeats, which displayed good sequence similarity to the α4 repeats with 36% sequence identity and 54% overall sequence homology, were also expressed in the insoluble fraction but refolded protein was produced with ligand binding activity and a well defined structural composition compatible with EF-hand-like motifs (Banères *et al.*, 1998). However, this negative result does not prove conclusively that the α4 repeats cannot be refolded correctly.

In comparison, the results from the α4 repeats I-VII were more promising, correlating with the proposed β-propeller model. The monomeric nature of the α4 repeats I-VII (personal communication, Dr. Y. Takada) and the presence of secondary structure elements, as demonstrated by CD analysis, suggested that the protein had a folded structure. The model spectra generated from CCA and LINCOMB analysis showed good correlation to the experimental CD spectra. Both analyses were in agreement showing the major contributing secondary structure element to be antiparallel β-sheet with little α-helix. Based on the α4 β-propeller model (Springer, 1997), 38% of the residues would contribute to the four stranded antiparallel β-sheet that form each blade of the propeller. The remainder of the protein is likely to predominantly adopt loop structures. The recent αVβ3 crystal structure shows the αV N-terminal repeats to adopt a β-propeller structure with 32% antiparallel β-strand and 3% α-helix. The CD data presented here correlated well with the secondary structure elements of the β-propeller with the averaged estimation from CCA and LINCOMB assigning a 32% contribution to antiparallel β-sheet and an 8% contribution to α-helix. The electron micrographs of α4 repeats I-VII show ring-like structures, a proportion of which appear

to have aggregated on the surface of the grid. This aggregation was likely to be an artifact of the EM procedure. Due to this problem, EM reconstruction could not be pursued to determine a low resolution structure of the repeats. However, the shape of the single species shown in the EM images did appear to correlate with the circular structure of the proposed β-propeller domain.

The recent publication of the αVβ3 extracellular segment structure (Xiong *et al.*, 2001) has revealed that the α subunit N-terminal repeats fold into a β-propeller structure, as discussed in section 1.4.1.2. The data from α4 repeats I-VII demonstrated that the domain had defined secondary structure, compatible with that of the β-propeller therefore correlating with the new αVβ3 structure. The requirement for a mechanism of ring closure in all known β-propeller domains and the use of the central hole in the domain to coordinate ligand or facilitate catalytic function in most propeller proteins (Fulop & Jones, 1999) suggests that folding of all the blades into the propeller structure is needed to form the structurally stable and functionally competent domain. The αVβ3 structure may explain the inability of the α4 repeats IV-V, VI-VII and IV-VII to form soluble fragments, as it would be most unlikely for part of the propeller to refold in the absence of the complete structure.

The ability of the α subunit β-propeller structure to fold independently of the β subunit has been questioned. Studies with monoclonal antibodies have shown that folding of specific domains requires association of the α and β subunits. The structure of the β subunit I domain has been shown to be dependent on the association with the αL subunit (Huang *et al.*, 1997a). The αL I domain was shown to fold independently of the putative α subunit β-propeller domain and the β subunit (Huang & Springer, 1997b). This is consistent with the fact that the αL I domain can be expressed and crystallised as an isolated domain (Qu & Leahy, 1995). In the same study, other results suggested that folding of the β-propeller domain was not completed until after association with the β subunit (Huang & Springer, 1997b). Another study with αMβ2

also demonstrated that the folding of the β-propeller is dependent on the association with the β2 subunit (Lu *et al.*, 1998). Similarly, the folding of the G protein β subunit β-propeller requires association with the G protein γ subunit (Garcia-Higuera *et al.*, 1996). However, the authors also demonstrate that unlike the G protein, the β-propeller domains from several other proteins were able to fold into globular domains without the aid of accessory subunits. Although the structure of the recombinant α4 repeats I-VII was not determined, the data presented here provide some evidence that the integrin α subunit β-propeller may be recombinantly produced. However, further studies with the α4 repeats I-VII were not pursued as the recombinant protein did not bind ligand (personal communication, Dr. Y. Takada). In addition, protein was not available to set up further crystallisation trials.

The identification of the β-propeller domain within the αVβ3 structure puts into the question the results of Banères *et al.* (1998), which were the basis for a large proportion of the work presented in this chapter. How could Banères *et al.* have produced soluble, functional fragments of the β-propeller domain with a 30-35% α helical content when the β-propeller domain is comprised of only anti-parallel β sheet and loop structures? In addition, conflicting results have been published subsequent to that of Banères *et al.*, which indicate that the α5 repeats IV-VII, which Banères *et al.* (1998) reported to bind ligand, do not confer ligand recognition. These results demonstrated that α5 repeats I-III provide ligand binding specificity to α5β1 with the ligand binding sites located in the upper surface loops of the β-propeller domain (Burrows *et al.*, 1999; Mould *et al.*, 2000). The proposal of Ca^{2+} providing a bridge between the proposed EF-hand-like domain and ligand and consequently facilitating binding can also be questioned as it has been established that Ca^{2+} plays an inhibitory role in integrin-ligand binding as discussed in section 1.5.3. In addition, an antibody to αMβ2, which recognises loops containing the proposed EF-hand-like motifs, binds only in the presence of Ca^{2+} and does not block ligand binding (Oxvig & Springer, 1998).

This result also conflicts with that of Banères *et al.* (1998) and Gulino *et al.* (1992) as their data demonstrated that the recombinantly expressed repeats containing the EF-hand-like motifs from α5 and αIIb would only support binding when all Ca^{2+} binding sites were fully occupied.

In conclusion, it is now clear the α subunit N-terminal repeats form a β-propeller structure rather than EF-hand-like domains. A structure of the ligand binding extracellular domains of the integrin in complex with a physiological ligand will be required to understand the quaternary mechanisms of integrin-ligand recognition and allosteric activation.

Chapter 3: Ligand binding and crystallisation of the αM I domain

3.1 Introduction

The α subunit I domain of integrins is an important region for ligand recognition and integrin activation. As previously discussed, the structure of the I domain from αMβ2 (CD11b/CD18, complement receptor type 3, Mac-1) has been determined in the open and closed states, thus making it a good candidate for co-crystallisation studies.

αMβ2 is expressed mainly on cells of myeloid lineage and plays an important role in the firm adhesion of leukocytes to the endothelium and their migration to sites of inflammation (Anderson *et al.*, 1989; Smith *et al.*, 1989), phagocytosis of infectious agents and the oxidative burst (Beller *et al.*, 1982) and activation of neutrophils and monocytes (Shappell *et al.*, 1990). αMβ2 also controls apoptosis of neutrophils (Coxon *et al.*, 1996). One of the defining characteristics of integrins is the capacity of its family members to bind multiple ligands. αMβ2 is no exception to this and recognises a wide range of ligands, as shown in table 1.1. Ligands include fibrinogen (Wright *et al.*, 1988), ICAM-1 (Diamond *et al.*, 1990), the blood-clotting factor X (Alteri & Edgington, 1988), the complement fragment iC3b (Ueda *et al.*, 1994), the hookworm neutrophil inhibitory factor (NIF) (Zhang & Plow, 1997) and denatured proteins (Davis, 1992). Binding of many of these ligands has been mapped to the αM I domain and many of their interactions shown to be divalent cation-dependent involving the MIDAS (Michishita *et al.*, 1993; Rieu *et al.*, 1994; Zhou *et al.*, 1994; Kamata *et al.*, 1995; Zhang

& Plow, 1996). αMβ2 ligands bind to overlapping, but not identical sites, within the I domain (Diamond *et al.*, 1993; Rieu *et al.*, 1996; Zhang & Plow, 1996; Zhang & Plow, 1999). The same short structural segments within the I domain may be involved in binding, but key residues may contact different ligands. The recognition sites for iC3b and NIF within αMβ2 I domain have been mapped to loop regions surrounding the MIDAS, as well as to helix 5 which is positioned on the side of the domain (Zhang & Plow, 1997; Zhang & Plow, 1999). Helix 5 of the I domain and a segment of the loop between helix 5 and β-strand D have been mapped as the binding interface for a fibrinogen peptide (Yakubenko *et al.*, 2001). There are few data describing the interaction sites for ICAM-1 and factor X and no direct evidence for the exact nature of any ligand interactions with αMβ2.

The αM I domain ligands which were used in this study shall be discussed below.

3.1.1 Intercellular cell adhesion molecule –1 (ICAM-1)

ICAM-1 is a glycosylated 90 kD cell surface transmembrane protein basally expressed on cells important in immune responses. Inflammatory mediators, bacterial antigens and cytokines further increase expression on these cells and induce expression on other cell types, such as endothelial, epithelial and fibroblastic cells (Springer, 1994). Increased ICAM-1 expression enhances leukocyte accumulation and leukocyte adhesion functions in immune and inflammatory responses (Hubbard & Rothlein, 2000).

ICAM-1 consists of a large extracellular domain with five tandem immunoglobulin (Ig)-like domains (D1-D5), a short transmembrane domain and a small carboxyl terminus cytoplasmic tail. Unlike many integrin ligands, ICAM-1 does not

contain an Arg-Gly-Asp (RGD) motif, but a larger more extended binding surface. Cation-dependent adhesion of ICAM-1 and αMβ2 is primarily between D3 and the I domain respectively (Diamond *et al.*, 1991; Diamond *et al.*, 1993; Zhou *et al.*, 1994; Feng *et al.*, 1998). Mutation of αM I domain MIDAS residues disrupts binding to ICAM-1 (Kamata *et al.*, 1995; McGuire & Bajt, 1995; Li *et al.*, 1998). Recently, a bicyclic nonapeptide based on a peptide sequence from D1 has been shown to bind to the isolated αM I domain in a cation-dependent manner (Koivunen *et al.*, 2001). Interestingly, this peptide does not contain an acidic residue, which is thought to be necessary for ligand binding to the I domain.

The exact nature of the interaction between the αM I domain and ICAM-1 is unknown. By comparison, more evidence is available for the interaction of ICAM-1 and the αL I domain, which is structurally very similar to αM I domain. The residues involved in αL I domain recognition have been mapped to a different Ig-like domain, D1, of ICAM-1 (Staunton *et al.*, 1990; Fisher *et al.*, 1997; Stanley & Hogg, 1998). Like the αMβ2-ICAM-1 interaction, the recognition site for ICAM-1 within αLβ2 has been located to MIDAS residues within the I domain (Huang & Springer, 1995; Edwards *et al.*, 1998). Crystal structures have been determined for D1 and D2 of ICAM-1 (Cassasnovas *et al.*, 1998; Bella *et al.*, 1998) revealing two tandem Ig-superfamily domains with a putative binding dimerisation interface on D1.

ICAM-1 exists predominantly on the cell surface as a dimer (Reilly *et al.*, 1995) and this dimerisation provides two ligand binding sites for αLβ2 (Jun *et al.*, 2001b). The binding site for αMβ2 in domain 3 of ICAM-1 is predicted to be on the same face of ICAM-1 as that for αLβ2 (Jun *et al.*, 2001a). Dimerisation of ICAM-1 would therefore leave both αMβ2 sites well exposed.

Mutational data and ultimately a structure of the complex between αMβ2 and ICAM-1 will be necessary to understand their interactions. Although D3 has been

identified as the primary binding site on ICAM-1, other Ig-like domains may play additional roles by maintaining the structural integrity of the ligand binding site in D3 as has been proposed for ICAM-1 binding to αLβ2 (Stanley *et al.*, 2000).

3.1.2 Fibrinogen

Fibrinogen is a 340 kDa glycoprotein found in the blood plasma of all vertebrates. It is composed of three pairs of homologous but nonidentical polypeptide chains ($\alpha_2\beta_2\gamma_2$) (Doolittle *et al.*,1998). It forms a triglobular structure with each of the two N-terminal globular domains containing the αβγ chains and a smaller central domain where all six N-termini are gathered together. The three-stranded connectors between domains can be broken by proteases generating two principle core fragments, D and E. Fragment E corresponds to the central domain and fragment D corresponds to the two terminal globules.

Fibrinogen is a ligand for αMβ2 (Altieri *et al.*, 1990) and engagement of fibrinogen by αMβ2 on leukocytes may play a role in mediating adhesion of leukocytes to the blood vessel wall (Sriramarao *et al.*, 1996) and facilitating their transendothelial migration (Languino *et al.*, 1995). The binding of deposited fibrinogen to αMβ2 is also thought to mediate leukocyte adhesion at extravascular sites of inflammation (Wu *et al.*, 1994). Engagement of αMβ2 with fibrinogen induces a series of intracellular signalling events and cellular responses, which are relevant to the inflammatory response including cytokine secretion and nuclear factor κB activation (Perez & Roman, 1995; Sitrin *et al.*, 1998)

The I domain from αMβ2 has been identified as the major recognition site for fibrinogen (Diamond *et al.*, 1993; Zhou *et al.*, 1994) and deletion of the I domain from

αMβ2 completely inhibits binding to fibrinogen (Yalamanchili *et al.*, 2000). The αMβ2 binding site has been localised to the γ-module of fragment D from fibrinogen (Altieri *et al.*, 1990). Two peptides, P1 (Altieri *et al.*, 1993) and P2 (Ugarova *et al.*, 1998) duplicating residues 190-202 and 377-395 respectively, from the γ chain of fibrinogen have been shown to competitively inhibit fibrinogen-dependent leukocyte adhesion events. Immobilised P1 and P2 supported efficient adhesion of αMβ2 expressing cells and both peptides specifically bound the αMβ2 I domain. There is conflicting evidence regarding the potency of P1. Binding of fibrinogen to the αM I domain was shown to be entirely recapitulated by P1 (Altieri *et al.*, 1993) but Zhou *et al.* (1994) have reported the affinity of P1 for αMβ2 to be substantially lower than that of intact fibrinogen. Also, P2 was found to be more potent than P1 in inhibiting adhesion of αMβ2-expressing cells to fragment D of fibrinogen (Ugarova *et al.*, 1998). The crystal structure of the fibrinogen γ chain has been determined (Yee *et al.*, 1996) and residues 190-202 and 377-395 (P1 and P2 respectively) reside in close proximity forming two anti-parallel β strands. It is hypothesised that the juxtapositioning of these two sequences may form the binding site for αMβ2 (Ugarova *et al.*, 1998).

Different studies identify the binding site for fibrinogen within the I domain to be located in different regions. The epitope for the monoclonal antibody CBRM1/5, which blocks the αMβ2-mediated adhesion to fibrinogen, has been mapped to a segment of helix 1 and the loop between the helix 3 and 4 of the I domain (Oxvig & Springer, 1999). The epitope for the monoclonal antibody 7E3, which also recognises the open αM I domain and blocks fibrinogen binding, has been mapped to the first β-strand and part of helix 1 (Plescia *et al.*, 1998). Mutagenesis studies suggest that the binding pocket for fibrinogen may include helix 6 and the MIDAS (Zhang & Plow, 1996). In addition, the binding site for part of the fibrinogen peptide, P2, has been localised to helix 5 and the loop preceding it within the αM I domain (Yakubenko *et al.*, 2001).

3.1.3 Factor X

αMβ2 adhesion to factor X can trigger monocyte degranulation and activation of factor X, leading to rapid fibrin formation (Plescia & Altieri, 1996). Three spatially distant surface loops in the catalytic domain of the coagulation factor X were found to mediate its interaction with αMβ2 (Altieri *et al.*, 1991). Unlike most αMβ2 ligands, binding to factor X is only partially mediated by the I domain (Zhou *et al.*, 1994; Yalamanchili *et al.*, 2000). A factor X peptide, duplicating residues 238 to 246, has been shown to block ligand binding to αMβ2 and prevent monocyte procoagulant activity (Mesri *et al.*, 1998). The peptide bound specifically to isolated αM I domain and inhibited cell attachment to ICAM-1 transfectants. It was suggested that the Factor X peptide defines an ICAM-1 binding site within the αM I domain and hypothesised that engagement of this site induces a conformational change in the receptor which disrupts a distant factor X binding site required for monocyte procoagulation activity.

3.1.4 Other peptides

The I domain MIDAS mediates ligand binding with an acidic residue from the ligand completing the coordination sphere of the metal. Direct evidence for this can be seen in the α2 I domain:collagen complex, where a glutamate from the collagen binds the metal directly through the MIDAS (Emsley *et al.*, 2000). In addition, the open form of the αM I domain was crystallised with a glutamate coordinating the metal at the MIDAS motif (Lee *et al.*, 1995a),

Peptides were used in co-crystallisation trials with αM I domain that would

potentially present an acidic residue to the MIDAS of the I domain. These peptides included RGD, RGEV and hydroxamic derivatives of the acidic residues in RGDV and RGEV, RGD(HA)V and RGE(HA)V, respectively.

3.1.5 Study aims

A three-dimensional structure of the αM I domain in complex with a ligand would demonstrate the conformational changes which occur upon ligand binding. If these were similar to the predicted changes for the αM I domain (Lee *et al.*, 1995a) and those occuring upon collagen binding to the α2 I domain (Emsley *et al.*, 2000), would this shape-shifting be a common mechanism for I domain-ligand recognition? The molecular mechanisms by which the αMβ2 I domain can interact with so many structurally unrelated ligands, and yet exhibit high affinity for each, is unknown. An αM I domain-ligand complex would provide an understanding of the structural and functional organisation of the I domain binding sites. The ligands, ICAM-1 and fragment D from fibrinogen, were the main focus of this study due to the lack of knowledge or clarity about their interactions with the αM I domain. As previously discussed, very little information is available about the adhesion of ICAM-1 to the αM I domain and different studies have identified various regions of the I domain to be involved in fibrinogen recognition.

The αM I domain has been shown to recapitulate many of the ligand binding properties of the intact αMβ2 integrin (Michishita *et al.*, 1993; Zhou *et al.*; Yalamanchili *et al.*, 2001). Determination of the structural elements involved in the αM I domain-ligand complex would therefore aid the design of antagonists to counter the harmful effects of αMβ2 in disease states. For example, sustained inflammation, reperfusion of ischemic tissue or sepsis, causes the excessive activation of αMβ2 and

subsequent inappropriately large mobilisation of phagocytic cells which is thought to contribute to tissue damage (von Asmuth *et al.*, 1991). Interruption of such neutrophil extravasation or the oxidative burst may be a means of damage control in such situations. The use of blocking antibodies directed towards ICAM-1 has been found to modulate autoimmune diseases, such as rheumatoid arthritis, and facilitate organ transplantation (Cosimi *et al.*, 1990; Isobe *et al.*, 1992; Kavanaugh *et al.*, 1994). Small molecule inhibitors, could also be designed based upon the structure of an αM I domain-ligand complex, to antagonise various disease states .

The experimental approach taken to solving the I domain-ligand complex would first test the functionality of the αM I domain and its ligands, sICAM-1 and fragment D, by surface plasmon resonance studies. This technique would also be used to determine the optimal binding conditions for the interaction of the I domain with sICAM-1 and fragment D. The I domain-ligand complex would then be isolated by size exclusion chromatography prior to co-crystallisation. Binding of peptides, listed in section 3.2, to the I domain may result in a conformation change so the peptides would first be co-crystallised with the I domain. Co-crystallisation trials would also be set up with a E314R αM I domain mutant. This mutation would remove the residue that makes the crystal contact at the MIDAS in crystals with the open conformation, thus preventing formation of this crystal form.

3.2 Materials and methods

All chemicals used in this chapter and chapter 4, unless otherwise stated, were purchased from Sigma (St. Louis, MI). Protein concentrations were calculated using the BCA protein assay reagent (Pierce, Rockford, IL). Restriction and modification enzymes were purchased from New England Biolabs (Beverley, MA) and used as per the manufactors' instructions. All PCR reactions were carried out in a Perkin-Elmer thermal cycler and all chromatography columns and FPLC units were purchased from Amersham Pharmacia Biotech (Piscataway, NJ). The recombinant αM I domain encoding residues G111-I319 cloned into a pGEX-2T vector, with an additional C-terminal vector sequence, GSPGIHRD, was provided by Glaxo Wellcome, U.K.

The following Mac-1 I domain ligands were used;

Factor X peptide (L^{238}YQAKRFKV^{246}) (Mesri *et al.*, 1998) (synthesised by GlaxoWellcome, U.K.)

Fibrinogen peptides P1 (G^{190}WTVFQKRLDGSV^{202}) (Altieri *et al.*, 1993) and P2 (Y^{377}SMKKTTMKIIPFNRLTIG^{395}) (Ugarova *et al.*, 1998) (synthesised by GlaxoWellcome, U.K.)

Five immunoglobulin domain (D1-D5) fusion of human ICAM-1 encoding residues 28-480, termed soluble ICAM-1 (sICAM-1), with a protein A conjugate ZZ tag, (provided by Glaxo Wellcome, U.K.)

Fibrinogen and fragment D from fibrinogen (a gift from Dr. R. Doolittle, University of California, San Diego)

RGD, RGEV (Sigma) and hydroxamic acid derivitives of RGD (RGD(HA)V) and RGEV (RGE(HA)V) (provided by Dr. J. Smith, The Burnham Institute, La Jolla)

3.2.1 Site-directed mutagenesis

Two complementary oligonucleotide primers both containing the desired codon change were used. *Pfu* DNA polymerase was used to extend and incorporate these oligos during temperature cycling to generate the mutated plasmid with nicked staggers. 50 µl PCR reactions were set up with *Pfu* DNA polymerase buffer as per the manufacturers instructions. The reactions were held at 95°C for 30 seconds, followed by 1 minute at 55°C and 6 minutes at 68°C for a total of 16 cycles. This PCR product was purified using a QIAprep spin column (Qiagen, Valencia, CA) and digested with *DpnI*, an endonuclease (target sequence 5' – $G^{m6}ATC$-3') specific for methylated and hemimethylated DNA, to digest the parental DNA. The digestion product was again purified and transformed into *Escherichia Coli* BL21(DE3) cells (Amersham Pharmacia Biotech, Piscataway, MI). Transformants were selected on LB plates plus 100 µg/ml ampicillin and grown overnight in 5 ml LB plus 100 µg/ml ampicillin. DNA was purified on QIAquick spin columns (Qiagen) and analysed by automated DNA sequencing. The following primers (synthesised by Genbase, San Diego, CA) were used:

E314R (forward) 5' AAC CAG CTT CGG AGG AAG ATC TTT GCG 3'

(reverse) 5' CGC AAA GAT CTT CCT CCG AAG CTG GTT 3'

3.2.2 Expression and purification of WT and mutant αM I domains

Escherichia Coli (BL21(DE3)) transformed with pGEX-2T constructs were stored as 10% glycerol stocks. A scraping from this glycerol stock was diluted into 3 ml TB media with 0.1 mg/ml ampicillin. 200 µl were used to innoculate 750 ml TB media

with 100 μg/ml ampicillin in one litre flasks and the cultures were grown at 30°C overnight. The temperature was increased to 37°C after the overnight incubation and grown to an OD_{600} ~ 0.6, induced with 0.5 mM IPTG and harvested after 4 hours of induction by centrifugation in a GSA rotor at 7500 rpm for 20 minutes, 4°C. The cell pellets were resuspended in 1 mM EDTA, 1 mM DTT, 0.1% Triton X-100, 1 mM PMSF in phosphate buffered saline (PBS) and frozen at –80°C.

The cell pellets were thawed in a 37°C water bath and lysed by sonication on ice with 2 second on/off pulses for 1 minute. The resulting crude extract was centrifuged in an SS34 rotor at 18000 rpm for 1 hour, 4°C. The lysate was incubated with a 10 ml slurry of glutatione-sepharose 4B beads (Amersham Pharmacia Biotech, Pistcataway, NJ) pre-equilibriated with PBS in a luer lock glass column (Sigma, St. Louis, MI) for 1 hour at room temperature with constant rocking. The beads were washed extensively with 100 ml 1% Triton X-100 in PBS followed by a wash with 50 ml PBS. The glutathione-S-transferase (GST) fusion protein could be released by competitive elution with 50 mM reduced glutathione in 20 mM Tris pH 8.0 after a 1 hour incubation at room temperature. Alternatively, the I domain was cleaved on the beads from GST by incubating with PBS containing 5 μg/ml thrombin for 3 hours at room temperature with constant rocking. The cleaved protein was pooled from elution after the thrombin incubation along with the eluate collected from washing the beads with 30 ml PBS. The GST beads could then be regenerated for re-use by washing with 6 M guanidine hydrochloride, 70% ethanol and high and low pH buffers. 16 N-terminal residues need to be removed in order for the I domain to crystallise (Lee *et al*, 1995b). The I domain was therefore digested overnight with 0.5% immobilised trypsin (Pierce, Rockford, IL) at 4°C in PBS to remove these N-terminal residues. The correct cleavage site was confirmed using N-terminal sequencing.

3.2.3 Iodoacetylation of WT and E314R αM I domain

The WT and mutant αM I domain contained a single cysteine which was capable of forming intermolecular disulphides as judged by dimer formation using size exclusion chromatography. Addition of reducing agent was not suitable as ligands containing disulphide bonds, which were to be used in subsequent binding studies, would be affected. Therefore the dimer formation was prevented by reacting the I domain with iodoacetamide to block the single cysteine with the neutral moiety H_2NCOCH_2S-. The protein was first reduced by incubation with 1 mM DTT at room temperature for 1 hour. It was then dialysed into 20 mM Tris, 150 mM NaCl, 5 mM $MgCl_2$, pH 8.0 to remove DTT and achieve the optimal pH for iodoacetamidation. The I domain was incubated with 10 mM iodoacetamide for 2 hours at room temperature and dialysed extensively to remove excess iodoacetamide. Completion of the reaction was judged by the monomeric nature of the protein on a 24 ml Superdex 75 gel filtration column HR 10/30, running at 0.5 ml/min with 20 mM Tris, 150 mM NaCl, 5 mM $MgCl_2$, pH 8.0. A standard curve (log molecular weight vs elution volume) was generated from the elution profile of thyroglobulin (670 kDa), γ-globulin (158 kDa), ovalbumin (44 kDa), myoglobin (17 kDa) and vitamin B12 (1.35 kDa) (Sigma, St Louis, MI) to allow molecular weight estimation of the sample proteins.

3.2.4 Ligand preparation

3.2.4.1 ICAM-1 fusion digestion

The sICAM-ZZ fusion was cleaved in 20 mM sodium phosophate buffer pH 7.2,

150 mM NaCl with restriction protease factor Xa (Roche, Indianapolis, IN), using a 1:20 w/w enzyme to substrate ratio, incubating at room temperature overnight. sICAM was seperated from the protein A tag by size exclusion chromatography using a 24 ml superdex 75 column HR 10/30, running at 0.5 ml/min with 20 mM sodium phosphate buffer, 150 mM NaCl, pH 7.2.

3.2.4.2 Fragment D desialyation

The crystal structure of fragment D was solved using desialyated protein (Spraggon *et al*, 1997). Fragment D used in these studies was purified from mammalian blood and therefore glycosylated. For crystallisation, fragment D was digested in 50 mM Tris pH 7.0, 5 mM $CaCl_2$ with neuraminidase (Roche, Indianapolis, IN) at a concentration of 0.1 U/mg substrate to remove sialic acids. Mass spectroscopy analysis revealed a decrease of 554 Da following digestion accounting for a loss of 2 sialic acids.

3.2.4.3 Mass spectroscopy

Matrix-assisted laser adsorption/ionisation-mass spectroscopy (MALDI-MS) spectra were obtained for all proteins and peptides with a Voyager DE-RP MALDI-TOF (time-of-flight) mass spectrometer (PerSeptive Biosystems, Framingham. MA), using reflector mode and α-cyano-4-hydroxycinnamic acid as a matrix. Peaks were assigned using the program PAWS (Proteometrics). The molecular weights assigned from these spectra were used to determine accurate molar ratios for co-crystallisation studies.

3.2.5 Surface plasmon resonance studies

A BIAcore 3000 surface plasmon resonance-based biosensor (BIAcore AB, Uppsala, Sweden) was used to measure binding parameters for the interaction between the αM I domain and ligands, fibrinogen, fragment D, sICAM-1. All proteins were dialysed extensively against Biacore running buffer, 20 mM Hepes, 150 mM NaCl, 0.005% polysorbate 20 (v/v), pH 7.5 (BIAcore AB), along with 5 mM $MgCl_2$, $MnCl_2$, $CaCl_2$ or EDTA. All binding experiments with fragment D were performed using 1mM Ca^{2+}, which is required to prevent degradation of the protein, and different cations were tested by adding a 5-fold excess of the test cation over Ca^{2+}. Samples were also purified by gel filtration in order to eliminate aggregated material which could interfere with affinity measurements. For clarification, the protein immobilsed onto the chip surface is termed the ligand and the protein flowed over the chip surface is the analyte. Prior to immobilisation and binding studies, the system was washed five times with Biacore running buffer. Protein immobilisation onto the carboxymethylated dextran gold surface of the BIAcore chip was carried out using the amine coupling method (Jonsson *et al.*, 1991), as illustrated in figure 3.1.

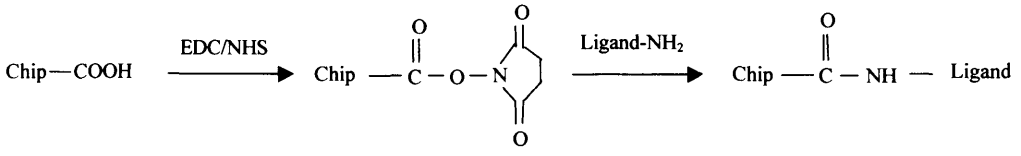

Figure 3.1 Basic mechanism for the amine-coupling method.

The chip surface was activated by mixing equal volumes of 100 mM NHS and 400 mM EDC and injecting the mixture over the chip at 5 µl/min for 8 minutes. Ligand binding to the activated surface was tested at different pHs to determine the optimal pH. This should be below the pI of the protein but as high as possible to increase covalent

attachment. The theoretical pI of the protein was determined using ProtParam in SWISS-PROT (ExPASy molecular biology server). After ligand immobilisation, 500 mM ethanolamine was flowed over the chip for 8 minutes at 5 µl/min to block the remaining active groups on the chip. For all measurements, a flow path involving all 4 flow cells was utilised at 25°C with a blank flow cell, which had been activated and blocked, to be used as a reference surface.

Initial binding studies used the GST tags of the αM I domain fusions to immobilise the I domain to CM5 sensor chips allowing freedom for the I domain to undergo any conformational changes. An excess of goat anti-GST IgG was immobilised onto the chip surface by amine coupling and the αM I domain-GST fusion was flowed over the cell at 5 µl/min to immobilise ~1000 response units (RU) (~1.0 ng/mm^2). Goat anti-GST IgG was also immobilised onto the reference surface for this analysis. Analytes, fibrinogen, fragment D and sICAM-1, were flowed over the chip at 20 µl/min for 2 minutes and the surface was regenerated with 10 mM glycine/HCl pH 2.2. Binding was not observed when the I domain was captured via GST to the chip.

Amine coupling was then used to directly immobilise the I domain (in 10 mM acetate pH 5.0), fibrinogen (in 10 mM acetate pH 4.5), fragment D (in 10 mM acetate pH 5.0) and sICAM-1 (in 10 mM acetate pH 4.5) to the chip. Binding was only observed by using the αM I domain as the analyte and immobilising the ligands, fibrinogen, fragment D and sICAM-1. Regeneration of the chip surface with the baseline returning to zero was achieved with 1 M NaCl. A surface stability test demonstrated that this regeneration condition did not affect the binding capacity of the ligand or cause any baseline drift.

Analytes were initially tested for binding with a 1 minute injection at 20 µl/min and a 10 µM analyte concentration. Steady state affinity experiments were performed on Pioneer B1 (BIAcore, AB) chips, which have a lower degree of carboxymethylation and

therefore less negatively charged than the CM5 chips, resulting in lower levels of non-specific binding. Fibrinogen, fragment D and sICAM-1 were immobilised at concentrations ranging from 200 to 1000 RU and the flow rate for all injections was 5 μl/min. A wide range of analyte concentrations was tested to ensure recovery of data suitable to obtain the equilibrium dissociation constant K_D. Typically, sensorgrams were obtained at 6 different concentrations for each analyte/ligand pair with an injection of 8 minutes to achieve steady state binding. The chip surface was regenerated with a 4 minute injection of 1 M NaCl and prior to each analyte injection and after regeneration, buffer was injected for 1 minute to stabilise the baseline. Each set of titrations included a running buffer injection to be used as an additional blank control.

All data collected were analysed using BIAevaluation 3.0, aligning injection start times, adjusting all baselines to zero and subtracting binding to the reference flow cell and the blank buffer injection to account for any non-specific binding. At equilibrium,

$$dR/dT = k_a C (R_{max} - R_{eq}) - k_d R_{eq} = 0$$

where R is the response, T is time, k_a is the association constant, k_d is the dissociation constant, C is the analyte concentration, R_{max} is the theoretical binding capacity and R_{eq} is the steady state binding capacity. From this, the following equation can derived;

$$R_{eq} = \frac{C R_{max}}{K_D C n}$$

where K_D is the equilibrium dissociation constant and n is a steric interference factor, specifying how many binding sites are on average blocked by one analyte molecule (a value of 1 was used, assuming one analyte molecule binds one ligand molecule).

For each sensorgram, the peak response levels achieved in the steady state region (R_{eq}) were plotted against analyte concentration (C). This plot was fit to a single site binding equation (Langmuir isotherm), as described above, to determine K_D values. The K_D for each analyte/ligand pair was measured in triplicate.

3.2.6 Using size exclusion chromatography to isolate the αM I domain in complex with fragment D and sICAM-1

sICAM-1 and the αM I domain were dialysed into 20 mM Tris, 150 mM NaCl, 5 mM $MgCl_2$, pH 7.5 and fragment D was dialysed into the same buffer with an addition of 1 mM $CaCl_2$. A 10-fold molar excess of αM I domain, at 0.4 mM, was used in each mixture with fragment D and sICAM-1. The concentration of each protein in the complex was greater than the K_D value, calculated by surface plasmon resonance, thus ensuring fragment D and sICAM-1 would be complexed with the I domain. 100 µl of each complex mixture was loaded onto a 24 ml superdex 200 gel filtration column HR 10/30, pre-equilibriated with 20 mM Tris, 150 mM NaCl, 5 mM $MgCl_2$, pH 7.5 with the addition of 1 mM $CaCl_2$ for the I domain-fragment D complex. A flow rate of 0.5 ml/min was used to elute the samples over 30 ml. A calibration curve, as previously described, was used to assess the molecular weights of the proteins eluted and 1 ml fractions were collected for further analysis by SDS PAGE.

3.2.7 Crystallographic studies

3.2.7.1 Co-crystallisation trials

All I domain crystal forms, as well as fragment D and D1-D2 ICAM-1, had been crystallised using PEG as a precipitant, as previously discussed in sections 1.4.1.1, 3.1.1 and 3.1.2. Initial screening for the crystallisation conditions of the αM I domain complexed to ligand were therefore carried out using the PEG precipitant solutions from the commercial screens Screen I and II (Hampton Research, Laguna Niguel, CA), Cryo I and II and Wizard I and II (Emerald Biostructures, Bainbridge Island, WA) at room temperature and 4°C. Trials were set up using the sitting drop vapour diffusion method with 100 µl precipitant in the well and 1 µl protein plus 1 µl precipitant in the drop. Prior to crystallisation, 5 mM $MgCl_2$ was added to each mixture of I domain and ligand as this cation was shown to support the highest level of binding from surface plasmon resonance studies.

The WT and E314R αM I domains were dialysed into 20 mM Tris, 150 mM NaCl, 5 mM $MgCl_2$, pH 7.5 and concentrated to 15 mg/ml in an Amicon ultrafiltration stirred cell with a YM10 membrane (Millipore, Bedford, MA). The ligands, sICAM-1 and fragment D in the same buffer, were added to obtain I domain-ligand molar ratios of 1:1, 1:0.9 and 1:1.1 and then concentrated to 10 mg/ml. The I domain-fragment D complex also contained 2 mM $CaCl_2$ to prevent degradation of fragment D. Additional trials were set up exchanging the Mg^{2+} in the protein buffer solution for Mn^{2+}, Co^{2+}, Zn^{2+}, Ni^{2+} or Cd^{2+}. The αM I domain peptides were dissolved in 20 mM Tris, 150 mM NaCl, 5 mM $MgCl_2$, pH 8.0 except for P1 which was dissolved in a 50% (v/v) DMSO solution. A 10-fold molar excess of peptide was added to the I domain and concentrated to 10 mg/ml.

Once crystallisation conditions were established, crystal growth was optimised using Linbro plates (Hampton Research, Laguna Niguel, CA) by mixing 2 µl protein with 2 µl preciptant in the drop over a reservoir containing 1 ml preciptant. Precipitant and salt concentrations, as well as pH, were varied. Crystals which were too small or intergrown and therefore unsuitable for data collection were optimised by streak seeding (Stura & Wilson, 1990). Trays were set up with progressively lower concentrations of PEG and left for 5 days for the drops to equilibriate with the reservoir solution. The reduced precipitant concentration should prevent spontaneous nucleation but be high enough to permit growth of seeds. Seeds were then collected by scratching the surface of a small crystal with a hair and transfering them to the pre-equilibriated drops. Seeding was optimised by reducing the number of seeds deposited into the drops by successively streak seeding 5 drops with the same well solution resulting in single crystal growth in the last drop. Examples of the different crystal morphologies grown are shown in figure 3.2.

3.2.7.2 Soaking ligands into WT αM I domain crystals

The fibrinogen peptide, P2, was soaked into αM I domain crystals with $P2_12_12_1$ and $P4_3$ symmetry. These crystal forms were chosen as the proposed P2 binding sites within the I domain were free of crystal contacts. Crystals with the $P2_12_12_1$ space group were grown in 0.2 M NaCl, 30% PEG 3000, 0.1 M Tris pH 7.0 and harvested in the same mother liquor with an additional 5% PEG 3000. The crystal was then transferred to a 10 µl drop containing 0.5 mM P2 in 0.2 M NaCl, 35% PEG 3000, 0.1 M Tris pH 7.0. P2 concentrations above 0.5 mM damaged the crystals, which then diffracted to only ~10 Å. Crystals with the $P4_3$ space group were grown in 20% PEG 300, 5% PEG 8000, 10% glycerol, 0.1 M Tris pH 8.5 and harvested in mother liquor with an

additional 5% PEG 300. The crystals were then transferred to a 10 µl drop with 250 µM P2, 25% PEG 300, 5% PEG 8000, 10% glycerol, 0.1 M Tris pH 8.5. P2 concentrations above 250 µM caused the crystals to completely deteriorate. Crystals were soaked with P2 overnight prior to data collection.

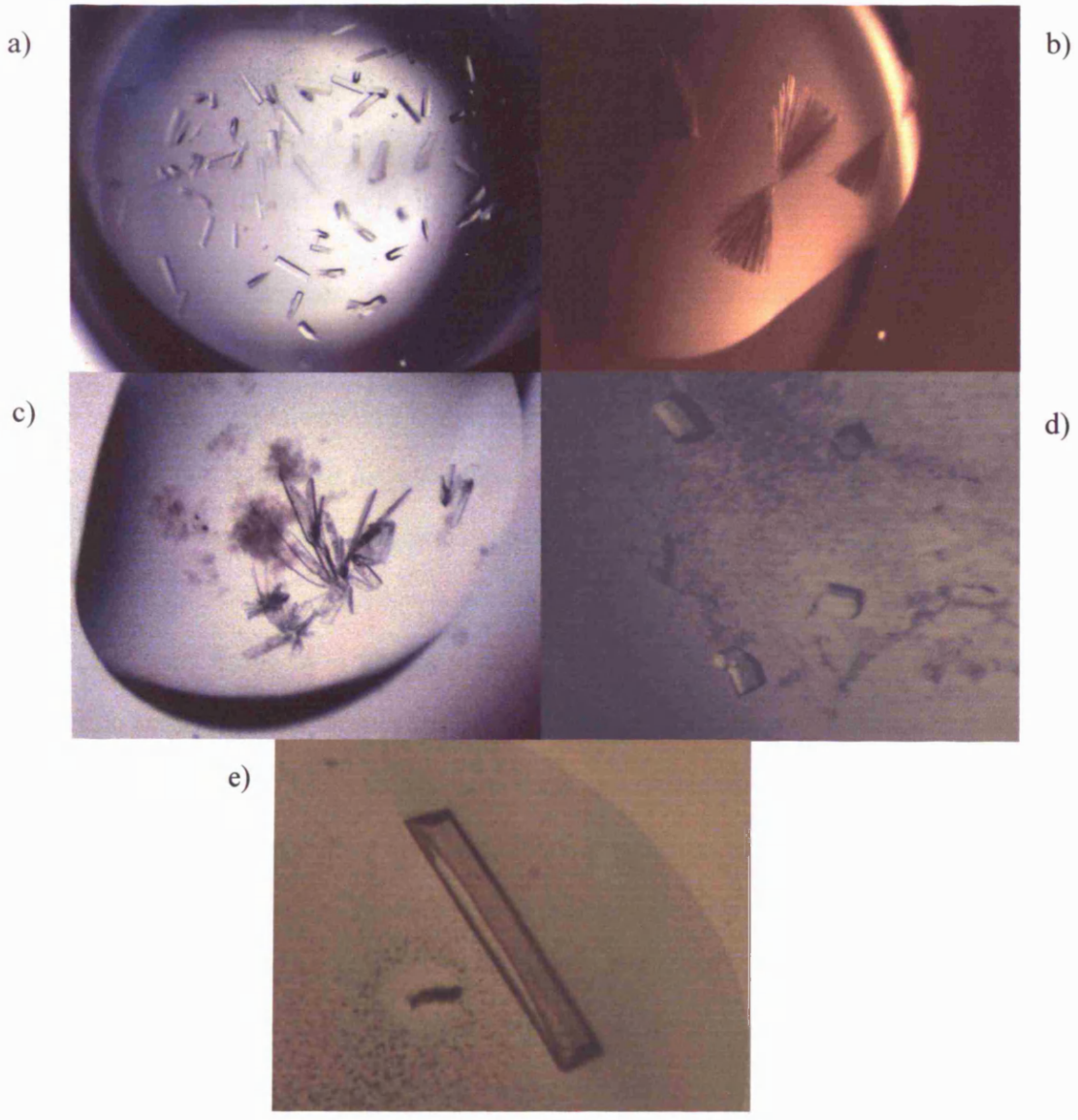

Figure 3.2 Different crystal forms of the WT αM I domain. (a) $P2_1$ (b) $P4_3$ (c) $P2_12_12$ (d) C2 (e) $P2_12_12_1$.

3.2.7.3 Data collection and processing

Data were collected from the crystals in table 3.1 with cryoprotectant conditions, as shown in table 3.2. Each crystal was harvested in mother liquor containing an additional 5% PEG precipitant to stabilise the crystal. The harvested crystal was then soaked in cryoprotectant and flash frozen in a cryo-stream of nitrogen at 100 K. A test exposure was taken so the unit cell could be indexed with DENZO (Otwinowski & Minor, 1997). PREDICT within the CCP4 suite of programs (CCP4, 1994) was then used to facilitate efficient data collection. All data were processed with the programmes DENZO and SCALEPACK (Otwinowski & Minor, 1997).

DENZO determines the crystal parameters for a single image in the data set using detector and X-ray parameters during autoindexing. Crystal parameters include lattice type, unit cell dimensions and orientation of the reciprocal lattice with respect to the detector. The X-ray and detector parameters include the wavelength and coordinates of the X-ray beam, the crystal-to-detector distance and the detector alignment parameters. DENZO then refines the crystal and detector orientation parameters for each processed image by a least squares method that minimises the deviation of the reflection centroids from their predicted positions and partiality refinement in which the intensity of the partially recorded reflections is compared to the predicted partiality multiplied by an average intensity in the same resolution range. DENZO calculates the diffraction intensity by subtracting the detector background from the reflection profile. It is assumed that the background is a linear function of the detector coordinates and pixels that deviate more than 3 standard deviations from the best fit to the background function are removed. The measured intensities are then integrated by profile fitting, which uses the radius of the area around each spot, containing neighbouring spots, to calculate the average reflection spot. Each spot is fitted to the average profile of all the spots within the specified radius.

Data set name	Ligand	Method	Crystallisation condition	Crystallisation temperature
FXa	FX	Co-crystal	0.2M $(NH_4)_2SO_4$, 30% PEG 4000	4°C
FXb	FX	Co-crystal	20% PEG 300, 5% PEG 8000, 10% glycerol, 0.1M Tris 8.5	RT
FXc	FX	Co-crystal	0.2M NaCl, 20% PEG 8000, sodium/phosphate pH 6.2	4°C
P1a	P1	Co-crystal	20% PEG 10000, 0.1M HEPES pH 7.5	RT
P1b	P1	Co-crystal	0.2M NaCl, 20% PEG 8000, 0.1M phosphate citrate pH 4.2	RT
P1c	P1	Co-crystal	0.2M $(NH_4)_2SO_4$, 25% PEG 4000, 0.1M sodium acetate pH 4.5	4°C
P1d*	P1	Co-crystal	0.2M Li_2SO_4, 30% PEG 4000, 0.1M Tris pH 8.5	RT
P2a	P2	Co-crystal	20% PEG 10000, 0.1M HEPES pH 7.5	RT
P2b	P2	Co-crystal	0.2M NaCl, 30% PEG 3000, 0.1M Tris pH 7.0	RT
P2c	P2	Soak	20% PEG 300, 5% PEG 8000, 10% glycerol, 0.1M Tris pH 8.5	RT
P2d	P2	Soak	0.2M NaCl, 30% PEG 3000, 0.1M Tris pH 7.0	RT
RGEVa	RGEV	Co-crystal	0.2M Li_2SO_4, 30% PEG 4000, 0.1M Tris pH 8.5	RT
RGE(HA)Va	RGE(HA)V	Co-crystal	20% PEG 10000, 0.1M HEPES pH 7.5	RT
RGE(HA)Vb	RGE(HA)V	Co-crystal	0.3M NaCl, 25% PEG 3350, 0.1M Tris pH 7.0	4°C
RGDa	RGD	Co-crystal	20% PEG 8000, 0.1M CHES pH 9.5	RT
RGD(HA)Va	RGD(HA)V	Co-crystal	0.2M $(NH_4)_2SO_4$, 30% PEG 4000	4°C
RGD(HA)Vb*	RGD(HA)V	Co-crystal	0.2M $MgCl_2$, 24% PEG 4000, 0.1M Tris pH 8.5	RT

Table 3.1 Crystallisation conditions for the αM I domain crystals tested. All crystals are the WT αM I domain except those labelled with * which denotes the E314R mutant.

Data set name	Cryoprotectant	Source	λ (Å)
FXa	15% glycerol	SRS 7-2	1.488
FXb	None	SSRL 9-1	0.976
FXc	20% glycerol	In-house	1.542
P1a	15% glycerol	SSRL 9-1	0.976
P1b	20% glycerol	SSRL 9-1	0.976
P1c	15% glycerol	In-house	1.542
P1d*	15% glycerol	In-house	1.542
P2a	20% glycerol	SSRL 9-1	0.976
P2b	15% glycerol	SSRL 9-1	0.976
P2c	None	In-house	1.542
P2d	15% glycerol	In-house	1.542
RGEVa	15% glycerol	In-house	1.542
RGE(HA)Va	20% glycerol	SSRL 9-1	0.976
RGE(HA)Vb	15% glycerol	SSRL 7-1	1.080
RGDa	15% glycerol	In-house	1.542
RGD(HA)Va	15% glycerol	SSRL 7-1	1.080
RGD(HA)Vb*	15% glycerol	SSRL 9-1	0.976

Table 3.2 Cryoprotectant conditions and x-ray sources used in data collection. * denotes the E314R αM I domain mutant. SSRL – Stanford synchrotron radiation laboratory, in-house - RU200 HB X-ray generator , SRS – Daresbury synchrotron.

The scaling and merging of intensities as well as the global refinement of crystal parameters is performed by SCALEPACK. This postrefinement allows for the separate refinement of each image but uses the same unit cell value for the whole data set. Additional parameters, such as mosaicity, are also refined at this stage. SCALEPACK

enlarges the estimated error of each measurement by a fraction of the expected intensity. This algorithm reduces the bias towards reflections with an integrated intensity below the average. Various statistics, such as the ratio of the intensity to the error of the intensity ($I/\sigma I$) and the agreement between symmetry related reflections (R_{merge}), are output upon scaling and merging of the data, which are used as a measure of the quality of the data set.

From the merged intensities (Is) and their standard deviations (σIs), structure factor amplitudes are calculated using TRUNCATE within the CCP4 suite (CCP4, 1994). The amplitudes are placed on an approximately absolute scale using the scale factor taken from the Wilson plot (Wilson, 1950). The Wilson plot determines the absolute scale and temperature factor from plotting observed intensities against resolution. The truncation procedure has the effect of forcing all negative observations of up to -4σ to be positive while increasing the weakest reflections (less than 3σ). The truncated data are then sorted into a standard order using CAD (CCP4).

The cell parameters for each crystal measured are shown in table 3.3. Reflection statistics for the highest resolution data set of each crystal form are shown in appendix table A.1.

The number of molecules in the asymmetric unit for each crystal form was assessed by calculating the Matthews coefficient (V_M) (Matthews, 1968), which is expected to be in the range of 1.7 to 3.5 $Å^3$/Da. Typical values for each crystal form are shown in table 3.4.

Data set name	Space group	a (Å)	b (Å)	c (Å)	α (°)	β (°)	γ (°)
FXa	$P2_12_12$ (a)	85.4	62.9	75.6	90.0	90.0	90.0
FXb	$P4_3$	45.7	45.7	94.9	90.0	90.0	90.0
FXc	$P2_12_12_1$	38.3	50.9	102.3	90.0	90.0	90.0
P1a	$P4_3$	45.8	45.8	94.6	90.0	90.0	90.0
P1b	$P2_12_12_1$	38.4	50.9	102.4	90.0	90.0	90.0
P1c	$P2_12_12$ (b)	122.0	47.7	74.8	90.0	90.0	90.0
P1d*	C2	135.7	36.6	37.8	90.0	92.9	90.0
P2a	$P4_3$	45.5	45.5	94.7	90.0	90.0	90.0
P2b	$P2_12_12_1$	38.2	50.8	102.2	90.0	90.0	90.0
P2c	$P4_3$	45.4	45.4	94.8	90.0	90.0	90.0
P2d	$P2_12_12_1$	38.1	50.7	102.3	90.0	90.0	90.0
RGEVa	C2	134.9	36.8	37.7	90.0	92.1	90.0
RGE(HA)Va	$P4_3$	45.3	45.3	94.8	90.0	90.0	90.0
RGE(HA)Vb	$P2_1$	36.8	75.8	70.1	90.0	105.2	90.0
RGDa	$P4_3$	45.6	45.6	95.0	90.0	90.0	90.0
RGD(HA)Va	$P2_12_12_1$	38.6	51.0	102.8	90.0	90.0	90.0
RGD(HA)Vb*	$P2_1$	38.6	74.2	70.1	90.0	105.2	90.0

Table 3.3 Cell parameters for each data set. Two different crystals grew in the $P2_12_12$ space group with different cell dimensions so the space groups for these data sets have been labelled with (a) and (b) for identification. * denotes the E314R αM I domain mutant.

Space group	Number of molecules in the asymmetric unit	Unit cell volume ($Å^3$)	V_M ($Å^3$/Da)	Solvent content (v/v) (%)
$P2_12_12_1$	1	2.0×10^5	2.2	43.0
$P2_12_12$ (a)	2	4.1×10^5	2.2	43.8
$P2_12_12$ (b)	2	4.3×10^5	2.4	47.5
C2	1	1.8×10^5	2.0	39.0
$P2_1$	2	1.9×10^5	2.1	39.5
P4	1	2.0×10^5	2.1	41.7

Table 3.4 Content of the unit cells for each crystal form.

3.2.7.4 Molecular replacement

After data processing, a molecular replacement search was performed with data from crystals with new space groups and cell dimensions. The open (PDB accession code 1IDO) and closed (PDB accession code 1JLM) conformations of the αM I domain were used as search models. Molecular replacement was performed with the program AMoRe (Navaza, 1994), within the CCP4 suite. The program incorporates rotation and translation searches followed by rigid body fitting. The rotation function is used to find the correct orientation of the model in the crystal lattice by testing the agreement between the Patterson functions (the maps of interatomic vectors) calculated from the model and the data at various relative orientations. At the correct orientation, which superimposes the model onto the crystal, the correlation of the two Patterson functions should have a large value. The rotation function includes vectors between atoms within the same molecule (self vectors), independent of the origin, while eliminating cross vectors, vectors between neighbouring molecules, as much as possible. The translation function investigates the correlation between the observed intensities and the cross vectors between the symmetry related molecules of the model as it is moved about the unit cell. Correct positioning of the model should result with the peaks of the translation function corresponding to the translation vectors (x,y,z) between the symmetry-related molecules. Rigid body refinement is then applied to the correct solution from the translation search to optimise the rotation and translation parameters. This method assigns rigid geometry to parts of the structure and minimises $(|F_{obs}|-|F_{calc}|)^2$ with respect to all positional coordinates and thermal parameters by the least squares method.

Practically, the program, AMoRe, is carried out in five steps. The program SORTING reformats the observed structure factors for use in later steps. This is followed by TABLING, which translates the search model to place its centre of gravity at the origin and rotates it to align the principal axes of inertia along x, y and z in real

space. This avoids using an unnecessarily large cell during the calculation of the continuous Fourier coefficients. A table of Fourier coefficients for the model in this new orientation is then calculated. Spherical harmonics are calculated from the structure factors of the crystal and the model during ROTING to facilitate the subsequent computation of the cross-rotation function. The rotation function finds the optimal orientation of the search model with respect to the diffraction data. A list of the highest peaks in the cross-rotation function is then output for use during the program TRAING. The best solutions of the rotation function are used in TRAING for the translation function search. Each possible orientation of the search model is translated through the asymmetric unit of the unit cell and the resulting Patterson calculated is compared with the Patterson derived from the diffraction data. The maximum overlap between the two Pattersons should correspond to the best solution. Once a potential translation function solution has been found in TRAING, FITING performs rigid body refinement to optimise the fit between the model and the data. The correct rotation and translation to apply to the initial model is then calculated. This also accounts for the original reorientation during which the centre of mass of the search model is placed at the origin.

Data from 8 to 3.5 Å were used, with a sphere radius of 15 Å and an angular search step of 2.5°, to calculate the rotation function. The rotation and translation functions along with the rigid body refinement for the highest resolution data set of each crystal form is shown in appendix table A.2.

3.2.7.5 Model building and refinement

Refinement of each model was calculated with CNS version 1.0 (Brünger *et al.*, 1998). Each data set was refined to an R_{free}value to at least below ~30% to identify the presence of additional density which would correspond to that of the ligand. The data set with the highest resolution for each space group was fully refined so that it could be used as a model for subsequent data sets with the same symmetry. The data sets with $P4_3$ and C2 symmetry were refined using the coordinates from the published αM I domain open (PDB accession code 1IDO) and closed (PDB accession code 1JLM) structures as the starting models. A random sample, containing 5% of the data, was excluded during the refinement of all the data sets and the difference between the observed and calculated structure factors of these reflections, the R_{free}, was monitored to avoid over modelling the diffraction data. These same reflections, initially chosen at random from the data sets to be used as models, were flagged again prior to beginning refinement of data sets with the same symmetry. This ensured that reflections that had previously been used during refinement were not used to calculate the R_{free} so it would remain an unbiased indicator of model quality.

Refinement for each model began with rigid body refinement, if this had not already been performed during molecular replacement. Simulated annealing with a starting temperature of 2500 K and a cooling rate of 25 K per step was then implemented to reduce any model bias. Phases were calculated for the new model and used to generate F_{obs}-F_{calc} and 2 F_{obs}-F_{calc} maps. Maps and models were displayed with Turbo-Frodo version 5.5 (Roussel & Cambillau, 1992) and during the first round of manual model building, side chains without interpretable density were given an occupancy of zero and alternative rotamer conformations were modelled. Refinement was then continued within CNS using positional and B factor refinement. After successive rounds of manual model building and positional and B factor refinement,

waters were added to the model. Waters were added in successive steps, at positions with density peaks higher than 3σ in the 2 F_{obs}-F_{calc} map, until all additional density peaks were accounted for. A maximum of 50 waters were added for each step of water picking. For data from crystals with more than one molecule in the asymmetric unit, non-crystallographic symmetry restraints were applied during the initial stages of refinement.

The stereochemical quality of the models were analysed using PROCHECK version 3.4.4 (Laskowski *et al.*, 1993). Waters with incorrect hydrogen-bonding partners were identified with XPAND version 1.3.1 (Kleywegt *et al.*, 2001) and subsequently deleted.

The final R values for all the data sets are given in table 3.5. A summary of refinement and model quality for the data sets with the highest resolution for each crystal form is given in appendix tables A.3 and A.4.

Data set name	Resolution (Å)	R_{work} (%)	R_{free} (%)
FXa	2.3	23.4	27.7
FXb	2.6	26.9	27.9
FXc	2.4	26.0	27.7
P1a	3.0	26.3	27.6
P1b	1.5	20.5	22.5
P1c	3.0	25.8	26.8
P1d*	2.6	24.7	25.0
P2a	2.0	27.3	28.1
P2b	1.9	19.7	22.3
P2c	2.8	24.3	22.4
P2d	2.3	25.6	28.1
RGEVa	2.4	23.2	24.8
RGE(HA)Va	2.2	23.8	27.6
RGE(HA)Vb	1.8	27.1	30.1
RGDa	3.0	27.5	28.1
RGD(HA)Va	2.1	25.9	28.8
RGD(HA)Vb*	2.8	28.6	30.6

Table 3.5 The highest resolution and final refinement statistics for each data set. * denotes the E314R αM I domain mutant. R_{work} (%) = 100 x $\sum_{hkl} | F_{obs} - F_{calc} | / \sum_{hkl} F_{obs}$ where F_{obs} and F_{calc} are the observed and calculated structure factors respectively. R_{free} (%) is the R_{work} (%) calculated using a random selected 5% of reflection data omitted from refinement.

3.3 Results

3.3.1 αM I domain purification

Figure 3.3 shows a SDS PAGE gel of a typical purification procedure of the WT αM I domain. About 2 mg of >95% pure protein was produced per litre of media. The E314R mutant was expressed and purified in a similar fashion (data not shown). Blocking the cysteine at position 128 with iodoacetamide produced monomeric protein as judged by size exclusion chromatography and non-reducing SDS PAGE (data not shown).

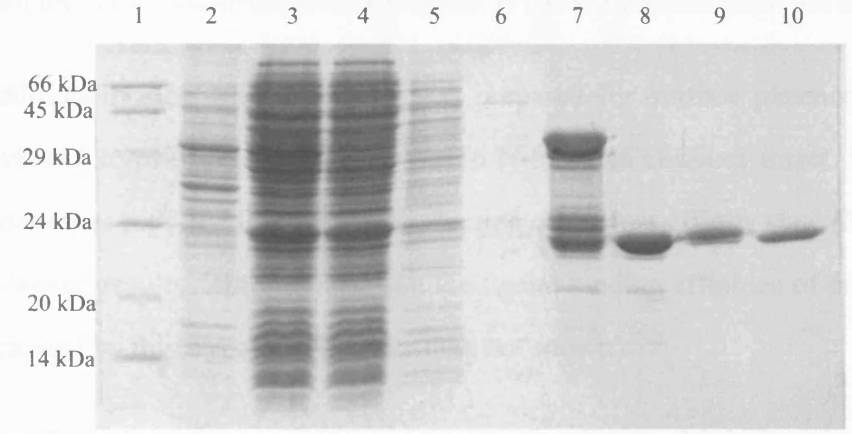

Figure 3.3 15% reducing SDS PAGE gel of the αM I domain purification
Lane 1 -molecular weight markers, lane 2 -pellet after cell lysis, lane 3 -supernatant after cell lysis, lane 4 -flow through from GST beads, lane 5 -first wash from GST beads, lane 6 -second wash from GST beads, lane 7 -GST-fusion on the beads, lane 8 -beads after thrombin digest, lane 9 -thrombin cleaved I domain, lane 10 -trypsin digested I domain.

3.3.2 Surface plasmon resonance studies

The αM I domain bound to fibrinogen, fragment D and sICAM-1 in a cation-dependent manner as shown in figure 3.4. All ligands bound with greater affinity in the presence of Mg^{2+} and binding was greatly decreased when EDTA was present. In the case of fibrinogen and sICAM-1, Mn^{2+} supported weaker binding than Mg^{2+}, and Ca^{2+} significantly reduced binding to the I domain. In contrast, Ca^{2+} supported more binding than Mn^{2+} for the interaction of fragment D with the αM I domain. The E314R αM I domain mutant was also tested to establish that the mutation did not affect ligand binding capacity of the I domain. Comparable binding was observed for the E314R mutant with the same cation-dependence as the WT αM I domain (data not shown).

Additionally, the αM I domain was prepared for surface plasmon resonance analysis without trypsin digest, leaving the 16 N-terminal residues intact. Removal of these residues was reported to result in production of the low affinity state (Xiong *et al.*, 2000). However, results demonstrated that the ligand binding affinities of the I domains were unchanged by this trypsin treatment (data not shown).

The K_D values from steady state analysis of the αM I domain binding to fibrinogen, fragment D and sICAM-1 are shown in table 3.6. All interactions were measured in the presence of Mg^{2+}. The K_D value for the I domain-fragment D interaction was measured with the addition of Ca^{2+}. Consequently, the interactions of fibrinogen and sICAM-1 with the αM I domain were also measured with the addition of Ca^{2+} for comparison. An example of a steady state binding experiment with the αM I domain and the ligand sICAM-1 is shown in figure 3.5.

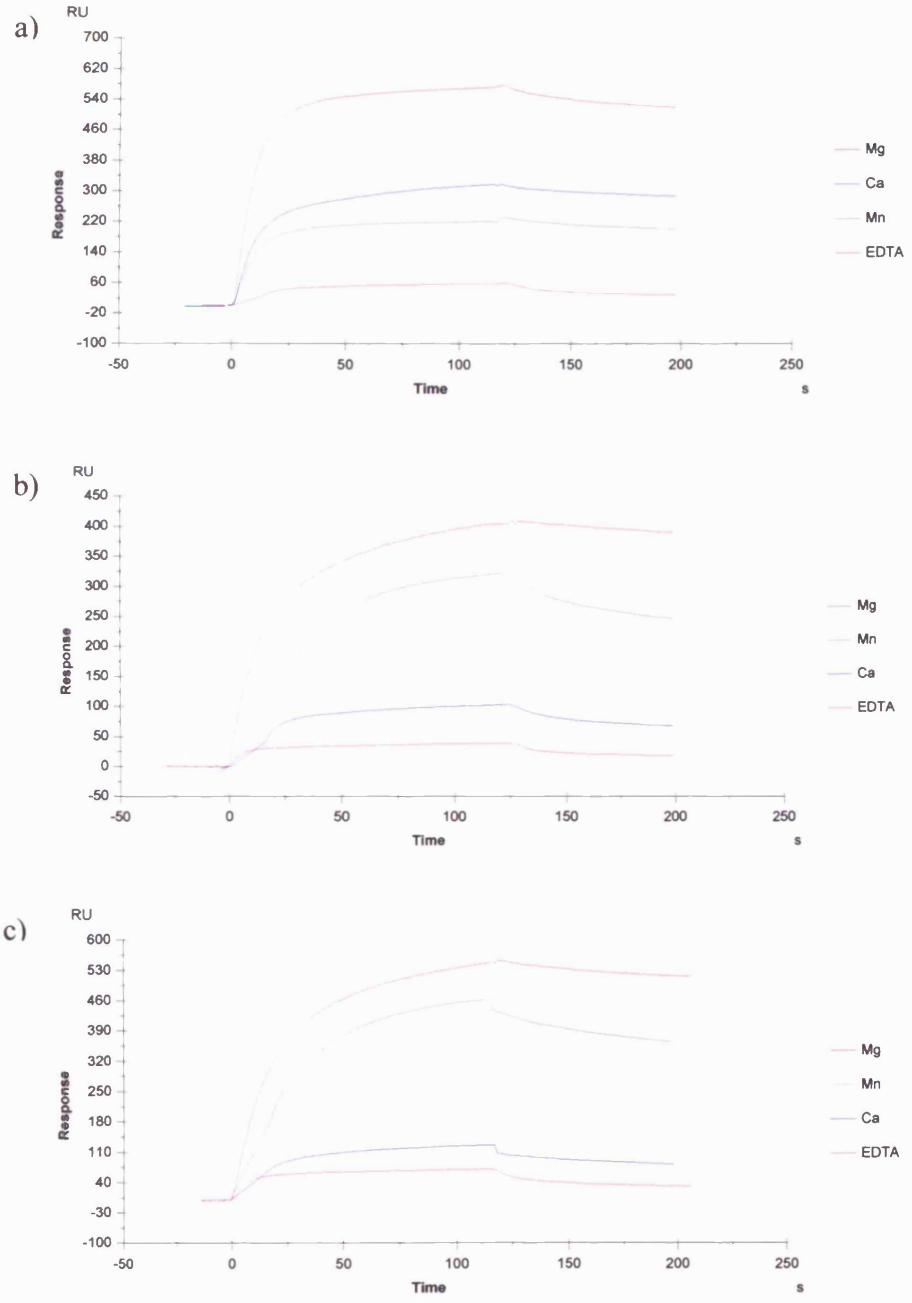

Figure 3.4 Sensorgram overlays showing the cation-dependence of the interaction of WT αM I domain with fragment D (a), fibrinogen (b) and sICAM-1 (c).

a)

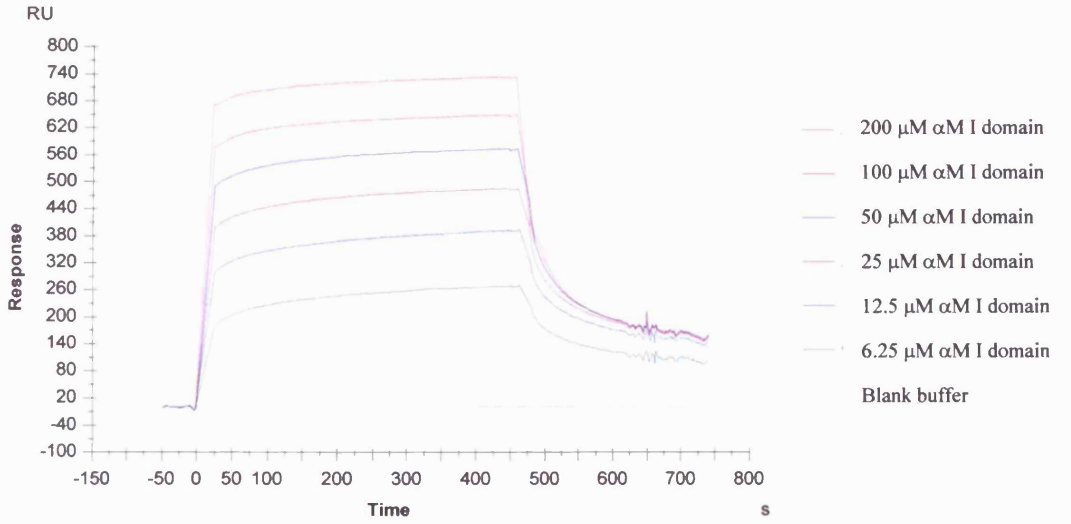

b)

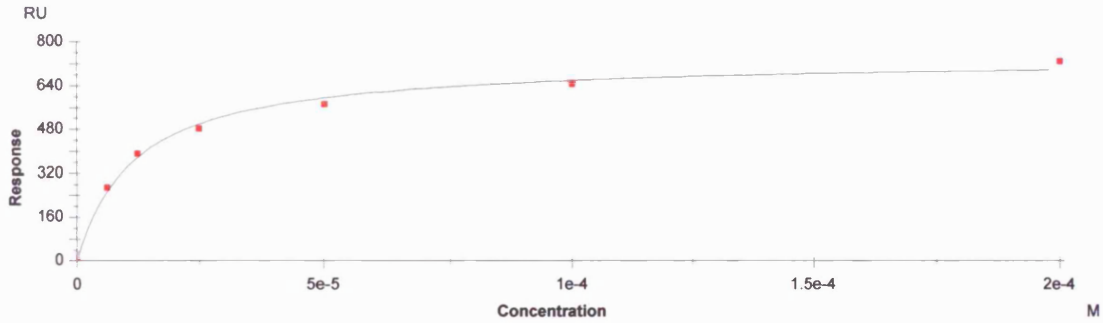

Figure 3.5 Equilibrium analysis of the WT αM I domain mutant binding to sICAM-1. a) Sensogram overlays for 6 different concentrations of the I domain binding to sICAM-1 immobilised on the chip surface. b) Langmuir isotherm displaying the peak response levels achieved at steady state (RU) against the analyte concentration. The K_D value calculated for this experiment was 6.07 μM.

	Fibrinogen (μM)	**Fragment D (μM)**	**sICAM-1 (μM)**
+ calcium	15.23 ± 2.86	19.37 ± 2.86	30.97 ± 6.31
- calcium	3.98 ± 0.86	-	6.45 ± 0.58

Table 3.6 K_D values of the interaction of αM I domain with fibrinogen, fragment D and sICAM-1 in the presence and absence of calcium. K_D ± S.D where n=3.

3.3.3 Size exclusion chromatography

Attempts to form the complexes, αM I domain-sICAM-1 and αM I domain-fragment D, were guided by the results from the surface plasmon resonance studies. This included using Mg^{2+}, which was shown to be the optimal cation for ligand binding, and concentrations, which were significantly higher than the calculated K_D values. However, the complexes were unable to be isolated by size exclusion chromatography as shown in figure 3.6.

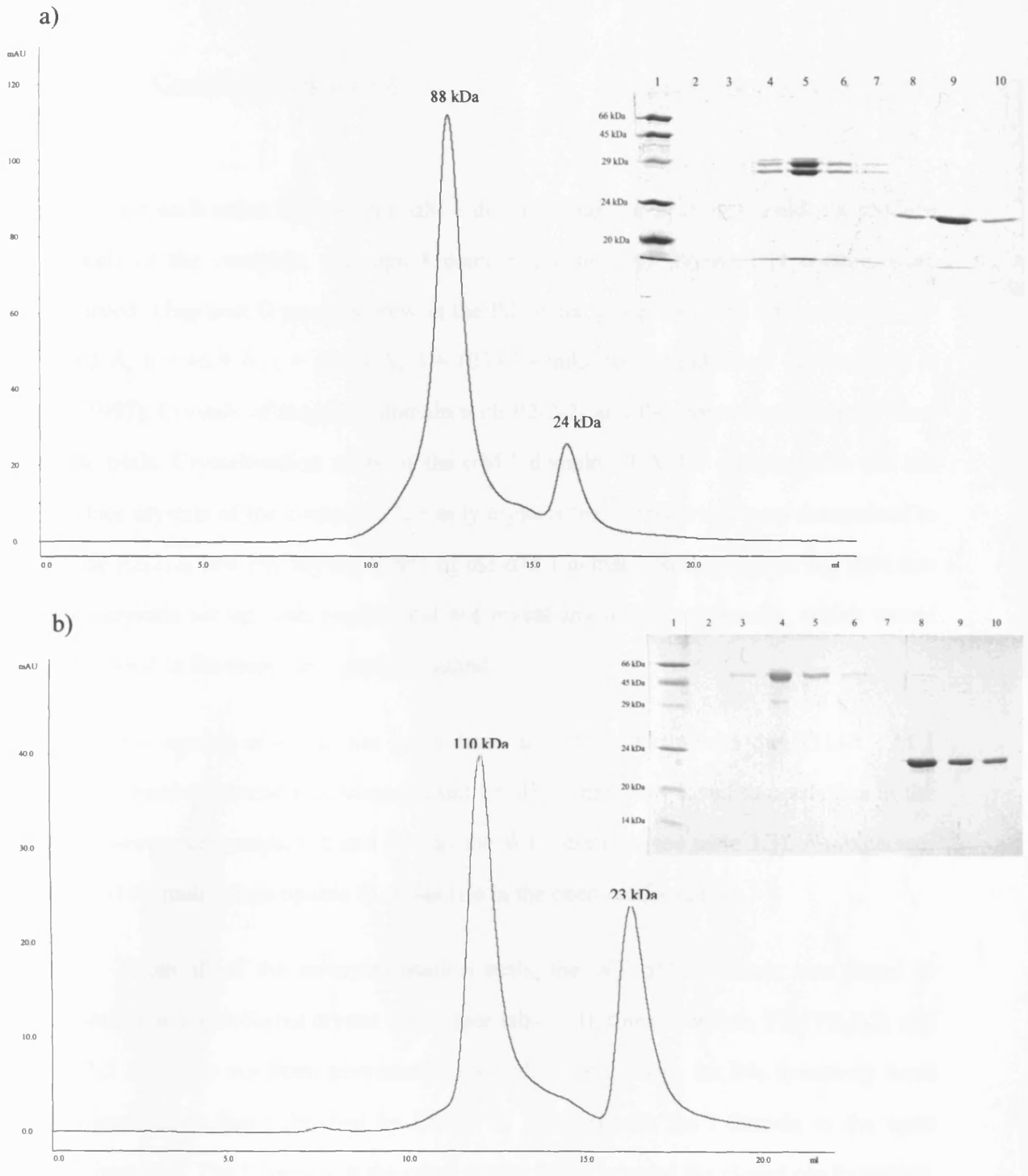

Figure 3.6 Elution profiles from a Superdex 200 gel filtration column of the αM I domain in solution with fragment D (a) and sICAM-1 (b). A 12% reducing SDS PAGE gel of the fractions is inset. Lane 1 -molecular weight markers and lanes 2 to 10 -1 ml fractions eluted from 9 ml to 17 ml.

3.3.4 Crystallographic studies

Crystallisation trials of the αM I domain-fragment D complex did not produce crystals of the complex, although I domain crystals and fragment D crystals were observed. Fragment D crystals grew in the $P2_1$ space group with cell dimensions of a = 106.5 Å, b = 46.9 Å, c = 164.9 Å, β = 105.0° similar to that published by Spraggon *et al.* (1997). Crystals of the αM I domain with $P2_12_12_1$ and $P4_3$ symmetry also grew from these trials. Crystallisation trials of the αM I domain-sICAM-1 complex also did not produce crystals of the complex. The only crystals from these trials were determined to be the $P2_12_12_1$ and $P4_3$ crystal forms of the αM I domain. Refinement of the data sets from crystals set up with peptide did not reveal any additional density, which would correspond to the respective peptidic ligands.

Co-crystals also did not grow from any of the trials with the E314R αM I domain mutant. Instead the uncomplexed E314R mutant was found to crystallise in the same two space groups, C2 and $P2_1$, as the WT I domain (see table 3.3). As expected, the E314R mutant was unable to crystallise in the open conformation.

From all of the co-crystallisation trials, the WT αM I domain was found to crystallise in six different crystal forms (see table 3.3), three of which, $P2_1$, $P2_12_12_1$ and $P2_12_12$ (a), have not been previously reported. Crystals with the $P4_3$ symmetry were isomorphous to that published by Lee *et al.* (1995a) with the I domain in the open conformation. The I domain in the other crystal forms adopted the closed conformation. The rmsd for the Cαs between the C2 crystal form and the $P2_1$ and $P2_12_12$ (b) crystal forms were 0.30 Å and 0.28 Å respectively. The rmsd for the Cαs between the C2 crystal form and the $P2_12_12$ (a) and $P2_12_12_1$ crystal forms were higher at 1.17 Å and

0.91 Å respectively. The major differences of interest between the structures are at the MIDAS. The $P2_12_12_1$ and $P2_12_12$ (a) crystal forms did not contain a Mg^{2+} ion coordinating the MIDAS, even though sufficient Mg^{2+} was present in the crystallisation buffer. Crystals were unable to grow upon addition of higher concentrations of metal to the crystallisation buffer. In addition, density for a metal ion was not observed when the crystals were soaked overnight in crystallisation buffer containing 10 to 50 mM $MgCl_2$ prior to data collection. The superimposed Cα traces of the $P2_12_12_1$ and $P2_12_12$ (a) crystal forms are shown in figure 3.7a. The $P2_1$, C2 and $P2_12_12$ (b) crystal forms possess a Mg^{2+} ion bound at the MIDAS coordinated directly by S142, S144 and D242 with 3 water molecules completing the coordination sphere, as illustrated in figure 1.4b. Cα trace superimpostions of the $P2_1$, C2 and $P2_12_12$ (b) crystal forms are shown in figure 3.7b. Compared to the closed conformation with metal bound, the absence of metal at the MIDAS was also accompanied by a 1 Å shift of S144 into the MIDAS pocket and side chain movements of D242 and S142, which have rotated 90 to 120° away from the pocket of the MIDAS. The differences between the positions of the coordinating residues in the MIDAS are shown in figure 3.8 using the C2 and $P2_12_12_1$ crystal forms as examples of the closed I domain with and without metal bound, respectively. An additional movement of helix 1 which is adjacent to the MIDAS is observed when the Cα traces of the closed conformations, with and without metal, are superimposed, as shown in figure 3.7c.

Analysis of the crystal contacts formed within the six different crystal forms of the αM I domain allowed for the identification of the appropriate crystals to use for soaking experiments. The fibrinogen peptide, P2, was chosen to use in soaking experiments as this peptide was reported to be the most effective peptide, from those available, to inhibit ligands, such as fibrinogen, binding to the αM I domain (Mesri *et al.*, 1998; Ugarova *et al.*, 1998). In addition, the binding site within the I domain for this peptide had also been located to helix 5 of the I domain and part of the loop preceding it

(Yakubenko *et al.*, 2001). Crystals with $P4_3$ and $P2_12_12_1$ symmetry were chosen for these experiments as these crystal forms did not involve crystal contacts at the reported P2 binding site and should therefore have room to accommodate the P2 peptide within the crystal lattice. Binding of the P2 peptide to the αM I domain was shown to be cation-independent (Yakubenko *et al.*, 2001) so this peptide should still be capable of binding the I domain crystals in the $P2_12_12_1$ form even though they do not possess metal at the MIDAS. However, soaking experiments were unsuccessful in forming a complex with the αM I domain.

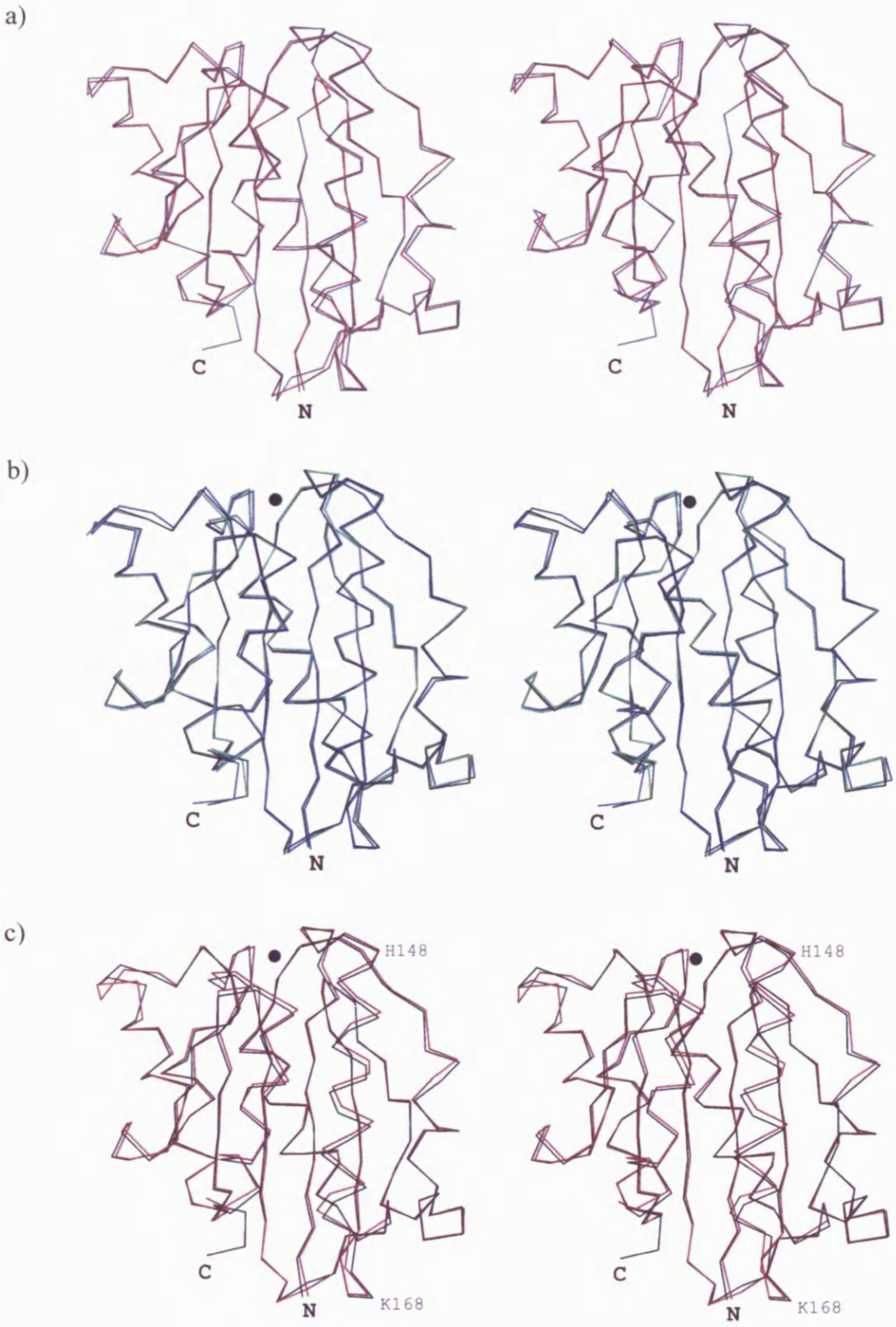

Figure 3.7 Stereo diagrams of the Cα superimpostions of the different crystal forms of the closed αM I domains. (a) shows the crystal forms, $P2_12_12_1$ (red) and $P2_12_12$ (grey), without metal , (b) the crystal forms C2 (blue), $P2_1$ (black) and $P2_12_12$ (green) with metal and (c) a comparison of the crystal forms with and without metal. The N- and C-termini are labelled and the metal at the MIDAS is represented as a black sphere. The first residues of helix 1 (H148) and the second β sheet (K168) are labelled in (c).

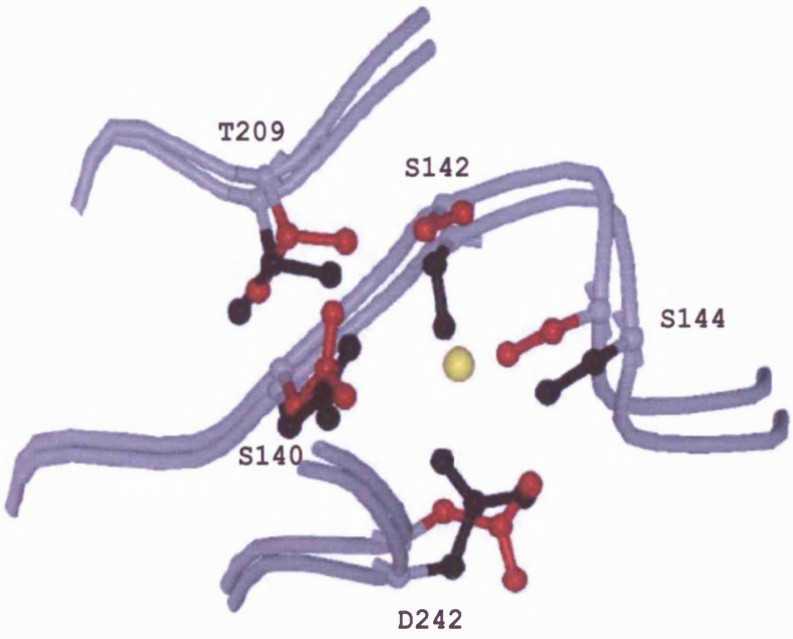

Figure 3.8 Superimposition of the MIDAS residue side chains of the crystal forms with and without metal, represented by the crystal forms C2 (black) and $P2_12_12_1$ (red) respectively. The Mg^{2+} in the C2 crystal form is represented as a yellow sphere and the Cα traces are shown as grey worms.

3.4 Discussion

3.4.1 αM I domain ligand binding and co-crystallisation trials

The recombinant αM I domain was found to be competent in binding the ligands, sICAM-1 and fragment D, which were to be used in co-crystallisation studies. The I domain bound fragment D with similar affinity to fibrinogen demonstrating that fragment D can entirely recapitulate the binding properties of fibrinogen for the interaction with the I domain. Cation-dependent binding was observed for sICAM-1, fibrinogen and fragment D indicating that binding is likely to be mediated through the MIDAS. The presence of Mg^{2+} was found to be optimal for ligand binding and consequently used in co-crystallisation experiments. Ca^{2+} was found to significantly reduce sICAM-1 and fibrinogen binding to the I domain. This may be explained by the very low binding constant, 1.2 mM, determined for Ca^{2+} binding to the isolated αM I domain (Baldwin *et al.*, 1998). As demonstrated in figure 3.4, the interaction of the I domain with fragment D exhibited a slightly different preference for cation. The highest affinity was displayed in the presence of excess Mg^{2+}, however, unlike the other ligands, more binding was observed with Ca^{2+} than with Mn^{2+}. The increased I domain affinity for fragment D in the presence of Ca^{2+} is likely to be merely a consequence of the increased stability of fragment D. Two of the three high affinity Ca^{2+} sites in fibrinogen are located in the γ C-terminal domains of fragment D and these sites need to be fully occupied to maintain the integrity of the conformation (Doolittle *et al.*, 1998). Unlike the isolated fragment D, fibrinogen does not require calcium for stability (Dr. R.F. Doolittle, University of California, San Diego, personal communication) explaining why this effect was not observed with fibrinogen.

Co-crystallisation trials with all the ligands available were unsuccessful in

producing an αM I domain-ligand co-crystal. It was recently suggested that deletion of the N-terminal extension of the αM I domain, 16 residues N-terminal to G127, locked the I domain in the low affinity state (Xiong *et al.*, 2000). The αM I domain used in the co-crystallisation studies was truncated to remove these N-terminal residues which would otherwise inhibit crystal growth. However, surface plasmon resonance studies demonstrated that truncation of the αM I domain used in these studies did not affect ligand binding. Additionally, other data have shown ligand binding to αM I domains with N-terminal truncations (Li *et al.*, 1998; Ugarova *et al.*, 1998; Yakubenko *et al.*, 2001). It can therefore be concluded that the inability of the I domain to co-crystallise with ligands was not due to the truncation at the N-terminus.

It is much more likely that the I domain was unable to form a crystalline complex with ligand due to only a small population (10%) of the I domain being present in the open high affinity state (Li *et al.*, 1998). This low affinity correlates with the equilibrium constants measured by surface plasmon resonance and the inability of the proteins to adhere during the size exclusion chromatography procedure. The presence of uncomplexed I domain crystals from the co-crystallisation trials with every ligand would also be expected if 90% of the I domain molecules were ligand-free prior to crystallisation.

Although the main reason for the failure of the co-crystallisation trials with peptide would have been due to the majority of I domain molecules being in the closed state, the peptides may not have recapitulated the important binding determinants of their respective ligands. The fibrinogen ligand , P2, which was reported to display the highest inhibitory activity of the two fibrinogen peptides was shown to bind the βD-α5 loop and adjacent helix 5 (Yakubenko *et al.*, 2001). These regions do not involve the MIDAS and the authors report the interaction of P2 with the I domain to be cation-independent. Moreover, the peptide does not contain an acidic residue which would mediate the interaction with metal at the MIDAS. However, the studies here

demonstrate that the interaction of fibrinogen and fragment D with the αM I domain is cation-dependent, indicating that this peptide does not represent a major recognition site for the I domain. It is also interesting to note that several regions of the I domain have been identified as binding sites for fibrinogen, as described in section 3.1.1.2. These data along with the absence of the classical RGD motif displayed by integrin ligands suggests that fibrinogen probably has a large recognition site which spreads over the I domain. The fibrinogen peptides, P1 and P2, would not supply sufficient binding energy to form a stable complex with the I domain if the additive binding energy of all the interactions in the large binding interface is important for the complex to form.

3.4.2 αM I domain crystal forms

Six different crystal forms of the αM I domain were identified from these trials. Only one of these crystal forms, $P4_3$, adopted the open conformation. This provides additional support for the hypothesis that the open conformation of the isolated αM I domain relies critically on the ligand-mimetic glutamate crystal contact that interacts with the MIDAS (Lee *et al.*, 1995a). It is of interest to note that two of the six crystal forms, $P2_12_12_1$ and $P2_12_12$ (a), did not show density for metal at the MIDAS even when excess Mg^{2+} was soaked into the crystals. A simulated annealing omit map, calculated by omitting all of the residues within a 5 Å sphere from the expected cation position, did not reveal any electron density feature that could correspond to the bound cation. Examination of these closed structures within the crystal lattice in comparison to the other closed crystal forms revealed two observations. Firstly, along with the movement of the MIDAS residues, as illustrated in figure 3.8 , the width of the MIDAS, as judged by the distance between the side chain oxygen atoms of S144 and T209, dictated the metal coordination that is possible. Table 3.7 shows the MIDAS widths of the different crystal forms to illustrate this point.

Space group	Conformation	Metal bound	MIDAS width (Å)
$P4_3$	Open	Mg^{2+}	4.3
C2	Closed	Mg^{2+}	6.1
$P2_1$	Closed	Mg^{2+}	5.9
$P2_12_12$(b)	Closed	Mg^{2+}	5.8
$P2_12_12$(a)	Closed	None	5.0
$P2_12_12_1$	Closed	None	4.9

Table 3.7 Width of the MIDAS in the different crystal forms of the αM I domain

The αL I domain has also been crystallised in the closed conformation with and without metal bound (Qu & Leahy, 1996). It is interesting to note that the width of the MIDAS with metal bound is 5.8 Å and 4.8 Å when metal is absent, similar to that observed here for the closed αM I domain. Secondly, superimposition of the closed crystal structures, as illustrated in figure 3.7c, showed that helix 1 undergoes ~1 Å upwards movement in the two structures without metal compared to the three structures with metal. This movement appears to be a consequence of crystal contacts with helix 1. Residues of helix 1 in the $P2_12_12_1$ crystal form make contacts in the crystal lattice with regions of helix 1, 3 and the loop region between helix 3 and 4 in an adjacent symmetry-related molecule. The other crystal form without a bound metal, $P2_12_12$ (a), also displays a crystal contact involving helix 1 in the crystal lattice. This interaction is between the end of helix 1 and residues in the middle of a symmetry-related helix 7. The movement of helix 1 has pushed the adjacent S144 further into the MIDAS pocket by ~1 Å, narrowing the width of the MIDAS. The side chains of D242 and S142, which directly coordinate the metal in the closed conformation, rotate away from the MIDAS due to steric hindrance. Metal would therefore be unable to bind the MIDAS in these crystal forms. It was also concluded that the absence of metal at the MIDAS of the closed αL I domain crystal structure was due to crystal contacts (Qu & Leahy, 1996). These crystal contacts resulted in a ~1 Å shift of S141, the homologue of S144 in the

αM I domain, narrowing the MIDAS in a similar manner to that of the αM I domain without metal bound. The two different crystal forms without bound metal are very similar with an rmsd for the Cαs of only 0.25 Å. They also display the same conformational changes at the MIDAS and in helix 1. It may therefore be concluded that the metal-free MIDAS is of some significance. The ability of the I domain to crystallise in the absence of metal may reflect the relatively weak binding of metal to the domain in the absence of ligand. A low binding constant of 555 μM has been calculated for Mg^{2+} binding to the isolated αM I domain (Baldwin *et al.*, 1998). The energy required for metal binding is therefore likely to be small compared with typical crystal lattice energies. These new crystal forms also reflect a degree of plasticity at the MIDAS and adjacent helix 1. The new crystal forms indicate that metal is not required to stabilise the tertiary structure of the αM I domain closed conformation. Metal ions are unlikely to regulate I domain adhesion as the extracellular Mg^{2+} concentration in the blood is millimolar, much higher than the calculated Mg^{2+} binding constant for the αM I domain (Baldwin *et al.*, 1998). The main role for metal in the α subunit I domains is likely to be only in the open conformation as a structural bridge to the ligand.

In conclusion, the results of the co-crystallisation trials demonstrate that the αM I domain would need to be stabilised in the open high affinity state in order to form a stable complex with ligand. Generation of a high affinity mutant for subsequent co-crystallisation trials is the subject of the next chapter.

Chapter 4: Designing the open high affinity conformation of the αM I domain

4.1 Introduction

Integrins switch from a low to a high affinity state in response to cell activation signals. The I domain has been shown to adopt a closed and open state, with low and high affinity for ligand, respectively (Lee *et al.*, 1995a; Li *et al.*, 1998; Oxvig *et al.*, 1999; Emsley *et al.*, 2000). Consequently, the recombinant I domain in solution is thought to be in dynamic equilibrium between the open and closed conformations. It was demonstrated that only 10% of the αM I domain in solution is in the open conformation (Diamond & Springer, 1993; Simon *et al.*, 1997; Li *et al.*, 1998). As attempts to crystallise the αM I domain in complex with ligand were unsuccessful, mutants were designed to shift the equilibrium so all of the I domain molecules were in the open state. This would enhance ligand binding in solution and eliminate the contamination of unliganded I domain molecules in co-crystallisation trials.

Different single and multiple residue mutations were reported to produce the open high affinity form of the αM I domain, prior to and during the course of these studies (Zhang & Plow, 1996, Li *et al.*, 1998; Oxvig *et al.*, 1999; Shimoaka *et al.*, 2000; Xiong *et al.*, 2000). However, it was unclear as to which mutant, if any, had successfully shifted the equilibrium to produce a constitutively high affinity I domain. For example, the αM I domain mutants displayed different magnitudes of activation compared to WT. Cell adhesion assays using the same mutant demonstrated varying degrees of activation depending on the type of cells used. In addition, the effect of some

of these mutations were not investigated in the isolated I domain. These gain-of-function mutants are briefly discussed below;

A number of mutations at the bottom of the domain, distal to the MIDAS were shown to be activating (Zhang & Plow, 1996; Oxvig *et al.*, 1999). The activating mutations were located in the interface between the I domain and the β-propeller. It was proposed that the mutations weakened the quaternary constraints that hold the I domain in the low affinity state, mimicking the physiological mechanisms of inside-out signalling. These studies were carried out using mutated I domains within the αMβ2 heterodimer. The I domain is structurally linked to the β-propeller (Springer, 1997) so these effects are likely to be influenced by the interdomain interactions of the heterodimeric receptor. It is therefore not known how these mutations would alter ligand binding affinity for the isolated I domain or if the allosteric regulation is intrinsic to the I domain.

Another study mutated a number of residues within the hydrophobic core of the αM I domain, filling in the cavities to prevent repacking of the core to form the closed state (Shimaoka *et al.*, 2000). An increase in ligand binding of 3-fold compared to WT was demonstrated in different cell lines using the mutated I domain in the intact receptor. Two other studies targeted specific residues (Li *et al.*, 1998; Xiong *et al.*, 2000). Li *et al.* mutated F302, which is buried in the αM I domain closed conformation but becomes solvent exposed in the open conformation. It was proposed that introduction of a bulky residue, such as tryptophan, to this position would prevent residue 302 from burying into the hydrophobic core thereby favouring the I domain to adopt the open conformation. Li *et al.* reported a 2.5-fold increase in the proportion of open conformation but this study also produced a confusing result as surface plasmon resonance studies revealed a similar dissociation constant (K_D) for the WT and mutant αM I domain. Xiong *et al.* suggested that the open conformation could be generated by deletion or mutation of I316, which is stabilised by a hydrophobic pocket in the closed

state. Introducing the I316G mutated I domain into the αMβ2 heterodimer produced a 5-fold increase in iC3b binding in COS cells.

The main objective of this research was to obtain a crystal structure of the αM I domain complexed with a physiological ligand, such as fragment D from fibrinogen or sICAM-1. These co-crystallisation trials would be aided by an engineered high affinity I domain. It would be necessary to detect high affinity ligand binding to the recombinant mutant I domain in solution prior to co-crystallisation. The aim of the work in this chapter was to introduce a mutation or minimal number of mutations into the αM I domain to lock the I domain in the open conformation. The mutant I domains would be ranked by ligand binding affinity using surface plasmon resonance studies, and K_D values determined for the most interesting mutants. High affinity mutants would be used in crystallisation studies to probe the structural basis for their functional properties and to determine a co-crystal structure with ligand. Two strategies for designing high affinity mutants were used. Firstly, three previously published single residue mutants were used to test their effect in the isolated I domain. Double mutants were also generated from these mutations in an attempt to further increase the binding capacity of the I domain. The second approach was to engineer a disulphide bond into the I domain, tethering the mobile C-terminal helix in an appropriate position to stabilise the open conformation. The experimental approach of fixing a protein in a particular conformation via an engineered disulphide bond has been previously successful with rhodopsin (Yu *et al.*, 1999).

4.2 Materials and methods

4.2.1 Structure-based design of intramolecular disulphide bond engineering

The coordinates of the αM I domain open and closed conformations, PDB accession codes 1IDO and 1JLM respectively, were superimposed using the program LSQKAB within the CCP4 suite (CCP4, 1994). The superimposed molecules were visualised with Turbo-Frodo version 5.5 (Roussel & Cambillau, 1992) to identify candidate residues to be utilised in an intramolecular disulphide bond. Pairs of residues were chosen to be mutated to cysteines by their close proximity in the open conformation compared to that in the closed conformation. The first double cysteine mutant to be made used the WT N-terminal C128. As previous models for the αM I domain did not contain residues 128 to 131, it was predicted that these N-terminal residues would extend the loop below the first B-strand. The 10 Å downward movement of C-terminal helix in the open conformation would therefore place the C-terminus in close proximity to C128. The C-terminal residue, A318, was consequently mutated to cysteine to form a disulphide bond with C128, in an attempt to stabilise the I domain in the open state. Residues chosen to mutate to cysteines for subsequent mutants are shown in figure 4.1.

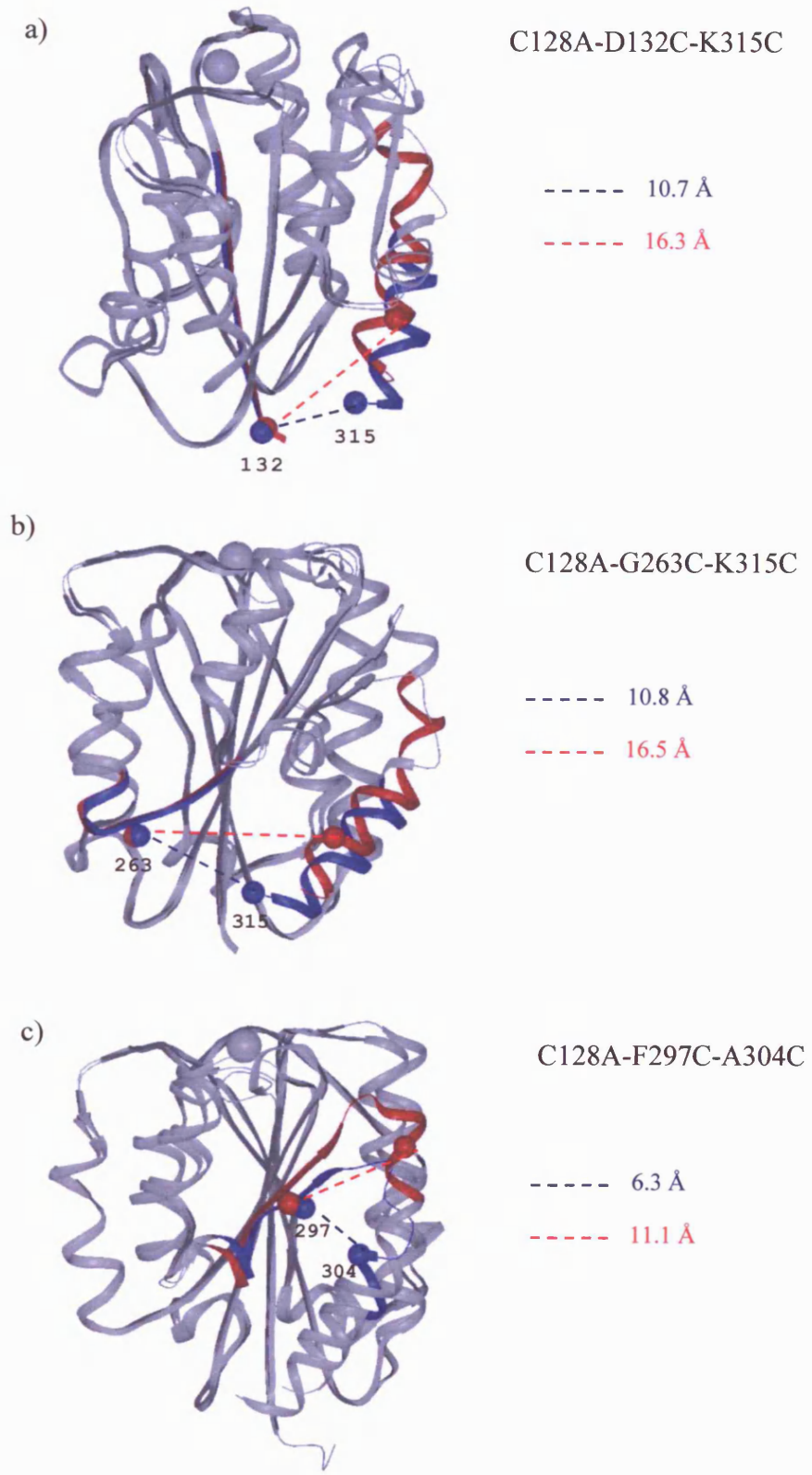

Figure 4.1 Superimpositions of the open and closed αM I domains to demonstrate the disulphide bond which would favour the stabilisation of the open conformation. Blue represents the open state and red the closed state with the metal at the MIDAS shown as a grey sphere. The Cα of the residues to be mutated to cysteines are represented as spheres and labelled in the open state. The distances between these Cαs are labelled with a dashed line.

4.2.2 Site-directed mutagenesis

Site-directed mutagenesis was carried out in the pGEX-2T vector as previously described in section 3.2.1. C128 was mutated to alanine in mutants that introduced two new cysteines into the I domain to prevent the formation of additional undesired disulphide bonds. The following primers were used:

C128A (forward) 5' GAG GCC CTC CGA GGG GCT CCT CAA GAG GAT AGT G 3'
(reverse) 5' C ACT ATC CTC TTG AGG AGC CCC TCG GAG GGC CTC 3'

C128A-D132C (forward) 5' GCT CCT CAA GAG TGT AGT GAC ATT GCC 3'
(reverse) 5' GGC AAT GTC ACT ACA CTC TTG AGG AGC 3'

L164F (forward) 5' ACT GTG ATG GAG CAA TTC AAA AAG TCC AAA ACC 3'
(reverse) 5' GGT TTT GGA CTT TTT GAA TTG CTC CAT CAC AGT 3'

G263C (forward) 5' GAG GCA GAC AGA GAG TGT GTC ATT CGC TAC G 3'
(reverse) 5' C GTA GCG AAT GAC ACA CTC TCT GTC TGC CTC 3'

F297C (forward) 5' CCT CGT GAT CAC GTG TGT CAG GTG AAT AAC TTT G 3'
(reverse) 5' C AAA GTT ATT CAC CTG ACA CAC GTG ATC ACG AGG 3'

F302W (forward) 5' TTC CAG GTG AAT AAC TGG GAG GCT CTG AAG ACC 3'
(reverse) 5' GGT CTT CAG AGC CTC CCA GTT ATT CAC CTG GAA 3'

A304C (forward) 5' GTG AAT AAC TTT GAG TGT CTG AAG ACC ATT CAG 3'
(reverse) 5' CTG AAT GGT CTT CAG ACA CTC AAA GTT ATT CAC 3'

E314R-K315C (forward) 5' CAG AAC CAG CTT CGG AGG TGT ATC TTT GCG ATC G 3'
(reverse) 5' C GAT CGC AAA GAT ACA CCT CCG AAG CTG GTT CTG 3'

K315C (forward) 5' AAC CAG CTT CGG GAG TGT ATC TTT GCG ATC GG 3'
(reverse) 5' CC GAT CGC AAA GAT ACA CTC CCG AAG CTG GTT 3'

I316G (forward) 5' CAG CTT CGG GAG AAG AGG TTT GGG ATC GGA TCC C 3'
(reverse) 5' G GGA TCC GAT CCC AAA CCT CTT CTC CCG AAG CTG 3'

A318C (forward) 5' CGG GAG AAG ATC TTT TGC ATC GGA TCC CCG GG 3'
(reverse) 5' CC CGG GGA TCC GAT GCA AAA GAT CTT CTC CCG 3'

The following mutant αM I domain constructs were made to be used in functional and structural analyses: L164F, F302W, I316G, A318C, L164F-F302W, L164F-I316G, F302W-I316G, C128A-D132C-K315C, C128A-F297C-A304C, C128A-G263C-K315C, C128A-D132C-E314R-K315C.

4.2.3 Expression and purification of WT and mutant αM I domains

The WT and mutant αM I domains were expressed and purified as previously described in section 3.2.2. The WT I domain and mutant I domains, except for the double cysteine mutants, were iodoacetylated as in section 3.2.3. After trypsin cleavage, the double cysteine mutants which were unable to spontaneously form intramolecular disulphide bonds were concentrated to ~20 μM and incubated with 0.1 mM $CuSO_4$ and 0.1 mM *o*-phenanthroline to promote disulphide bond formation (Lee *et al.*, 1994). The oxidation reaction was allowed to proceed for 4 hours with rocking at room temperature.

4.2.4 αM I domain characterisation

Prior to crystallisation and surface plasmon resonance studies, all αM I domain samples were analysed on a 24 ml Superdex S75 gel filtration column HR 10/30 (Pharmacia, Piscataway, NJ) to monitor monomer formation. The S75 running buffer

(20 mM Hepes pH 7.5, 150 mM NaCl, 5 mM $MgCl_2$) was filtered through a 0.22 μm membrane and degassed. Protein samples were dialysed into S75 running buffer and then filtered. The column was equilibriated with two column volumes (48 ml) of S75 running buffer at a flow rate of 0.5 ml/min and 100 μl (between 0.2 and 1 mg) sample injected per run. 1.25 column volumes (30 ml) were allowed to flow through the column at a flow rate of 0.5 ml/min to elute the protein and 1 ml fractions were collected. A standard curve (log molecular weight vs elution volume) was generated from the elution profile of thyroglobulin (670 kDa), γ-globulin (158 kDa), ovalbumin (44 kDa), myoglobin (17 kDa) and vitamin B12 (1.35 kDa) to allow molecular weight estimation of the experimental proteins eluted.

4.2.5 5, 5' dithio-bis (2-nitrobenzoic acid) (DTNB) titration

Disulphide formation in mutants, which eluted as a single monomeric peak on a gel filtration column, was determined by titration against DTNB. Free sulphydryl groups can be detected with DTNB by the production of the fluorescent thionitrobenzoate molecule, as shown in figure 4.2.

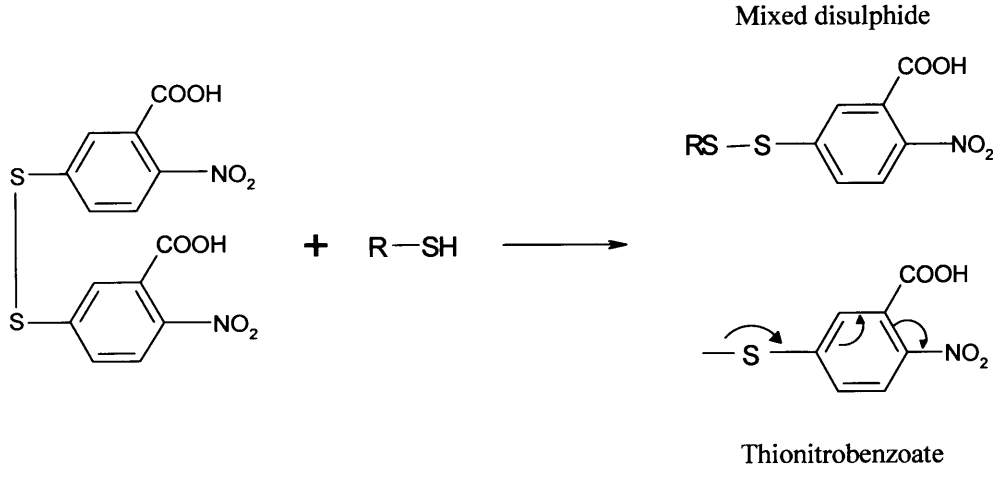

Figure 4.2 Diagram showing the reaction of DTNB with a protein containing a free cysteine.

Thionitrobenzoate absorbs at 412 nm with a molar extinction coefficient of 13600 $M^{-1}cm^{-1}$. L-cysteine, ranging from 1.5 to 100 μM, was used to generate a standard curve for calibration and all αM I domain samples were titrated at a concentration of 10 μM. All samples, in duplicate, were diluted in 990 μl 20 mM Tris-HCl, 6 M guanidinium hydrochloride, pH 8.0. 10 μl 0.1 M DTNB, dissolved in DMSO, was added at 30 s intervals to each sample so that each reaction could proceed for the same amount of time. After 10 minutes at room temperature, the samples' absorbances were measured at 412 nm. Each reaction was blanked against 20 mM Tris-HCl, 6 M guanidinium hydrochloride, pH 8.0. The number of free cysteines for the αM I domain could then be determined from the L-cysteine calibration curve.

4.2.6 Crosslinking the A318C αM I domain mutant

Homobifunctional, sulphydryl-reactive crosslinkers of different spacer arm lengths, as shown in figure 4.3, were used to crosslink the cysteine residues in the A318C αM I domain mutant. Bismaleimidohexane (BMH), 1,4-bismaleimidyl-2,3,-dihydroxybutane (BMDB), bis-maleimidoethane (BMOE) were purchased from Pierce (Rockford, Illinois) and dibromobimane (bBBr) from Molecular Probes (Eugene, OR). The crosslinking protocols were based on the manufacturers instructions. Prior to addition of cross-linker, the A318C αM I domain was incubated at room temperature with 1 mM DTT for two hours. The protein was dialysed extensively into 20 mM Hepes, 150 mM NaCl, 5 mM EDTA, pH 7.0 at 4°C to remove DTT and adjust the pH and buffer conditions to the optimum for the crosslinking reaction. The I domain concentration was adjusted to 25 μM for each crosslinking reaction and each crosslinker was dissolved in DMSO at 20 μM. A 10-fold molar excess of crosslinker was incubated with I domain samples for 2 hours at room temperature avoiding exposure to light. The

reactions were quenched with a 5-fold excess of β-mercaptoethanol over crosslinker. Each reaction was then dialysed extensively at 4°C to remove β-mercaptoethanol and excess crosslinker. Introduction of the crosslinkers, BMH, BMOE and BMDB, into the I domain was assessed by matrix-assisted laser adsorption/ionisation-mass spectroscopy. The reaction of the I domain cysteines with bBBr was monitored by spectrophotometric measurements. bBBr develops a new absorption maxima at 392 nm with a molar extinction coefficient of 5700 $M^{-1}cm^{-1}$ when both of its alkylating groups have reacted with two sulphydryl groups.

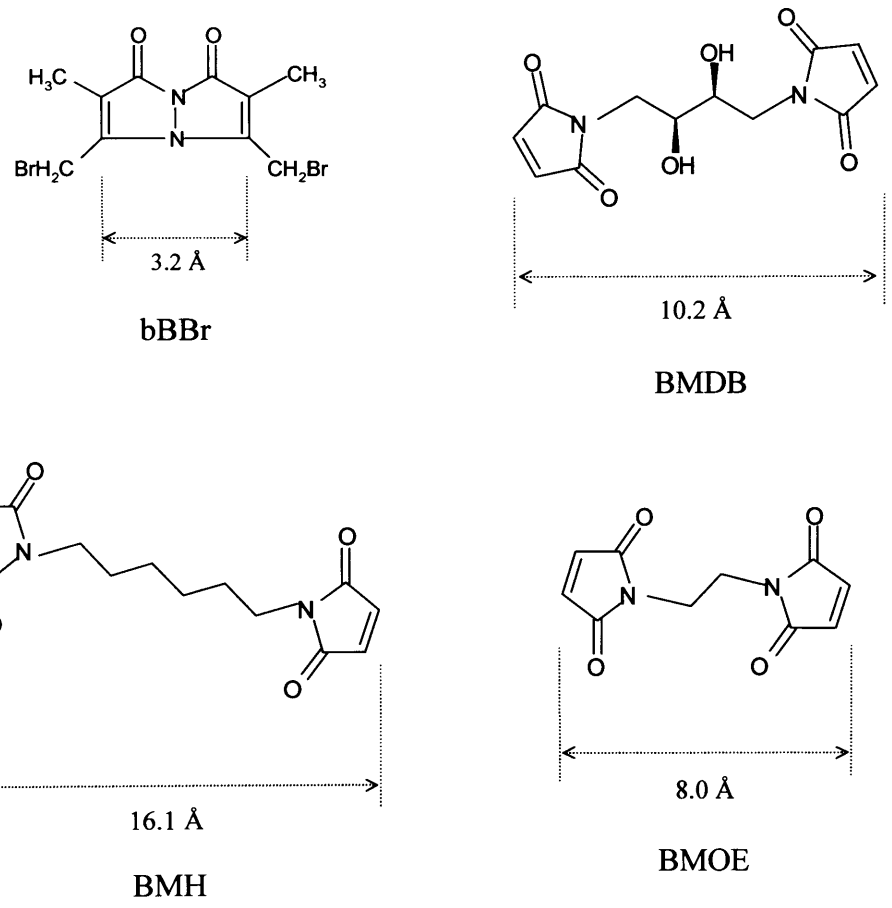

Figure 4.3 The crosslinkers used to substitute for the disulphide bond in the A318C αM I domain mutant. The length of each crosslinker is shown for each structure.

4.2.7 Surface plasmon resonance studies

Surface plasmon resonance studies with the mutant αM I domains were carried as previously described in section 3.2.5. Briefly, between 200 and 1000 RU of fibrinogen, fragment D and sICAM-1 were immobilised onto a B1 Pioneer chip by amine coupling. The remaining flow cell was activated and blocked and used as a reference surface. Interactions with fibrinogen and sICAM-1 were measured in Biacore buffer, 20 mM Hepes, 150 mM NaCl, 0.005% (v/v) polysorbate 20, 5 mM $MgCl_2$, pH 7.5. Fragment D requires the presence of calcium for stability so the interaction of fragment D with the mutant I domains was analysed in Biacore buffer with the addition of 1 mM $CaCl_2$. All mutant αM I domains were purified by gel filtration, dialysed into running buffer and filtered prior to being flowed over the chip surface. Analytes were initially tested for binding with a 1 minute injection at 20 μl/min and a 10 μM analyte concentration. The equilibrium dissociation constants for the interactions were calculated, as previously described, using steady state binding with a range of 6 different analyte concentrations.

4.2.8 Crystallisation trials

The purified mutant αM I domains, A318C, oxidised C128A-D132C-K315C, oxidised C128A-D132C-E314R-K315C and reduced C128A-D132C-K315C were dialysed into 20 mM Tris, 100 mM NaCl, 5 mM $MgCl_2$, pH 7.5 and concentrated to 10 mg/ml in an Amicon stirred cell with a YM10 membrane (Millipore, Bedford, MA). Crystallisation trials were set up as described in section 3.1.7.1.

Crystals of A318C αM I domain grew from 22-30% (w/v) PEGMME 2000, 0.2 M ammonium sulphate, 0.1 M sodium acetate, pH 4.6 at 4°C. Typically, the crystals grew after 5 days as plates with typical dimensions of 0.3 mm x 0.1 mm x 0.05 mm.

Crystals of the reduced form of C128A-D132C-K315C grew from 0.2 M NaCl, 20% PEG 3000, 0.1 M Hepes, pH 7.5 at room temperature. Crystals grew as stacked plates within one week with dimensions of 0.1 mm x 0.05 mm x 0.01 mm.

4.2.9 Data collection and processing

Data from the A318C αM I domain crystals were collected on beamline 7-1 (λ = 1.08 Å) at the Stanford Synchrotron Radiation Laboratory. A crystal was soaked in reservoir buffer containing 15% (v/v) glycerol and flash frozen in a cryo-stream of nitrogen at 100 K. A data set to 1.25 Å resolution was collected using a 345 mm diameter MAR image plate, with a crystal to detector distance of 120 mm, an exposure time of 90 s and an oscillation range of 1.0° per frame. Due to the number of overloaded reflections at low resolution, an additional data set was collected with the same crystal. The second data set was collected to 2.5 Å resolution with the smaller 180 mm diameter MAR image plate using a larger crystal to detector distance of 190 mm, an exposure time of 10 s and an oscillation range of 1.0° per frame.

The data were processed as described in section 3.2.8.4. using DENZO and SCALEPACK. The crystal belonged to the $P2_12_12_1$ space group with unit cell dimensions a = 38.6 Å, b = 51.0 Å, c = 102.4 Å and a mosaicity of 0.3°. The asymmetric unit contained one molecule with a solvent content of 43.5% (v/v). Data processing statistics are shown in table 4.1.

Resolution shells (Å)	Unique reflections	Total measurements	Completeness (%)	I/σI	R_{merge} (%)
20.00-3.39	3054	17717	98.9	51.7	2.1
3.39-2.69	2869	14159	97.7	42.4	3.3
2.69-2.35	2824	11231	97.5	37.5	4.4
2.35-2.14	2764	10471	96.9	34.5	5.0
2.14-1.98	2759	8875	96.0	31.6	5.0
1.98-1.87	2713	7545	95.3	30.0	3.6
1.87-1.77	2725	7485	96.1	26.3	4.1
1.77-1.70	2715	7439	95.8	22.9	4.7
1.70-1.63	2709	7374	95.4	19.7	5.4
1.63-1.57	2678	7365	94.8	17.3	6.2
1.57-1.53	2652	7261	94.1	15.5	6.7
1.53-1.48	2647	7282	94.0	12.9	8.1
1.48-1.44	2661	7263	94.3	9.9	9.9
1.44-1.41	2632	7203	93.6	7.8	12.5
1.41-1.38	2626	7118	94.6	6.8	14.6
1.38-1.35	2642	7146	93.6	5.7	16.7
1.35-1.32	2594	7045	91.9	5.1	18.7
1.32-1.29	2562	6945	91.5	4.6	20.3
1.29-1.27	2492	6693	89.7	4.1	21.8
1.27-1.25	2503	6569	89.4	3.4	25.0
20.00-1.25	53821	170186	94.6	43.9	2.7

Table 4.1 Data collection statistics for the A318C αM I domain mutant crystal. R_{merge} (%) = 100 x $\sum_h\sum_j |I_{hj} - I_h| / \sum_h\sum_j I_{hj}$ where I_h is the weighted mean intensity of the symmetry related reflections I_{hj}.

Crystal surgery was first performed on the stacked reduced C128A-D132C-K315C αM I domain crystals to isolate a single crystal for data collection. The isolated crystal was soaked in reservoir buffer containing 15% (v/v) glycerol and flash frozen in a cryo-stream of nitrogen at 100 K. Data were collected 'in-house' with an RU200 HB X-ray generator using a copper target (Cu Kα 1.542 Å wavelength) with focusing

mirrors and a Rigaku Raxis4 imaging plate. The data set was collected to 2.5 Å resolution with a crystal to detector distance of 200 mm, an exposure time of 20 minutes and an oscillation range of 1.0° per frame.

The reduced C128A-D132C-K315C αM I domain crystals belonged to the $P4_3$ space group with unit cell dimensions a = 44.2 Å, c = 99.9 Å with a typical mosaicity of 1.0°. The asymmetric unit contained one molecule with a solvent content of 41.6% (v/v). Data processing statistics are shown in table 4.2.

Resolution shells (Å)	**Unique reflections**	**Total measurements**	**Completeness (%)**	**I/σI**	**R_{merge} (%)**
20.00-5.35	601	1443	89.7	20.4	6.5
5.35-4.26	634	1504	95.2	20.6	6.3
4.26-3.73	609	1443	94.0	17.8	8.1
3.73-3.39	597	1413	93.9	14.0	9.5
3.39-3.15	626	1458	95.3	9.7	12.3
3.15-2.96	635	1469	97.4	7.0	15.2
2.96-2.81	639	1488	97.6	5.7	19.7
2.81-2.69	638	1495	97.7	4.4	22.7
2.69-2.59	608	1411	97.0	3.6	30.5
2.59-2.50	647	1507	97.6	2.9	34.7
20.00-2.50	6234	14631	95.5	10.7	11.1

Table 4.2 Data collection statistics for the reduced C128A-D132C-K315C αM I domain mutant crystal. R_{merge} is defined in the legend for table 4.1.

4.2.10 Molecular replacement

Molecular replacement was carried out using AMoRe (CCP4, 1994) as described in section 3.2.7.5. The closed conformation of the αM I domain (PDB accession code 1JLM) was used as a search model to find the molecular replacement solution for the A318C αM I domain mutant. The cross-rotation function gave one clear peak, as shown in table 4.3a. After applying the Euler angles from ROTING peak 1, a translation search revealed an unambiguous solution. A list of the 5 best solutions from the translation function are presented in table 4.3b. 10 cycles of rigid body refinement using TRAING peak 1 gave a final solution, with R factor of 34.4% and a correlation value of 68.8%, indicating an excellent initial fit to the data.

ROTING peak	α	β	γ	Peak height
1	178.96	92.85	302.57	25.3
2	253.63	93.62	122.57	19.4
3	175.39	36.46	304.32	19.1
4	29.53	53.64	129.36	18.3
5	172.47	83.62	105.46	17.9

TRAING peak	x	y	z	C	R (%)
1	0.3185	0.2606	0.3516	63.7	37.4
2	0.1557	0.2618	0.3512	41.8	45.8
3	0.3276	0.2615	0.1257	41.2	46.6
4	0.4790	0.2640	0.3510	40.7	46.5
5	0.3305	0.2624	0.3311	40.6	46.6

Table 4.3 Molecular replacement solutions for the A318C αM I domain. a) shows the 5 highest peaks for the rotation function and b) the 5 best translation function solutions. C is the standard linear correlation coefficient between the observed and calculated structure factor amplitudes defined as $C=[\sum_{hkl}(|F_{obs}|-<|F_{obs}|>)x(|F_{calc}|-<|F_{calc}|>)]/ [\sum_{hkl}(|F_{obs}|-<|F_{obs}>)^2x\sum_{h}(|F_{calc}|-<|F_{calc}|>)2]^{½}$. R (%) = $100\ x\sum_{hkl}|F_{obs}-F_{calc}| / \sum_{hkl} F_{obs}$ where F_{obs} is observed structure factor amplitudes and F_{calc} is the calculated structure factor amplitudes.

4.2.11 Crystallographic refinement

Initial refinement of the A318C mutant model was carried out using CNS version 1.0 (Brünger *et al.*, 1998), as previously outlined in section 3.2.8.6. Refinement was later completed using Shelx-97 (Sheldrick & Schneider, 1997). Throughout all refinement, the same 5% of reflections were excluded from the refinement to calculate the R_{free}, which was used as a guide for correct modelling and refinement without over-fitting. The progress of refinement is summarised in table 4.4. The model from AMoRe was first refined by simulated annealing to reduce any model bias. Phases were then calculated for the new model and used to generate F_{obs}-F_{calc} and 2 F_{obs}-F_{calc} maps. Maps and models were displayed with Turbo-Frodo version 5.5 (Roussel & Cambillau, 1992). The difference map generated after simulated annealing showed strong positive density for the N-terminal residues C128 to E131 and the mutated A318C at the C-terminus. These residues were built into the model and at this stage clear density for a disulphide bond of 2 Å was observed between residues 128 and 318. Addition of these residues followed by positional and B factor refinement greatly improved the quality of the maps and the R_{free} decreased by 3.5%. After further improvement of the model by addition of water molecules, extra density at the C-terminus was observed in the maps. Consequently, I319, G320 and S321 were added to the model and subsequent refinement decreased the R_{free} by 1.7%. When refinement within CNS was no longer significantly improving the R_{free} value, the refinement package SHELX was used. Each round of SHELX refinement comprised of 10 cycles of positional and B factor refinement. After initial B factor isoptropic refinement within this package, all atoms were made anisotropic for further B factor refinement. Due to this type of refinement, the number of parameters increases from 4 to 9 per atom, leading to the risk of over-fitting the data. In this case, the ratio of unique reflections: refinement parameters is 3.0 making this type of refinement justifiable. Anisotropic refinement resulted in a 3.6%

decrease in the R_{free} value. After further improvement of the model, alternative conformations of the side chains of S142, S172, R181, S197 and T209 were visable and subsequently added to the model. A final round of automated water picking was performed using alternate cycles of ARP (Lamzin & Wilson, 1997) within the CCP4 suite to pick waters followed by two cycles of anisotropic restrained refinement within SHELX. The stereochemical quality of the model was analysed using PROCHECK version 3.4.4 (Laskowski *et al.*, 1993). Waters with incorrect hydrogen-bonding partners were identified with XPAND version 1.3.1 (Kleywegt *et al.*, 2001) and subsequently deleted. Finally, hydrogens were added to the model within SHELX. Figure 4.4 shows a section of density for residues 232 to 236 of the A318C mutant before and after refinement.

The open conformation of the αM I domain (PDB accession code 1IDO) was used as a starting model for the refinement of the reduced C128A-D132C-K315C αM I domain data set. Alternate steps of manual model building and refinement within CNS, as previously described, was used to complete refinement. A summary of the steps used to refine these data is shown in table 4.5.

Round	Procedure	Refinement package	R_{work} (%)	R_{free} (%)
1	Simulated annealing	CNS	31.3	33.5
2	Manual modelling and minimisation refinement	CNS	29.9	31.6
3	B factor refinement	CNS	28.8	30.0
4	Water picking (127 waters)	CNS	26.1	29.2
5	Manual modelling and minimisation refinement	CNS	25.6	27.6
6	B factor refinement	CNS	25.5	27.5
7	Refinement of all parameters	SHELX	25.2	27.0
8	Anisotropic B factor refinement	SHELX	20.0	23.4
9	Manual modelling, addition of alternative conformations and refinement of all parameters	SHELX	18.9	23.0
10	Water picking (102 waters)	ARP (CCP4) and SHELX	17.6	22.7
11	Deletion of waters following PROCHECK analysis (18 waters), manual modelling and refinement of all parameters	SHELX	17.0	22.6
12	Addition of hydrogens	SHELX	16.6	22.3

Table 4.4 Model building and refinement statistics for A318C αM I domain. The solution from AMoRe was used as the initial model for these rounds of refinement. Refinement within CNS was carried out using data from 20 to 2 Å. Refinement with SHELX used data from 8 to 1.25 Å. Map inspection for each refinement round and model modification was performed with Turbo-Frodo. R_{work} (%) = 100 x $\sum_{hkl} | F_{obs} - F_{calc} | / \sum_{hkl} F_{obs}$ where F_{obs} and F_{calc} are the observed and calculated structure factors respectively. R_{free} (%) is the R_{work} (%) calculated

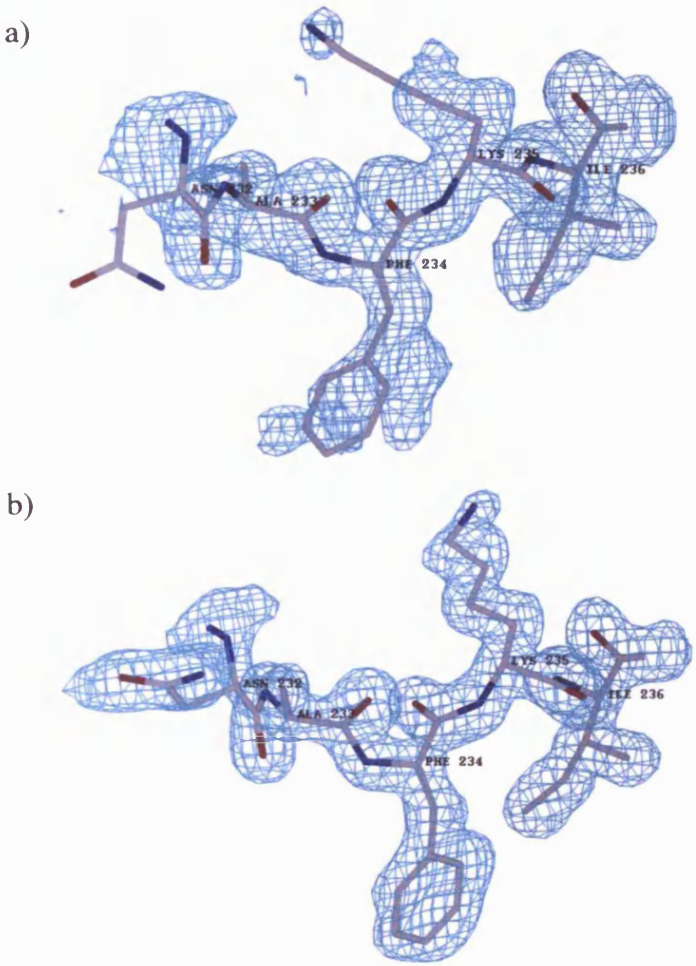

Figure 4.4 Part of the A318C αM I domain model superimposed onto the 2FoFc electron density map contoured at 1σ, using 8 to 1.25 Å resolution data, before (a) and after (b) refinement.

Round	Procedure	R_{work}	R_{free}
1	Rigid body refinement	31.2	36.9
2	Simulated annealing	28.0	33.8
3	Manual modelling and minimisation refinement	27.0	30.8
4	Manual modelling and minimisation refinement	25.5	29.6
5	B factor refinement	24.9	29.0
6	Manual modelling and B factor refinement	24.2	27.9
7	Manual modelling and B factor refinement	24.1	27.7

Table 4.5 Model building and refinement statistics for the reduced C128A-D132C-K315C αM I domain, using 20 to 2.5 Å resolution data. R_{work} and R_{free} are previously defined in the legend of table 4.4.

4.2.12 Quality of the model

Refinement statistics for the A318C αM I domain mutant are displayed in table 4.6. Density is present for residues A128 to S321 although fragmentary for the side chains of nine residues. There are no non-glycine residues in the disallowed region of the Ramachandran plot and 92.4% of main chain dihedral angles lie in the most favoured regions, with two residues in the generously allowed region. The Ramachandran plot for the A318C mutant is shown in figure 4.5.

Table 4.6 shows the refinement statistics for the reduced form of the C128A-D132C-K315C αM I domain. The model spans residues D132 to C318 and includes a magnesium ion at the MIDAS. Density is fragmentary for several side chains and the loop between the first α-helix and the second B-strand has particularly poor density. The Ramachandran plot shows that 89.3% of the main chain dihedral angles lie in the most favoured regions with one residue in the disallowed regions and one residue in the generously allowed regions.

	A318C	**C128A-D132C-K315C**
Protein atoms in asymmetric unit	1577	1486
Solvent atoms in asymmetric unit	229	0
Heterogen atoms in asymmetric unit	0	1 Mg^{2+}
R_{work} (%)	16.6	24.1
R_{free} (%)	22.3	27.7
Rmsd bond lengths (Å)	0.012	0.013
Rmsd bond angles (°)	2.30	1.71
Average B factor ($Å^2$)	29.2	22.9

Table 4.6 Refinement statistics for the A318C (8 to 1.25 Å resolution) and reduced C128A-D132C-K315C (20 to 2.5 Å resolution) αM I domain mutants. R_{work} and R_{free} are previously defined in the legend of table 4.4.

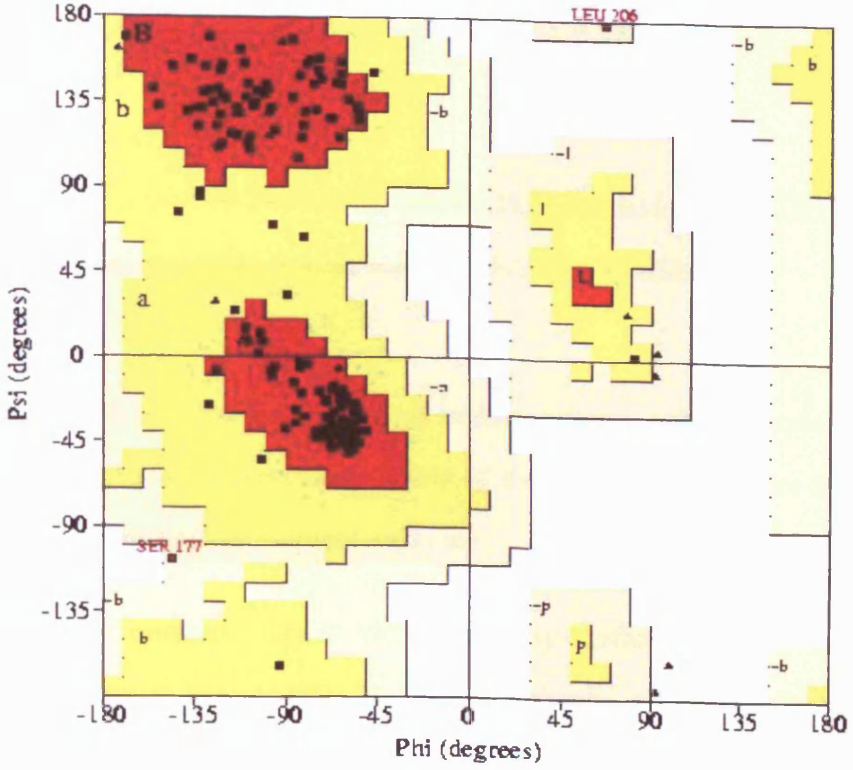

Plot Statistics

Residues in most favoured regions (A, B, L)	158	92.4%
Residues in additional allowed regions (a, b, l, p)	11	6.4%
Residues in generousl allowed regions (-a, -b, -l, -p)	2	1.2%
Residues in disallowed regions	0	0.0%
	---	---
Number of non-glycine and non-proline residues	171	100.0%
Number of end residues (excl. Gly and Pro)	2	
Number of glycine residues (shown as triangles)	12	
Number of proline residues	9	

Total number of residues	194	

Figure 4.5 Ramachandran plot of the main chain dihedral angles for the A318C αM I domain mutant. Glycine residues are represented by triangles, while other residues are denoted by squares. The most favourable regions are shown in red with the disallowed regions in white. Additional allowed regions are coloured yellow and generously allowed regions are progressively darker shades of yellow.

4.3 Results

4.3.1 Surface plasmon resonance studies with the L164F, F302W, I316G, L164F-F302W, L164F-I316G, F302W-I316G αM I domain mutants

Expression and purification of all of the mutants, with the exception of I316G, were comparable to WT. Expression levels of the mutant I316G were too low to purify sufficient protein for any subsequent analyses.

The αM I domain mutants were tested by surface plasmon resonance to rank their binding affinities against WT. The relative change in binding compared to WT for the three ligands was similar for each mutant analysed. Incubation of each mutant with 10 mM EDTA significantly reduced ligand binding, similar to that of WT, indicating cation-dependent ligand binding (data not shown). Figure 4.6 shows the sensorgram overlays of the mutant and WT αM I domains binding to sICAM-1. All αM I domain mutants demonstrated an increase in ligand binding compared to WT. However, the largest increase in affinity, displayed by the I316G-L164F mutant, was only about 4-fold.

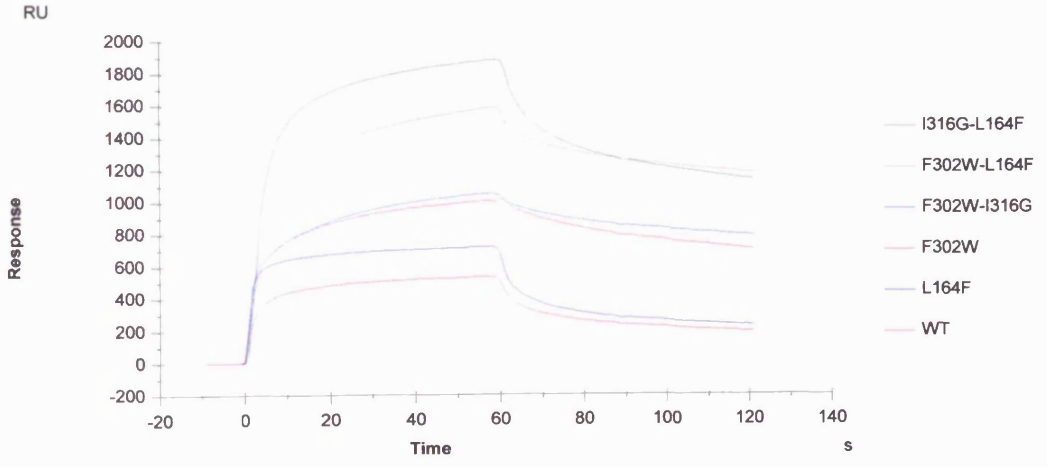

Figure 4.6 Sensorgram overlays of the L164F, F302W, I316G, L164F-F302W, L164F-I316G, F302W-I316G and WT αM I domains binding to sICAM-1.

4.3.2 Ligand binding properties of the A318C αM I domain mutant

The A318C mutant, which was designed to form a disulphide between residues 128 and 318, fixing the domain in the open conformation, eluted as a monomer on a gel filtration column. Free cysteines were not detected by titrating the A318C mutant against DTNB, demonstrating that an intramolecular disulphide bond had been made. Initial surface plasmon resonance studies revealed that the A318C mutant supported very poor binding to all of the ligands tested. Figure 4.7 illustrates the decrease in ligand binding affinity displayed by the A318C mutant compared to WT, using the ligand fibrinogen as an example.

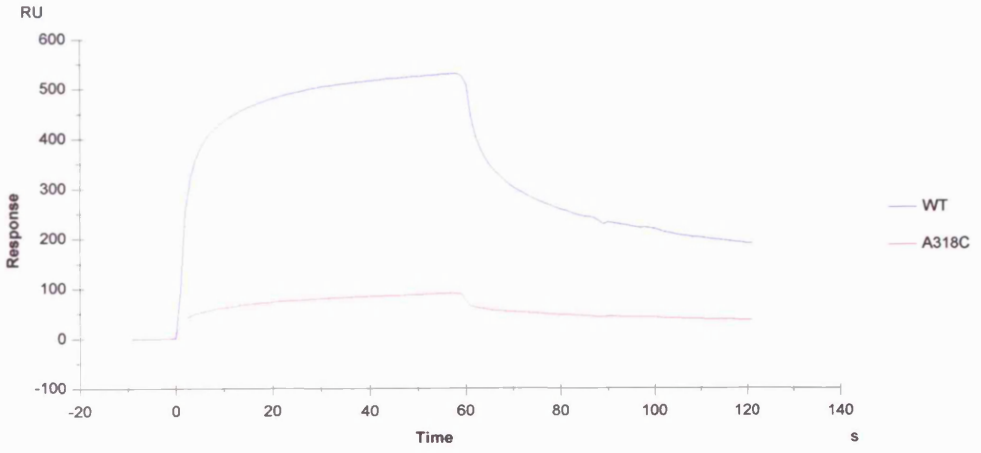

Figure 4.7 Sensorgram overlay of WT and the A318C mutant αM I domain binding to fibrinogen.

The K_D values from steady state analysis for the interaction of the A318C αM I domain with fibrinogen and sICAM-1 are presented in table 4.7, along with the WT values for comparison. The K_D value for the interaction of the A318C mutant with fragment D could not be measured as the addition of Ca^{2+} reduced ligand binding to a level that was too low to determine accurate measurements. A 5- to 6.5-fold decrease in

affinity was observed upon ligand binding to the A318C mutant.

	Fibrinogen K_D (μM)	D1-D5 ICAM-1 (μM)
A318C I domain	25.80 ± 2.60	31.67 ± 5.32
WT I domain	3.98 ± 0.86	6.45 ± 0.58

Table 4.7 K_D values calculated by surface plasmon resonance steady state analysis for the interactions of the A318C and WT αM I domains with fibrinogen and sICAM-1. K_D ± S.D. (n=3).

Incubating the A318C mutant with 10 mM DTT for 1 hour at room temperature increased affinity to the ligands, allowing the I domain to resume comparative WT binding. This is illustrated in figure 4.8, showing binding to fibrinogen as an example. The same reducing treatment with the WT αM I domain did not alter ligand binding (data not shown).

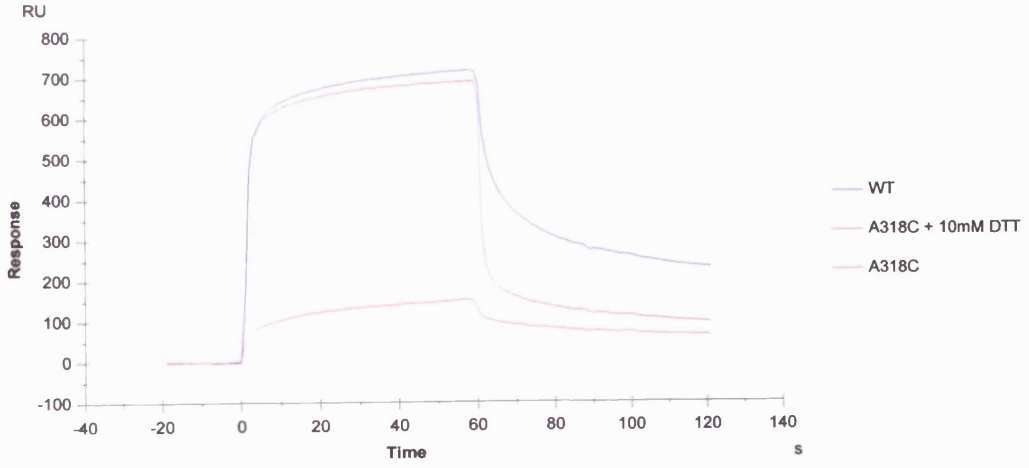

Figure 4.8 Sensorgrams demonstrating the effect of reducing the disulphide bond in the A318C αM I domain mutant.

4.3.3 Structure of the A318C αM I domain mutant

The crystal structure of the A318C αM I domain mutant, illustrated in figure 4.9, was determined to 1.25 Å resolution and displayed the typical conformation observed for all I domains crystallised in the closed conformation. The mutated A318C and disulphide bond between residues 128 and 318 can clearly be seen, as shown in figure 4.10. The disulphide bond links the C-terminal helix to a loop preceding the first β-strand. The A318C mutant crystallised in the same $P2_12_12_1$ space group as the WT αM I domain, described in chapter 3. Figure 4.11 shows the Cα superimposition of the A318C closed mutant and the WT closed conformation with the same $P2_12_12_1$ symmetry. The last four residues of the C-terminal helix can be seen to shift ~1 Å down towards the N-terminal cysteine to form the disulphide bond. The A318C mutant, similar to the WT I domain crystallised with the same symmetry, did not possess a metal bound at the MIDAS. Inspection of the pocket formed by the MIDAS revealed a peak of density, the strength and coordination of which were consistent with a water molecule. Addition of metal to the crystallisation buffer and soaking the crystals with 10 to 50 mM $MgCl_2$ did not result in metal binding at the MIDAS. The metal-coordinating residues at the MIDAS undergo the same conformational changes as that of the WT αM I domain crystallised with $P2_12_12_1$ symmetry, described in section 3.2.4. Figure 4.12 illustrates the conformational changes which occur at the MIDAS of the A318C mutant compared to that of the metal-bound WT closed conformation.

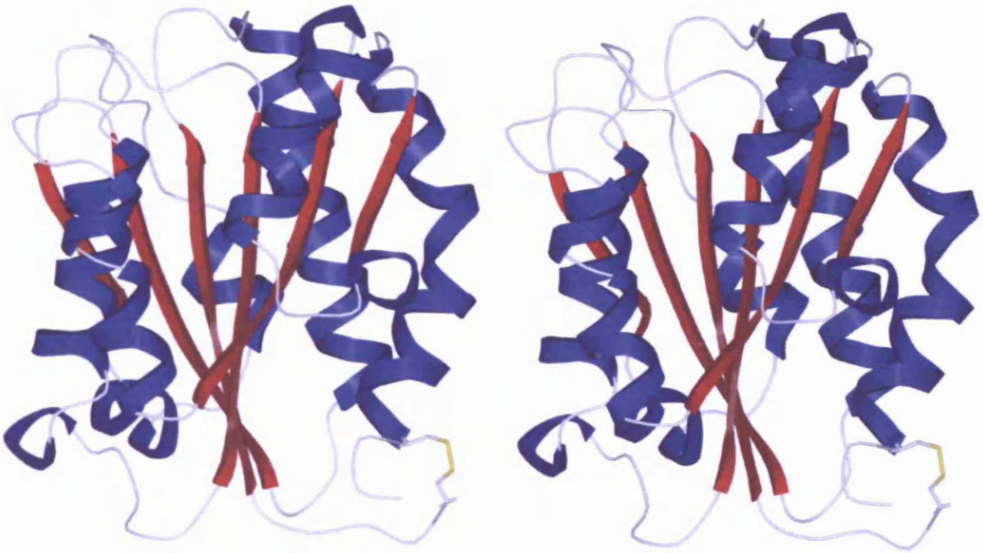

Figure 4.9 Stereo view of the A318C αM I domain mutant. β-strands are shown in red with α-helices in blue. The disulphide bond between residues 128 and 318 is represented in yellow.

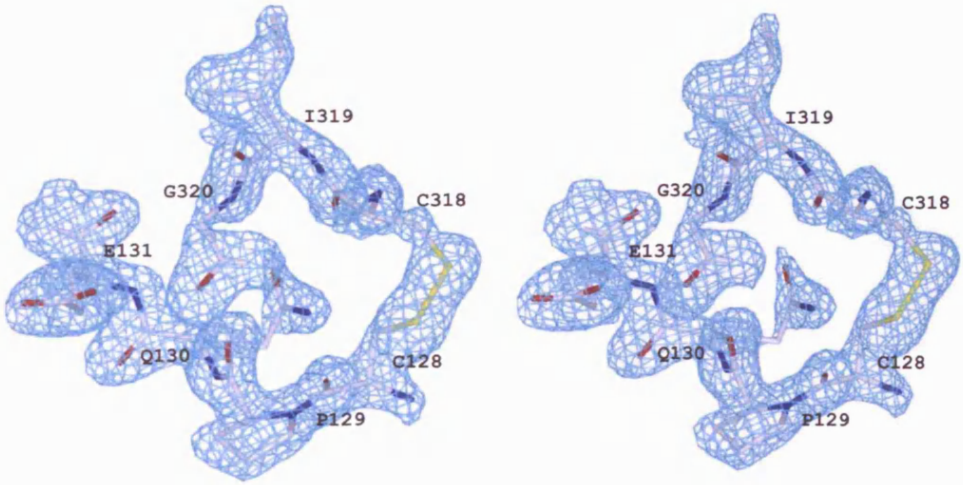

Figure 4.10 Stereo diagram of the disulphide bond between residues 128 and 318 in the A318C αM I domain mutant with the $2F_oF_c$ map, contoured at 1σ, superimposed, using 8 to 1.25 Å resolution data. Carbon atoms are coloured grey, oxygen atoms are red, nitrogen atoms are blue and sulphur atoms are yellow.

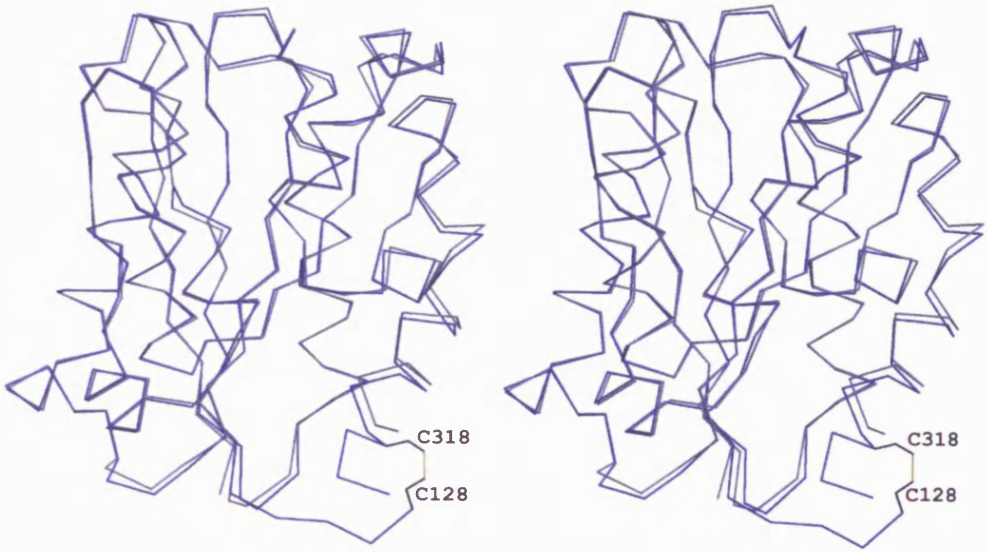

Figure 4.11 Stereo view of the Cα trace superimposition of the WT αM I domain closed conformation, coloured grey, and the α318C αM I domain mutant, coloured blue. The disulphide bond of the mutant between residues 128 and 318 is shown in yellow.

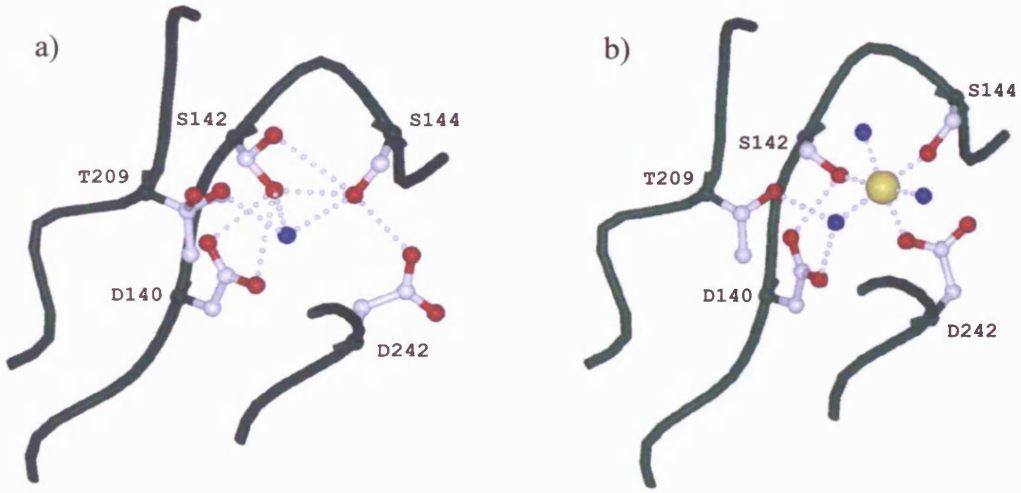

Figure 4.12 Ball and stick representations of the MIDAS of the A318C mutant (a) and theWT αM I domain closed conformation (b). Side chains are shown for each MIDAS residue with carbon atoms coloured grey, oxygen atoms coloured red and the Cα trace is represented as a green worm. Water molecules are shown as blue spheres and the Mg^{2+} of the WT closed conformation is represented as a yellow sphere. Dashed lines denote hydrogen bonds. (a) also illustrates the alternative conformations of T209 and S142.

4.3.4 Crosslinking reactions with the A318C closed mutant αM I domain

Crosslinkers of different lengths were reacted with the cysteine residues of the A318C mutant αM I domain in an attempt to fix the I domain in the open conformation. Mass spectroscopy analysis of the crosslinking reactions between the A318C mutant and crosslinkers, BMOE, BMDB and BMH, indicated that the crosslinkers had not been incorporated into the I domain. The crosslinker, bBBr, did react with the I domain as the crosslinked I domain sample was found to absorb at 391 nm and an equimolar ratio of I domain molecules to BBBr molecules was observed (data not shown).

Surface plasmon resonance studies with the A318C αM I domain crosslinked with bBBr revealed similar binding to fibrinogen and sICAM-1 as the A318C mutant without crosslinker (data not shown).

4.3.5 Generating the open αM I domain mutant

As the A318C mutant formed the closed rather than the open conformation and crosslinkers were unable to change this conformation, new mutants were designed to form a disulphide bond which would lock the I domain in the open conformation. All of the double cysteine mutants except for the C128A-D132C-K315C αM I domain expressed with low yields (~0.5 mg/L culture) and 80-90% of the protein oligomerised as judged by gel filtration chromatography. An example of a chromatogram from C128A-F297C-A314C is shown in figure 4.13a. When the eluted monomeric peaks of C128A-G263C-K315C and C128A-F297C-A304C were collected and injected again onto the gel filtration column, numerous peaks corresponding to oligomerised I domain were observed. The C128A-D132C-K315C mutant expressed ~6 mg/L culture and after purification two free cysteines were titrated with DTNB. After oxidative treatment, these cysteines were no longer titratable with DTNB and ~90% of the protein was

monomeric, as shown in figure 4.13b, indicating that an intramolecular disulphide bond had been formed.

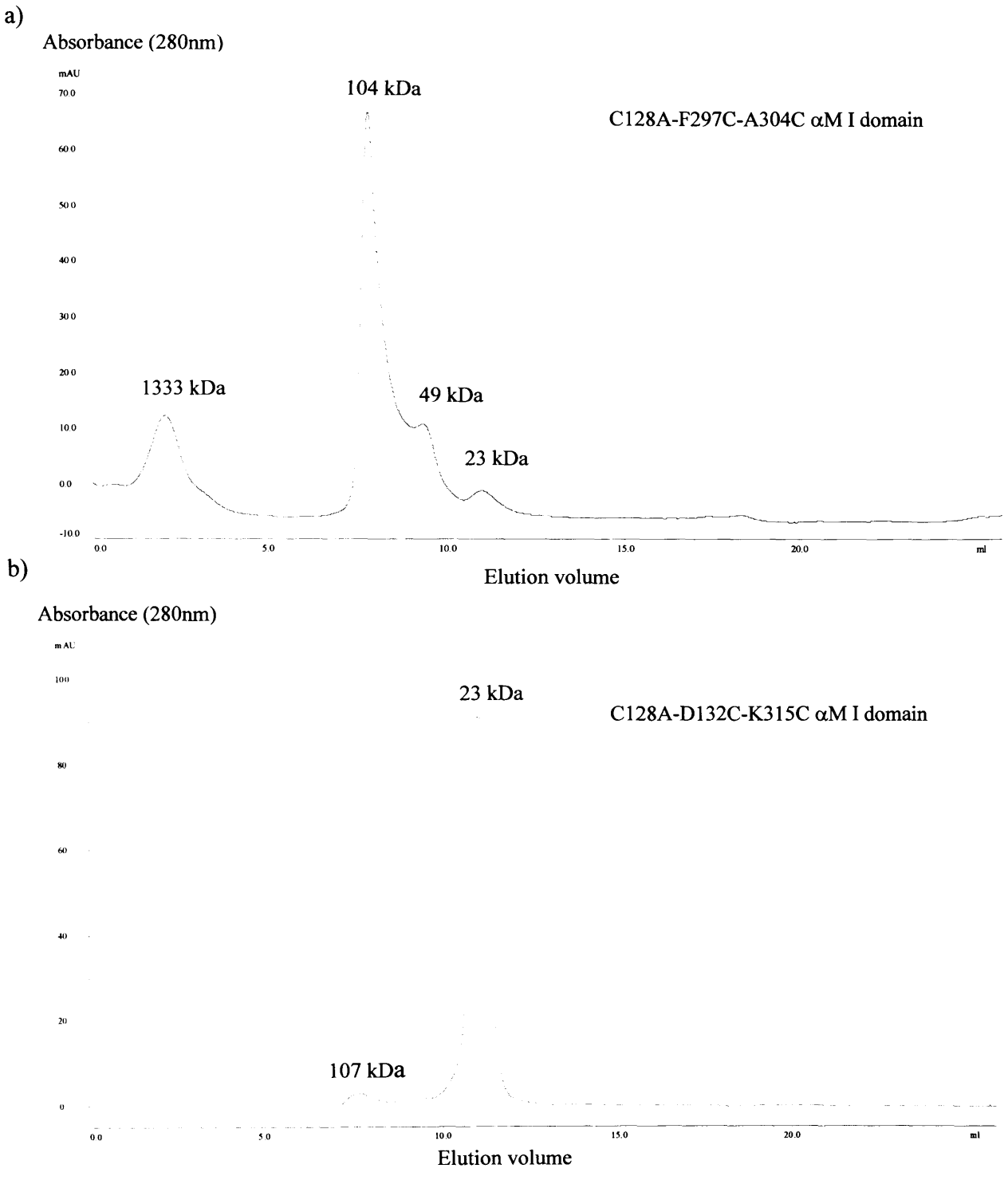

Figure 4.13 Superdex 200 gel filtration elution profiles of the C128A-F297C-A304C (a) and oxidised C128A-D132C-K315C (b) mutant αM I domains. The I domain has a molecular weight of 23 kDa. The three major peaks of chromatogram (b) show oligomerised and aggregated protein.

4.3.6 Ligand binding properties of the open (C128A-D132C-K315C) αM I domain mutant

Binding of the C128A-D132C-K315C mutant to fibrinogen, fragment D and sICAM-1 was markedly increased compared to WT. This increase in ligand binding affinity is illustrated in figure 4.14 using the ligand sICAM-1 as an example.

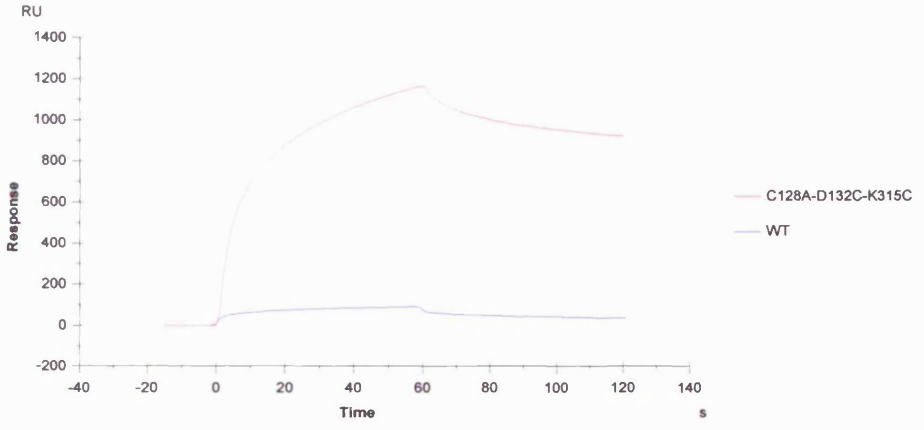

Figure 4.14 Sensorgram overlay of the oxidised C128A-D132C-K315C and WT αM I domain binding sICAM-1.

The K_D values from steady state analysis for the interaction of the C128A-D132C-K315C αM I domain with fibrinogen, fragment D and sICAM-1 are presented in table 4.8, along with the WT values for comparison. An 8- to 10.5-fold increase in affinity for all three ligands was displayed by the C128A-D132C-K315C mutant.

	Fibrinogen K_D (μM)	**Fragment D K_D (μM)**	**sICAM-1 K_D (μM)**
WT αM I domain	3.98 ± 0.86	19.37 ± 2.86 *	6.45 ± 0.58
Open αM I domain	0.49 ± 0.02	1.93 ± 0.96 *	0.62 ± 0.03

Table 4.8 K_D values for the interactions of fibrinogen, fragment D and sICAM-1 with WT and the open mutant αM I domain. K_D ± S.D. (n=3). * indicates the K_D values which were measured in the presence of Ca^{2+}.

Reducing the disulphide bond in the C128A-D132C-K315C mutant markedly reduced binding to the ligands, as shown in figure 4.15, lowering it to a level comparable to WT binding. K_D values were also measured for the reduced form of the mutant when two free cysteines could be detected. K_D values of 3.47 μM binding to sICAM-1 and 3.15 μM to fibrinogen were obtained. Similar binding was observed when the cysteine residues were blocked by iodoacetamide. As with the WT and others mutants, the C128A-D132C-K315C mutant displayed cation-dependent ligand binding.

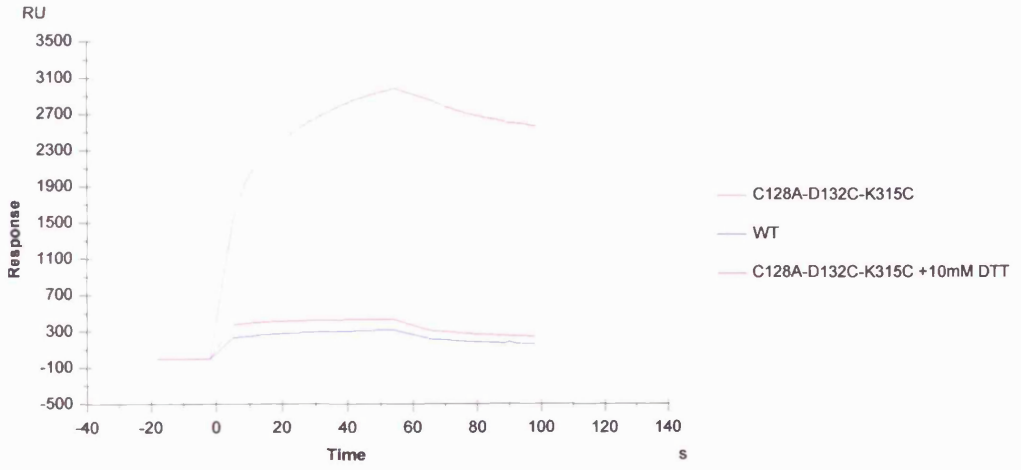

Figure 4.15 Sensorgrams demonstrating the effect of reducing the disulphide bond in the C128A-D132C-K315C αM I domain mutant.

4.3.7 Crystallisation trials with the open αM I domain mutant

Crystals of the oxidised C128A-D132C-K315C αM I domain were unable to grow. Crystallisation trials were also set up with the oxidised C128A-D132C-E314R-K315C mutant, which had the additional E314R mutation to prevent the I domain from

crystallising in the primitive tetragonal space group. A crystal structure of the open conformation with this mutant would demonstrate that the I domain had adopted the open conformation due to the disulphide bond rather than the crystal contact which dictates the crystal structure of the WT open conformation. However this mutant was also unable to crystallise. Crystallisation trials were therefore set up with the reduced C128A-D132C-K315C αM I domain, without the disulphide bond, to verify that the mutated residues were not disrupting the conformation of the domain and preventing crystallisation.

The reduced C128A-D132C-K315C αM I domain mutant crystallised in the same space group, $P4_3$, as the WT open conformation. As can be seen from table 3.3, crystals of the WT αM I domain in the primitive tetragonal space group are isomorphous. In contrast, the mutant crystals were non-isomorphous with the WT crystals, varying about 1% along a* and b* and about 5% along c*. The crystal structure of the mutant revealed a similar conformation to the WT open state. Figure 4.16 shows the superimposition of the reduced C128A-D132C-K315C mutant and the WT open conformation, the rmsd between the structures was 1.1 Å. The electron density was poor at the N- and C-termini where the cysteines were located. However, there was no evidence for a disulphide bond and the potential interacting –SH groups were 6.6 Å apart. The coordination at the MIDAS was similar to the WT closed structure with Mg^{2+} directly coordinating S142, S144, T209 and E314 from a neighbouring molecule in the crystal lattice. The main difference between the open WT and C128A-D132C-K315C αM I domain structure is ~ 2 Å downward movement of the C-terminal helix in the mutant structure.

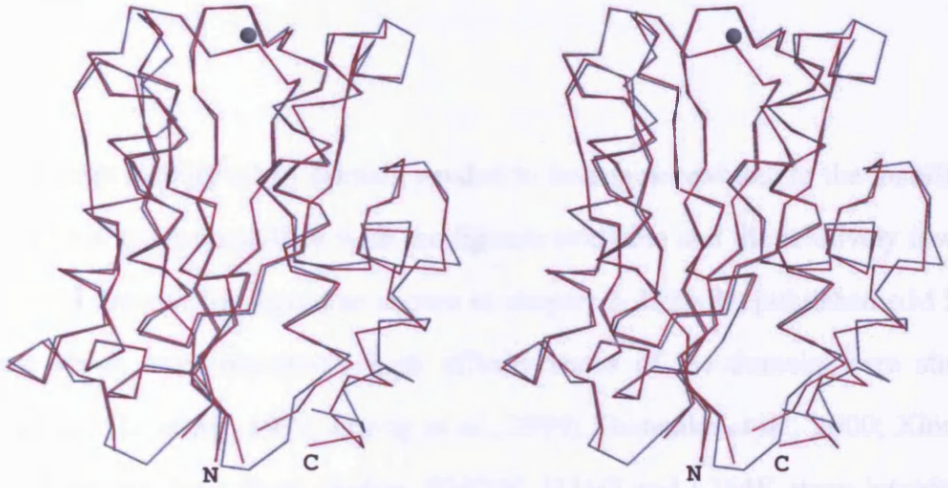

Figure 4.16 Stereo view of the Cα trace superimposition of the WT αM I domain open conformation, coloured grey, and the reduced C128A-D132C-K315C αM I domain mutant, coloured red. The N- and C-termini of the mutant I domain are labelled. The Mg^{2+} at the MIDAS is represented as a grey sphere.

4.4 Discussion

A high affinity αM I domain needed to be engineered due to the inability of the αM I domain to co-crystallise with the ligands available and the relatively low affinity of the αM I domain for ligand as shown in chapter 3. Initially, published αM I domain mutants which were reportedly high affinity states of the domain were studied for potential use (Li *et al.*, 1998; Oxvig *et al.*, 1999; Shimoaka *et al.*, 2000; Xiong *et al.*, 2000). Mutations from these studies, F302W, I316G and L164F, were introduced into the αM I domain to make single and double mutants. Previous data had demonstrated that 10% of the αM I domain were present in the open conformation (Diamond & Springer, 1993; Simon *et al.*, 1997; Li *et al.*, 1998). A theoretical maximum 10-fold increase in ligand binding, compared to WT, was therefore expected for a high affinity I domain mutant.

All of the mutants assessed displayed the typical cation dependence for ligand binding as has been demonstrated for the WT αM I domain (data not shown). Binding to fibrinogen, fragment D and sICAM-1 was significantly reduced with EDTA treatment suggesting that binding by all of the mutants were mediated by the MIDAS.

4.4.1 L164F, F302W, I316G, L164F-F302W, L164F-I316G, F302W-I316G αM I domain mutants

The F302W αM I domain mutant bound to ligands with a ~2-fold increase compared to WT. This is in agreement with previous data of this mutation within the isolated I domain and the αMβ2 heterodimer (Li *et al.*, 1998; Shimoaka *et al.*, 2000).

However, the F302W mutant, with a 2-fold increase in affinity, was likely to still have a significant population present in the closed conformation.

Mutation or deletion of I316 was reported to produce the high affinity form of the αM I domain (Xiong *et al.*, 2000). In addition to ligand binding studies, Xiong *et al.* provided crystallographic data to support their hypothesis. The αM I domain with the I316 mutation or truncation after residue 315 was reported to crystallise in the open conformation. These crystals grew with the same $P4_3$ space group as the WT open conformation, with the ligand mimetic glutamate completing the coordination of the metal ion at the MIDAS. Conversely, Xiong *et al.* reported that the αM I domain construct without the mutation or truncation crystallised in the closed conformation and was unable to crystallise in the open conformation. However, it was not reported whether the constructs with the I316G mutation or truncation after residue 315 were able to crystallise in the closed conformation. Xiong *et al.* concluded that crystallisation of the mutant and truncated I domain in the published open conformation with the $P4_3$ symmetry indicated that a high affinity αM I domain had been engineered. The αM I domain can not be assumed to adopt the open conformation in solution based on this observation. As previously discussed, this crystal form adopts the open conformation due to a crystal contact acting as a ligand mimetic. The contribution of a mutation, such as I316G, or the crystal contact towards generating the closed conformation with this crystal form would be indistinguishable. In my opinion, the crystallographic data presented by Xiong *et al.* does not accurately support their hypothesis. Ligand binding studies with the I316G αM I domain were not undertaken due to very poor protein expression so the use of the I316G mutant as a high affinity I domain was not pursued further.

Another residue that was a target for mutation, L164, is present in the loop between the first α-helix and the second β-strand and is buried by the C-terminal helix. Previous data showed that mutation of this residue to a bulky phenalanine in the context

of the heterodimeric receptor produced a 5- to 6-fold increase in ligand binding (Oxvig *et al.*, 1999). It was suggested that this mutation might loosen the packing of the C-terminal helix against the side of the I domain. The C-terminal helix connects to the β-propeller domain and the L164F mutation may lead to a weakening of the quaternary constraints that hold the I domain in the closed conformation. Results here show that the effect of the same mutation within the isolated I domain was not as marked with only a 1.5-fold increase in ligand binding compared to the WT I domain. This decreased enhancement of ligand binding may be explained by the absence of the discussed quaternary constraints.

Combining the three mutations, L164F, F302W and I316G, to produce double mutants did not markedly increase the ligand binding affinity of the I domain. The maximal increase in affinity of ~4-fold, compared to WT, was observed for the L164F-I316G mutant.

A number of published activating mutants of the αM I domain, including L164F which was tested in this study, involve residues at the interface between the I domain and the β-propeller (Zhang & Plow, 1996; Oxvig *et al.*, 1999). Movement of the I domain C-terminal helix at the β-propeller-I domain interface is proposed to facilitate an interdomain movement which unmasks ligand binding sites on the β-propeller (Loftus & Liddington, 1997). Therefore, activating mutations at the interface of these two domains may function by disrupting the quaternary constraints involved in allosterically regulating integrin function. Consequently, certain mutations localised to the αM I domain may only be effective in enhancing ligand binding when present in the intact αMβ2 receptor as demonstrated by these studies with the L164F mutant.

None of the mutants achieved the 10-fold increase in affinity, as expected for the stabilised open conformation. Therefore an alternative approach was adopted to mimic the conformational restraints that the β-propeller-I domain interface impinges on the I

domain. This involved engineering a disulphide bridge to lock the flexible C-terminal helix into the correct position for the I domain to adopt the open conformation.

4.4.2 The closed αM I domain mutant

The first mutant, A318C, constructed to generate a disulphide to tether the C-terminal helix in the open formation utilised the WT cysteine at position 128. Density for residues preceding D132 was not present in any previously published αM I domain structure, probably due to disorder. C128 was therefore predicted to be in a position where it would be closer to the mutated A318C in the open conformation than that of the closed conformation and therefore lock the open state. A disulphide bond was detected by biochemical analysis and confirmed by the A318C crystal structure. The structure revealed that the previously disordered residues preceding the first β-strand formed a loop, which was likely to be relatively flexible, as judged by their high B values. Consequently, C128 was presented in a position closer to the A318C in the closed conformation than that of the open conformation. The disulphide bond between residues 128 and 318 had therefore locked the αM I domain in the closed conformation. Functional studies, using surface plasmon resonance, correlated with the structure demonstrating a significant loss in ligand binding affinity. This decrease in affinity was shown to be reversible as reduction of the disulphide bond allowed the I domain to resume WT ligand binding affinity. Unlike other I domain-inhibiting mutants which completely destroy ligand binding by mutating residues directly involved in ligand recognition (Michishita *et al.*, 1993; McGuire & Bajt, 1995), the closed mutant presented here still displays some affinity for ligands. This could be explained by the ability of the loop region (C128-E131), which displays a degree of flexibility, to allow some downward movement of the C-terminal helix, slightly shifting the equilibrium to

allow some of the I domain molecules to adopt the open conformation. As the helix is tethered by a disulphide bond to the side of the domain, movement of the helix is more restrained than the WT, hence the reduced ligand binding affinity demonstrated by the mutant.

The closed mutant crystal structure showed no density for a metal at the MIDAS. The WT αM I domain also crystallised in the same $P2_12_12_1$ space group with similar cell dimensions. These crystals, as described in section 3.2.4, also do not have a metal bound at the MIDAS demonstrating that the absence of metal is not a consequence of the A318C mutation or the formation of the disulphide bridge. Movement of the cation coordinating residues in the A318 mutant, as shown in figure 4.12, are identical to that observed in the WT αM I domain crystals with $P2_12_12_1$ symmetry. As described in 3.4.2, the absence of a bound metal at the MIDAS can be attributed to crystal contacts.

4.4.3 The open αM I domain mutant

After the crystal structure of the closed mutant was determined and crosslinkers were unable to fix this mutant in the open state, a new set of mutants were generated to introduce cysteines into positions which were of a less flexible nature. Only one of the three double cysteine mutants generated, C128A-D132C-K315C, was able to form an intramolecular disulphide bond. This disulphide bridged the C-terminal helix to the first β-strand. In contrast to the closed mutant, the disulphide bond formed in this mutant linked regions of the I domain which were more structurally stable, producing a conformation which was likely to be more rigid. Surface plasmon resonance studies demonstrated an approximate 10-fold increase in binding to all three ligands tested. As with the closed mutant, the increase in affinity with the C128A-D132C-K315C mutant

was shown to be reversible by reduction of the disulphide bond. This increase in ligand binding affinity was also linked to disulphide bond formation as comparable WT K_D values for the interaction of ligands with the C128A-D132C-K315C mutant were obtained when the cysteines were blocked to prevent disulphide bond formation.

The apparent K_D for WT binding is taking into account two processes: the equilibrium between the open and closed states and the affinity for the open state for binding ligand. This is assuming that the closed state affinity for ligand is very small and therefore negligible. If the I domain is fixed in the open state then the calculated K_D excludes contributions from the equilibrium between the open and closed states. As the equilibrium constant between the open and closed states has been determined as 0.1 (Li *et al*, 1998), the 10-fold increase in K_D for the open mutant compared to WT demonstrates that the equilibrium between the two states is now absent and the I domain has been frozen in the open state. This is consistent with the observation that fibrinogen binding to αMβ2 was increased about 10-fold following activation, as monitored by the ligand mimetic monoclonal antibody 7E3 which can only bind αMβ2 in its active state (Simon *et al.*, 1997). In addition, αM/αL I domain chimeras that produced a constitutively active holoreceptor also adhered to fibrinogen 10-fold greater than WT αMβ2 (Zhang & Plow, 1996).

As a 10-fold increase in ligand binding, compared to WT, was observed for the C128A-D132C-K315C αM I domain mutant, it was concluded that this mutant was successfully locked in the open conformation by the disulphide bridge. In the case of certain ligands such as fibrinogen, the αM I domain has been shown to be solely responsible for ligand binding (Yalamanchili *et al.*, 2000). It is therefore interesting to note that the ligand binding affinity of the open mutant αM I domain is comparable to ligand binding with purified αMβ2 (K_D ~ 12.5-200 nM) (Berman *et al.*, 1993; Cai & Wright, 1995).

As the oxidised C128A-D132C-K315C and C128A-D132C-E314R-K315C open mutants were unable to crystallise, the reduced form of the C128A-D132C-K315C mutant was crystallised to analyse the consequence of mutating the three chosen residues. The crystal structure revealed that the mutated residues did not disrupt the conformation of the domain as the protein was still able to crystallise in the open conformation. Reduced C128A-D132C-K315C mutant displayed WT affinities for ligands suggesting that the I domain had not been locked in the open conformation. This functional analysis therefore correlated with the crystal structure, which demonstrated that the cysteines were too far apart to form a disulphide bond. Apart from the mutations, the only difference between the WT and reduced C128A-D132C-K315C mutant crystal structures was a ~2 Å downward shift of the C-terminal helix. This may reflect the inherent flexible nature of the C-terminal helix, which has previously been observed in I domains (Qu & Leahy, 1996; Legge *et al.*, 2000). It can be observed from the reduced C128A-D132C-K315C mutant structure that the I domain may be unable to form the disulphide bond in this $P4_3$ crystal form. As illustrated in figure 4.17, the crystal contact between E314 and the metal at the MIDAS of the neighbouring molecule positions the C-terminal helix against the upper surface of the I domain. Formation of the disulphide bond would require the N- and C-termini to move into close proximity with one another. Repositioning of the C-terminal helix is unlikely to be accommodated by the $P4_3$ space group due to the crystallographic restraints imposed upon the C-terminal helix. Unlike the closed αM I domain mutant, which was able to crystallise in the same space group as the WT closed state, the C128A-D132C-K315C would probably need to crystallise in a different space group to that of the WT open state. The additional mutation of E314R to the open mutant was designed to prevent the I domain from crystallising in the $P4_3$ space group, allowing other crystal forms to develop. Unfortunately, crystals of both the oxidised C128A-D132C-K315C and C128A-D132C-E314R-K315C αM I domain mutants were unable to grow.

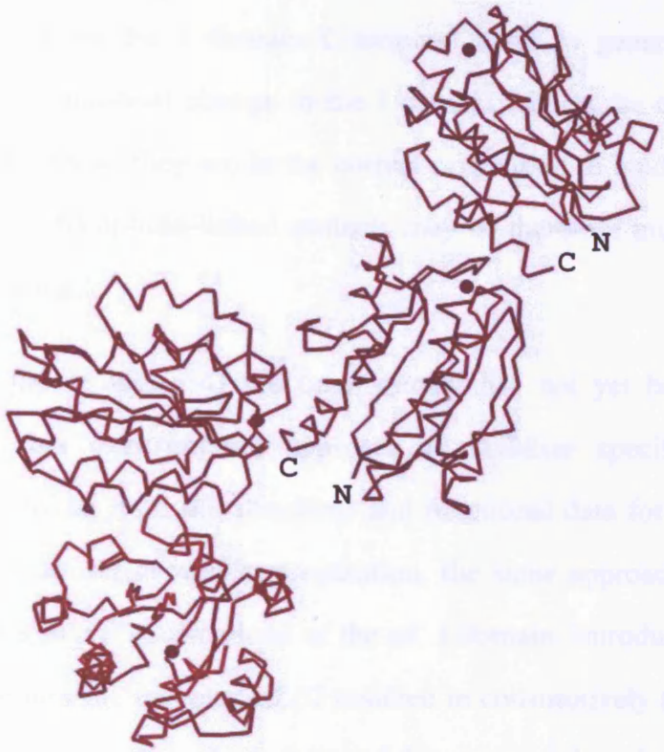

Figure 4.17 Diagram showing the crystal packing in the reduced C128A-D132C-K315C $P4_3$ crystal form. The Cα traces of 4 molecules are shown with the C- and N-termini of 2 molecules labelled. The red spheres represent the Mg^{2+} at the MIDAS.

The open αM I domain mutant demonstrates that the requirement for activation to the high affinity state is the shift of the C-terminal helix, thus reinforcing the idea of a two-state model for the α subunit I domain. Locking the C-terminal helix in the open position enables the metal coordinating residues at the MIDAS to adopt the correct conformation to accommodate ligand binding. In the context of the intact integrin, the I domain is inserted into the β-propeller domain of the α subunit (Springer, 1997), which also associates with the β subunit, and in turn is linked through the transmembrane to the cytoplasmic tails. Effectors binding the cytoplasmic integrin tails could transmit a

signal to the α subunit I domain via interdomain movements and shape shifting mechanisms, pulling on the I domain C-terminal helix to generate a high affinity receptor. This conformational change in the I domain adjusts the conformation of the residues at the MIDAS so they are in the correct orientation to bind ligand through the bound metal. These disulphide-linked mutants may be therefore mimicking the effects of inside-out signalling.

Although the structure of the open mutant has not yet been elucidated, the rationale behind this experimental approach to stabilise specific αM I domain conformations is proven with the structural and functional data for the closed mutant. While this thesis manuscript was in preparation, the same approach was successfully adopted to lock the two conformations of the αL I domain. Introduction of the mutant open αL I domain into the receptor αLβ2 resulted in constitutively active cell adhesion (Lu *et al.*, 2001) demonstrating the validity of this structure-based protein engineering. Unfortunately, due to time constraints, the use of open mutant αM I domain in co-crystallisation trials was not pursued further.

Unlike other gain- and loss-of-function mutants published for the αM I domain (Li *et al.*, 1998; Shimaoka *et al.*, 2000; Xiong *et al.*, 2000), the open and closed mutants presented here are fully reversible. Also the low affinity conformation has been generated without disrupting residues critical to ligand binding. These will provide very useful tools for future studies to understand the regulatory interactions among the integrin domains and will simplify ligand binding studies with the isolated I domain and intact receptor. Locking the I domain in specific conformations may also enable further elucidation of the biological functions of αMβ2. In addition, the ability to isolate the open and closed form of the αM I domain has broad pharmaceutical applications. αMβ2 is present on the surface on leukocytes and plays a critical role in leukocyte-endothelial interactions, which are involved in many immune and inflammatory functions. Many disorders, such as rhematoid arthritis, asthma and multiple sclerosis,

are the result of uncontrolled leukocyte migration (Curley *et al.*, 1999). The open I domain would therefore be valuable in screens to develop antagonists against integrin function in various diseases states.

Chapter 5: Further work

5.1 Ligand binding and activation in integrins without α subunit I domains

The structure of the extracellular domains of αVβ3, as previously described in chapter 1, provides for the first time a view of the quaternary organisation of the ligand binding regions in an integrin. However, some conclusions drawn from the structure by Xiong et al (2001) require further clarification as there are discrepancies with the proposed model of integrin activation as discussed in section 1.5.2.2. The α subunit β-propeller and β subunit I domain in the headpiece of the αVβ3 structure display a striking similarity to the Gα and Gβ domains of G proteins. This similarity was predicted and consequently the integrin heterodimer was proposed to behave in an analogous manner to G proteins (Loftus & Liddington, 1997), with the I domain and β-propeller domain completely separating from one another upon activation, unmasking the ligand binding sites on the β-propeller. A movement of the β-propeller domain relative to the β subunit I domain in integrins, as well as a complete dissociation of these domains, has also been observed upon ligand binding (Mould *et al.*, 1998b; Hantgan *et al.*, 1999). The structure of αVβ3 places the β-propeller domain and the β subunit I domain in close proximity with six of the seven blades in contact with the I domain even though αVβ3 is reported to be in its active, ligand-competent state. Xiong *et al.* (2001) propose that the ligand binding regions in the αV propeller and the β3 I domain are clustered at the top of the integrin head and are not buried by the β-propeller-I domain interface. This raises the possibility that a more conservative movement of the β-propeller in relation to the β subunit I domain may occur. The structure of the low affinity state and/or the ligand-bound integrin would clarify this

issue.

Another point concerns the β3 subunit I domain. The I domain, which is highly homologous to the α subunit I domain, was proposed to be in the open conformation due to the similarity of the position of its C-terminal helix with that of the open α subunit I domain. Experimental data with the α-subunit I domain, as discussed in section 1.5.2.2, has provided indirect evidence that shape shifting between the open and closed conformations is linked to an interdomain movement with the β-propeller, thus regulating integrin activation. However, Xiong *et al.* (2001) propose that the β subunit I domain may not undergo a similar conformational change as it is held in this open position by contacts with its adjoining hybrid domain and may only exist in this state. Does this mean that the β-subunit I domain is regulated by a different mechanism to the α-subunit I domain? Would this mechanism involve the regions of the β-subunit I domain that are in contact with the β-propeller, such as the 3_{10} helix, which is the analogous helix in the G proteins that undergoes a major conformation upon activation? Again, this question could only be answered by the structures of the low affinity form of the integrin. It would also be important to determine the structure of the integrin in complex with a ligand to determine that the features observed in the new αVβ3 structure are physiologically relevant.

The αVβ3 crystal structure has also located the bound divalent cations, which are proposed to regulate integrin binding and activation. Structure-function studies using integrin mutants, which would prevent the coordination of these cations, would help define the role of cations in allosterically regulating integrins.

5.2 Ligand binding and activation in integrins containing α subunit I domains

The design of the open high affinity αM I domain mutant in this thesis will now facilitate the structure determination of the I domain in complex with a physiological ligand. This structure would demonstrate ligand-induced conformational changes and deconstruct the binding site within αMβ2, which is capable of binding a diverse range of ligands. It would also be of interest to analyse the effect of substituting the I domain in αMβ2 with the mutant αM I domains locked open and closed by disulphide bonds. Would the open mutant I domain in the context of the intact integrin produce a constitutively active receptor? Conversely, would the closed mutant I domain in αMβ2 abolish constitutive and activatable adhesion?

It has been suggested that shape shifting in the α subunit I domain leads to an interdomain movement which unmasks ligand binding sites on the α subunit β-propeller domain, as discussed in section 1.2.2.2. The structures of the integrin extracellular binding domains with the locked open and closed α subunit I domains would provide valuable information regarding the interdomain movements which occur. If the α subunit I domain is sufficient for the full adhesive activity of the integrin, as demonstrated for the αL I domain (Lu *et al.*, 2001a), what is the role of the α subunit β-propeller and β subunit I domain in integrins which contain an α subunit I domain? The structure of these extracellular domains complexed to ligand would demonstrate the role each domain plays in ligand binding and allosteric regulation of integrins.

Appendix

Table A.1 Reflection statistics for the αM I domain data sets with the highest resolution for each space group

Data set RGEVa (C2 symmetry, 20 – 2.4 Å resolution)

Resolution shells (Å)	Unique reflections	Total measurements	Completeness (%)	I/σI	R_{merge} (%)
20.00-5.16	717	2003	90.1	36.5	3.7
5.16-4.10	721	1989	95.6	35.4	3.8
4.10-3.58	741	1999	96.6	35.8	4.2
3.58-3.25	718	1883	96.5	33.4	4.5
3.25-3.02	726	1880	97.1	31.9	4.2
3.02-2.84	718	1892	96.1	31.1	4.2
2.84-2.70	703	1852	95.8	27.9	5.2
2.70-2.58	720	1789	95.5	25.7	5.6
2.58-2.48	699	1774	95.1	23.9	5.6
2.48-2.40	647	1406	87.7	20.5	5.8
20.00-2.40	7110	18467	94.6	33.1	4.0

RGE(HA)Vb data set ($P2_1$ symmetry, 20 – 1.8 Å resolution)

Resolution shells (Å)	Unique reflections	Total measurements	Completeness (%)	I/σI	R_{merge} (%)
20.00-3.87	3192	10671	90.3	38.8	2.6
3.87-3.07	3329	11038	96.2	38.0	2.7
3.07-2.69	3367	10982	97.3	34.5	2.9
2.69-2.44	3368	10953	97.9	31.3	3.4
2.44-2.27	3361	10906	97.7	29.7	3.8
2.27-2.13	3375	10852	97.9	27.3	4.7
2.13-2.03	3358	10765	98.0	23.9	5.6
2.03-1.94	3341	10805	98.1	19.7	6.0
1.94-1.86	3325	10670	96.3	14.1	7.7
1.86-1.80	3216	8991	93.2	11.3	8.4
20.00-1.80	33232	106633	96.3	31.2	2.9

P1b data set ($P2_12_12_1$ symmetry, 20 – 1.5 Å resolution)

Resolution shells (Å)	Unique reflections	Total measurements	Completeness (%)	I/σI	R_{merge} (%)
20.00-3.12	3717	12990	95.0	37.8	1.9
3.12-2.48	3672	12943	98.8	34.5	2.5
2.48-2.16	3648	12919	99.4	29.0	3.4
2.16-1.97	3623	12838	99.6	22.6	4.8
1.97-1.83	3607	12940	99.8	16.8	6.5
1.83-1.72	3639	12753	99.9	11.4	9.7
1.72-1.63	3610	12579	100.0	8.7	11.9
1.63-1.56	3579	12348	99.8	6.8	15.8
1.56-1.50	3565	12090	99.3	5.4	18.7
1.50-1.45	3328	10737	92.9	3.9	22.2
20.00-1.45	35988	125137	98.4	25.9	2.5

P2a data set ($P4_3$ symmetry, 20 – 2.0 Å resolution)

Resolution shells (Å)	Unique reflections	Total measurements	Completeness (%)	I/σI	R_{merge} (%)
20.00-4.30	1259	3587	93.1	26.3	6.1
4.30-3.41	1269	3446	95.9	23.3	5.9
3.41-2.98	1282	3764	97.3	17.1	9.0
2.98-2.71	1293	4055	98.3	12.8	12.2
2.71-2.51	1288	4263	98.2	8.9	18.1
2.51-2.36	1278	4214	98.6	7.7	20.6
2.36-2.25	1306	4207	99.1	6.1	24.8
2.25-2.15	1279	3792	98.8	4.8	26.0
2.15-2.07	1275	3276	97.6	3.5	30.0
2.07-2.00	1115	2398	85.4	2.6	33.7
20.00-2.00	12644	37002	96.2	14.8	7.2

FXa data set ($P2_12_12$ symmetry, 20 – 2.3 Å resolution)

Resolution shells (Å)	Unique reflections	Total measurements	Completeness (%)	I/σI	R_{merge} (%)
20.00-4.83	1649	7949	77.0	42.2	2.8
4.83-3.84	1634	7555	79.8	44.7	3.1
3.84-3.36	1637	7516	81.4	41.8	3.8
3.36-3.05	1640	7329	82.4	37.4	4.6
3.05-2.83	1645	7528	82.7	32.5	5.3
2.83-2.67	1654	7475	83.8	27.3	6.4
2.67-2.53	1647	7357	84.5	22.8	7.3
2.53-2.42	1689	7512	84.5	18.6	8.4
2.42-2.33	1668	7409	85.3	13.9	10.2
2.33-2.25	1684	7106	85.6	11.4	11.0
20.00-2.25	16547	74736	82.6	33.5	4.5

P1c data set ($P2_12_12$ symmetry, 20 – 3.0 Å resolution)

Resolution shells (Å)	Unique reflections	Total measurements	Completeness (%)	I/σI	R_{merge} (%)
20.00-6.43	953	2796	92.4	19.9	4.2
6.43-5.10	946	2896	99.3	9.6	10.0
5.10-4.46	922	2849	99.6	13.4	8.9
4.46-4.05	916	2855	99.1	12.9	9.2
4.05-3.76	907	2822	98.7	10.1	11.4
3.76-3.54	901	2771	98.6	7.8	14.5
3.54-3.36	887	275	98.6	6.2	18.1
3.36-3.22	903	2763	98.6	4.5	24.9
3.22-3.09	882	2665	98.0	3.8	28.6
3.09-3.00	832	2463	91.9	2.9	32.8
20.00-3.00	9049	275950	97.4	8.8	10.8

R_{merge} (%) = 100 x $\sum_h\sum_j |I_{hj} - I_h| / \sum_h\sum_j I_{hj}$ where I_h is the weighted mean intensity of the symmetry related reflections I_{hj}.

Table A.2 Molecular replacement solutions for the αM I domain data sets with the highest resolution for each space group. The five highest peaks are given for each rotation and translation function.

Rotation function solutions for the RGE(HA)Vb data set

ROTING peak	α	β	γ	Peak height
1	90.08	90.00	90.47	9.0
2	269.86	90.00	270.48	7.6
3	202.3	35.92	130.16	4.6
4	253.20	61.36	330.65	4.2
5	193.70	66.86	156.02	4.0

Translation function solutions for the RGE(HA)Vb data set.
Fixing the Euler angles from ROTING peaks 1 and 2.

TRAING 1 peak	x	y	z	C	R (%)
1	14.87	10.25	64.60	61.1	35.1
2	23.82	71.18	1.56	37.2	45.8
3	24.11	37.08	1.51	36.9	45.7
4	5.68	37.48	1.52	36.2	45.8
5	7.91	61.91	12.30	36.6	45.6

Rotation function solutions for the P1b data set

ROTING peak	α	β	γ	Peak height
1	41.82	52.40	73.14	19.8
2	139.59	52.59	205.09	14.0
3	6.80	53.28	210.28	13.5
4	152.34	55.29	204.57	13.4
5	21.49	58.04	206.88	13.3

Translation function solutions for the P1b data set.

Fixing the Euler angles from ROTING peak 1.

TRAING 1 peak	x	y	z	C	R (%)
1	12.53	13.33	36.08	60.7	40.9
2	12.37	13.48	12.82	36.0	51.2
3	12.50	24.13	36.15	33.8	52.0
4	12.50	7.90	36.11	32.8	51.4
5	12.60	15.93	36.09	35.1	51.6

Rotation function solutions for the FXa data set

ROTING peak	α	β	γ	Peak height
1	89.5	53.9	61.2	17.0
2	154.5	52.5	62.8	16.6
3	234.2	35.1	56.3	10.2
4	35.6	53.2	69.6	9.5
5	164.0	63.2	46.3	8.7

Translation function solutions for the FXa data set.

Fixing the Euler angles from ROTING peaks 1 and 2.

TRAING 1 peak	x	y	z	C	R (%)
1	0.106	0.219	0.380	34.4	47.4
2	0.349	0.221	0.376	25.6	50.5
3	0.107	0.219	0.168	24.8	50.2
4	0.107	0.219	0.117	24.2	50.2
5	0.108	0.218	0.283	23.6	50.6

Rotation function solutions for the P1c data set

ROTING peak	α	β	γ	Peak height
1	23.5	50.8	62.5	19.6
2	40.0	52.6	64.1	16.3
3	23.0	59.6	73.5	10.9
4	37.3	60.2	70.0	10.1
5	22.4	9.4	16.4	8.7

Translation function solutions for the P1c data set.

Fixing the Euler angles from ROTING peaks 1 and 2.

TRAING 1 peak	x	y	z	C	R (%)
1	0.134	0.443	0.031	43.6	44.4
2	0.135	0.444	0.318	31.1	48.6
3	0.135	0.378	0.029	30.7	48.5
4	0.133	0.023	0.032	30.6	48.7
5	0.134	0.440	0.462	30.5	48.4

C is the standard linear correlation coefficient between the observed and calculated structure factor amplitudes defined as $C=[\sum_{hkl}(|F_{obs}|-<|F_{obs}|>)x(|F_{calc}|-<|F_{calc}|>)]/ [\sum_{hkl}(|F_{obs}|-<|F_{obs}>)^2x\sum_h(|F_{calc}|-<|F_{calc}|>)2]^{½}$. R (%) = 100 $x\sum_{hkl}|F_{obs}-F_{calc}| / \sum_{hkl} F_{obs}$ where F_{obs} is observed structure factor amplitudes and F_{calc} is the calculated structure factor amplitudes.

Table A.3 Summary of refinement progress for the αM I domain data sets with the highest resolution for each space group.

RGEVa data set (20 – 2.4 Å resolution)

Round	Procedure	R_{work}	R_{free}
1	Rigid body refinement	25.4	28.7
2	Simulated annealing	24.6	27.0
3	Manual modelling, positional and B factor refinement	24.3	26.9
4	3 rounds of water picking (55 waters)	23.4	25.3
5	Manual modelling, positional and B factor refinement	23.2	24.8

RGE(HA)Vb data set (20 – 1.8 Å resolution)

Round	Procedure	R_{work}	R_{free}
1	Rigid body refinement	34.6	34.8
2	Simulated annealing	33.2	33.9
3	Manual modelling, positional and B factor refinement	30.1	32.5
4	Manual modelling, positional and B factor refinement	29.0	30.6
5	3 rounds of water picking (126 waters)	27.7	28.9
6	Manual modelling, positional and B factor refinement	27.0	28.5

P1b data set (20 – 1.5 Å resolution)

Round	Procedure	R_{work}	R_{free}
1	Rigid body refinement	39.0	40.3
2	Simulated annealing	35.2	36.6
3	Manual modelling and positional refinement	29.6	30.5
4	Manual modelling, positional and B factor refinement	26.5	28.2
5	3 rounds of water picking (141 waters)	22.6	24.3
6	Manual modelling, positional and B factor refinement	21.2	23.1
7	2 rounds of water picking (61 waters)	20.6	22.7
8	Water deleting (22 waters), manual modelling, positional and B factor refinement	20.5	22.5

P2a data set (20 – 2.0 Å resolution)

Round	Procedure	R_{work}	R_{free}
1	Rigid body refinement	31.3	31.9
2	Simulated annealing	29.7	31.3
3	Manual modelling, positional and B factor refinement	27.3	28.1
4	Manual modelling and B factor refinement	26.1	27.0
5	2 rounds of water picking (52 waters)	24.5	24.7
6	B factor refinement	24.2	24.6

FXa data set (20 – 2.3 Å resolution)

Round	Procedure	R_{work}	R_{free}
1	Rigid body refinement	32.4	34.9
2	Simulated annealing	28.6	32.0
3	Manual modelling and positional refinement	27.4	30.9
4	2 rounds of water picking (78 waters)	26.2	29.2
5	Manual modelling, positional and B factor refinement	25.4	28.4
6	2 rounds of water picking (72 waters)	24.2	27.9
7	Water deleting (20 waters), manual modelling, positional and B factor refinement	23.4	27.7

P1c data set (20 – 3.0 Å resolution)

Round	Procedure	R_{work}	R_{free}
1	Rigid body refinement	33.1	34.5
2	Simulated annealing	32.3	33.1
3	Manual modelling	30.8	31.0
4	Manual modelling and B factor refinement	30.2	30.5
5	Manual modelling and positional refinement	26.6	29.6
6	Manual modelling	27.2	28.1
7	Manual modelling, positional and B factor refinement	26.8	27.8
8	2 rounds of water picking (45 waters)	25.8	26.8

R_{work} (%) = 100 x $\sum_{hkl} | F_{obs} - F_{calc} | / \sum_{hkl} F_{obs}$ where F_{obs} and F_{calc} are the observed and calculated structure factors respectively. R_{free} (%) is the R_{work} (%) calculated using a random selected 5% of reflection data omitted from refinement.

Table A.4 Refinement statistics for the αM I domain data sets with the highest resolution for each space group.

	RGEVa	RGE(HA)Vb	P1b	P2a	FXa	P1c
Resolution (Å)	20 - 2.4	20 - 1.8	20 - 1.5	20 - 2.0	20 - 2.3	20 - 3.0
Protein atoms in asymmetric unit	1516	3030	1688	1491	3030	3030
Solvent atoms in asymmetric unit	55	126	180	52	130	45
Heterogen atoms in asymmetric unit	1 Mg^{2+}	2 Mg^{2+}	0	1 Mg^{2+}	0	2 Mg^{2+}
R_{work} (%)	23.2	27.0	20.5	24.2	23.4	25.8
R_{free} (%)	24.8	28.5	22.5	25.4	27.7	26.8
Rmsd bond lengths (Å)	0.007	0.007	0.004	0.012	0.006	0.010
Rmsd bond angles (°)	1.34	1.36	1.24	1.60	1.38	1.91
Average B factor ($Å^2$)	27.6	17.1	17.7	29.8	25.7	24.3

References

Altieri, D.C. & Edgington, T.S. (1988) The saturable high affinity association of factor X to ADP-stimulated monocytes defines a novel function of Mac-1 receptor. *J. Biol. Chem.* **263,** 7007-7012.

Altieri, D.C., Agbanyo, F.R., Plescia, J., Ginsberg, M.H., Edgington, T.S. & Plow, E.F. (1990) A unique recognition site mediates the interaction of fibrinogen with the leukocyte integrin Mac-1 (CD11b/CD18). *J. Biol. Chem.* **265,** 12119-12122.

Altieri, D.C., Etingin, O.R., Fair, D.S., Brunck, T.K., Geltosky, J.E., Hajjar, D.P. & Edgington, T.S. (1991) Structurally homologous ligand-binding of integrin Mac-1 and viral glycoprotein-C receptors. *Science* **254,** 1200-1202.

Altieri, D.C., Plescia, J. & Plow, E.F. (1993) The structural motif glycine190-valine202 of the fibrinogen gamma chain interacts with CD11b/CD18 integrin (alphaM beta2, Mac-1) and promotes leukocyte adhesion. *J. Biol. Chem.* **268,** 1847-1853.

Anderson, D.C., Rothlein, R., Marlin, S.D., Krater, S.S. & Smith, C.W. (1989) Impaired transendothelial migration by neonatal neutrophils: abnormalities of Mac-1 (CD11b/CD18)-dependent adherence reaction. *Blood* **76,** 2613-2618.

Bajt, M.L., Goodman, T. & McGuire, S.L. (1995) β2 (CD18) mutations abolish ligand recognition by I domain integrins LFA-1 (αLβ2, CD11a/CD18) and MAC-1 (αMβ2, CD11b/CD18). *J. Biol. Chem.* **270,** 94-98.

Baldwin E. T., Sarver, R.W., Bryant, G.L., Curry, K.A., Fairbanks, M.B., Finzel, B.C., Garlick, R.L. *et al.* (1998) Cation binding to the integrin CD11b I domain and activation model assessment. *Structure* **6,** 923-935.

Banères, J-L., Roquet, F., Green, M., LeCalvez, H. & Parello, J. (1998) The cation-binding domain from the α subunit of integrin α5β1 is a minimal domain for fibronectin recognition. *J. Biol. Chem.* **273,** 24744-24753.

Bauer, T.R. & Hickstein, D.D. (2000) Gene therapy for leuckocyte adhesion deficiency. (2000) *Curr. Opin. Mol. Ther.* **2,** 383-388.

Bella, J., Kolatkar, P.R., Marlor, C.W., Greve, J.M. & Rossmann, M.G. (1998) The structure of the two amino-terminal domains of human ICAM-1 suggests how it functions as a rhinovirus receptor and as an LFA-1 integrin ligand *Proc. Natl. Acad. Sci. USA* **95,** 4140-4145.

Beller, D.I., Springer, T.A. & Schreiber, R.D. (1982) Anti-Mac-1 selectively inhibits the mouse and human type three complement receptor. *J. Exp. Med.* **156,** 1000-1009.

Benson, D.L., Schnapp, L.M., Shapiro, L. & Huntley, G.W. (2000) Making memories stick: cell-adhesion molecules in synaptic plasticity. *Trends Cell Biol.* **10,** 473-482.

Berman, P.W., Nakamura, G., Riddle, L., Chiu, H., Fisher, K., Champe, M., Gray, A. & Fong, S. (1993) Biosynthess and function of membrane bound and secreted forms of recombinant Mac-1. *J. Cell. Biochem.* **52,** 183-195.

Berton, G. & Lowell, C.A. (1999) Integrin signalling in neutrophils and macrophages. *Cell. Signal.* **11,** 621-635.

Bleijs, D.A., van Duijnhoven, G.C.F., van Vilet, S.J., Thijssen, J.P.H., Figdor, C.G. & van Kooyk, Y. (2001) A single amino acid in the cytoplasmic domain of the β2 integrin lymphocyte function-associated antigen-1 regulates avidity-dependent inside-out signalling. *J. Biol. Chem.* **276,** 10338-10346.

Blystone, S.D., Lindberg, M.P., Williams, K.P., McHugh, E.J. & Brown, E.J. (1997) Requirement of integrin β_3 tyrosine 747 for β_3 tyrosine phosphorylation and regulation of $\alpha_V\beta_3$ avidity. *J. Biol. Chem.* **272,** 28757-28761.

Brünger, A.T., Adams, P.D., Clore, G.M., DeLano, W.L., Gros, P., Grosse-Kunstleve, R.W., Jiang, J.S., Kuszewski, J., Nilges, M., Pannu, N.S., Read, R.J., Rice, L.M., Simonson, T. & Warren G.L. (1998) Crystallography and NMR system: A new software suite for macromolecular structure determination. *Acta. Cryst.* **D54,** 905-921.

Burrows, L., Clark, K., Mould, A.P. & Humphries, M.J. (1999) Fine mapping of inhibitory anti-α5 monoclonal antibody epitopes that differentially affect integrin-ligand binding. *Biochem. J.* **344,** 527-533.

Cai, T.Q. & Wright, S.D. (1995) Energetics of leukocyte integrin activation. *J. Biol. Chem.* **270,** 14358-14365.

Calderwood, D.A., Tuckwell, D.S., Eble, J., Kuhn, K. & Humphries, M.J. (1997) The integrin alpha 1 A-domain is a ligand binding site for collagens and laminins. *J. Biol. Chem.* **272,** 12311-12317.

Calderwood, D.A., Zent, R., Grant, R., Rees, D.J., Hynes, R.O. & Ginsberg, M.H. (1999) The talin head domain binds to integrin beta subunit cytoplasic tails and regulates integrin activation. *J. Biol. Chem.* **274,** 28071-28074.

Camper, C., Hellman, U. & Lundgren-Åkerland, E. (1998) Isolation, cloning, and sequence analysis of the integrin subunit α10, a β1-associated collagen binding integrin expressed on chondrocytes. *J. Biol. Chem.* **273,** 20383-20389.

Cao, Z., Huang, K. & Horwitz, A.F. (1998) Identification of a domain on the integrin alpha5 subunit implicated in cell spreading and signaling. *J. Biol. Chem.* **273,** 31670-31679.

Cary, L.A. & Guan, J.-L (1999) Focal adhesion kinase in integrin-mediated signalling. *Front. Biosci.* **4,** d102-113.

Cassasnovas, J.M., Stehle, T., Liu, J.-H., Wang, J.-H. & Springer, T.A. (1998) A dimeric crystal structure of the N-terminal two domains of intercellular adhesion molecule-1. *Proc. Natl. Acad. Sci. USA* **95,** 4134-4139.

CCP4 (1994) The CCP4 suite: programs for protein crystallography. *Acta Cryst.* **D50,** 760-763.

Chang, L. & Karin, M. (2001) Mammalian MAP kinase signalling cascades. *Nature* **410,** 37-40.

Clemetson, K. J. & Clemetson, J. M. (1994) Molecular abnormalities in Glanzmann's thrombasthenia, Bernard-Soulier syndrome, and platelet-type von Willebrand's disease. *Curr. Opin. Hematol.* **1,** 388-393.

Clezardin, P. (1998) Recent insights into the role of integrins in cancer metastasis. *Cell. Mol. Life. Sci.* **54:** 541-548

Coller, B.S. (1997) Platelet GPIIb/IIa antagonists: the first anti-integrin receptor therapeutics. *J. Clin. Invest.* **99,** 1467-1471.

Cosimi, A., Conti, D., Delmonico, F.L., Preffer, F.I., Wee, S.L., Rothlein, R., Faanes, R. & Colvin, R.B. (1990) In vivo effects of monoclonal antibody to ICAM-1 (CD54) in nonhuman primates with renal allografts. *J. Immunol.* **144,** 4604-4612.

Coppolino, M.G. & Dedhar, S. (2000) Bi-directional signal transduction by integrin receptors. *Int. J. Biochem. Cell Biol.* **32,**171-188.

Coppolino, M.G., Woodside, M.J., Demaurex, N., Grinstein, S., St-Arnaud, R. & Dedhar, S. (1997) Calreticulin is essential for integrin-mediated calcium signalling and

cell adhesion. *Nature* **386,** 843-847.

Coxon, A., Rieu, P., Barkalow, F.J., Askari, S., Sharpe, A.H., Von Andrian, U.H., Arnaout, M.A. & Mayadas, T.N. (1996) A novel role for the beta 2 integrin CD11b/CD18 in neutrophil apoptosis: a homeostatic mechanism in inflammation. *Immunity* **5,** 653-666.

Critchley, D.R. (2000) Focal adhesions – the cytoskeletal connection. *Curr. Op. Cell Biol.* **12,** 133-139.

Crowe, D.T., Chiu, H., Fong, S. & Weissman, I.L. (1994) Regulation of the avidity of integrin α4β7 by the β7 cytoplasmic domain. *J. Biol. Chem.* **269,** 14411-14418.

Curley, G.P., Blum, H. & Humphries, M.J. (1999) Integrin antagonists. *Cell. Mol. Life Sci.* **56,** 427-441.

Davies, G.E. (1992) The Mac-1 and p150,95 β2 integrins bind denatured proteins to mediate leukocyte cell-substrate adhesion. *Exp. Cell Res.* **200,** 242-252.

De Arcangelis, A. and Georges-Labouesse, E. (2000) Integrin and ECM functions: roles in vertebrate development. *Trends in Genetics* **16:** 389-395.

Diamond, M.S., Garcia-Aguilar, J., Bickford, J.K., Corbi, A.L. & Springer, T.A. (1993) The I domain is a major recognition site on the leukocyte integrin Mac-1 (CD11b/CD18) for four distinct adhesion integrins. *J. Cell Biol.* **120,** 1031-1043.

Diamond, M.S. & Springer, T.A. (1993) A subpopulationof Mac-1 (CD11b/CD18) molecules mediates neutrophil adhesion to ICAM-1 and fibrinogen. *J. Cell Biol.* **120,** 545-556.

Diamond, M.S., Staunton, D.E., de Fougerolles, A.R., Stacker, S.A., Garcia-Aguilar, J., Hibbs, M.L. & Springer, T.A. (1990) ICAM-1 (CD54): a counter-receptor for Mac-1

(CD11b/CD18). *J. Cell. Biol.* **111,** 3129-3139.

Diamond, M.S., Staunton, D.E., Marlin, S.D. & Springer, T.A. (1991) Binding of the integrin Mac-1 (CD11b/CD18) to the third immunoglobulin-like domain of ICAM-1 (CD54) and its regulation by glycosylation. *Cell* **65,** 961-971.

Dickeson, S.K., Bhattacharyya-Pakrasei, M., Mathis, N.L., Schlesinger, P.H. & Santoro, S.A. (1998) Ligand binding results in divalent cation displacement from the alpha 2 beta 1 integrin I domain: evidence from terbium luminescence spectroscopy. *Biochemistry* **37,** 11280-11288.

D'Souza, S.E., Haas, T.A., Piotrovicz, R.S., McGrath, D.E., Soule, H.R., Cierniewski, C., Plow, E.F. & Smith, J,W. (1994) Ligand and cation binding are dual functions of a discrete segment of the integrin β3 subunit: cation displacement is involved in ligand binding. *Cell* **70,** 659-667.

Doolittle, R.F., Spraggon, G. & Everse, S.J. (1998) Three-dimensional structural studies on fragments of fibrinogen and fibrin. *Curr. Op. Struct. Biol.* **8,** 792-798.

Edwards, J.G., Hameed, H. & Campbell, G. (1988) Induction of fibroblast and spreading by Mn2+: a possible role for unusual binding sites for divalent cation in receptors for protein containing Arg-Gly-Asp. *J. Cell Sci.* **89,** 507-513.

Edwards, C.P., Champe, M., Gonzales, T., Wessinger, M.E., Spencer, S.A., Presta, L.G., Berman, P.W. & Bodary, S.C. (1995) Identification of amino acids in the CD11a I-domain important for binding of the leukocyte function-associated antigen-1 (LFA-1) to intercellular adhesion molecule-1 (ICAM-1). *J. Biol. Chem.* **270,** 12635-12640.

Edwards, C.P., Fisher, K.L., Presta, L.G., Berman, P.W. & Bodary, S.C. (1998) Mapping of the intercellular adhesion molecule-1 and –2 binding site on the inserted domain of leukocyte function-associated antigen-1. *J. Biol. Chem.* **273,** 28937-28944.

Emsley, J., King, S.L., Bergelson, J.M. & Liddington, R.C. (1997) Crystal structure of the I domain from the integrin α2β1. *J. Biol. Chem.* **272,** 28512-28517.

Emsley, J., Knight, C.G., Farndale, R.W., Barnes, M.J. & Liddington, R.C. (2000) Structural basis of collagen recognition by integrin α2β1. *Cell* **101,** 47-56.

Epler, J.A., Liu, R. & Shimizu, Y. (2000) From the ECM to the cytoskeleton and back: how integrins orchestrate T cell action. *Dev. Immunol.* **7,** 155-170.

Erb, E.-M., Tangemann, K., Bohrmann, B., Müller, B. and Engel, J. (1997) Integrin αIIbβ3 reconstituted into lipid bilayers is non-clustered in its activated state but clusters after fibrinogen binding. *Biochemistry* **36,** 7395-7402.

Feng, Y., Chung, D., Garrard, L., McEnroe, G., Lim, D., Scardina, J., McFadden, K., Guzzetta, A., Abraham, J., Liu, D. & Endemann, G. (1998) Peptides derived from the complementarity-determining regions of anti-Mac-1 antibodies block intercellular adhesion molecule-1 interaction with Mac-1. *J. Biol. Chem.* **273,** 5625-5630.

Filardo, E.J., Brooks, P.C., Deming, S.L., Damsky, C. & Cheresh, D.A. (1995) Requirement of the NPXY motif in the integrin β3 subunit cytoplasmic tail for melanoma cell migration *in vitro* and *in vivo. J. Cell Biol.* **130,** 441-450.

Fisher, K.L., Lu, J., Riddle, L., Kim, K.J., Presta, L.G. & Bodary, S.C. (1997) Identification of the binding site in intercellular adhesion molecule 1 for its receptor, leukocyte function-associated antigen 1. *Mol. Biol. Cell* **8,** 501-515.

Forsyth, C.B., Plow, E.F. & Zhang, L. (1998) Interaction of the fungal pathogen *Candida albicans* with integrin CD11b/CD18: recognition by the I domain is modulated by the lectin-like domain and the CD18 subunit. *J. Immunol.* **161,** 6198-6205.

Frisch, S. M. & Francis, H. (1994) Disruption of the epithelial cell-matrix interactions induces apoptosis. *J. Cell. Biol.* **124,** 619-626.

Frisch, S. M. & Ruoslahti, E. (1997) Integrins and anoikis. *Curr. Opin. Cell Biol.* **9,** 701-706.

Frisch, S., Vuori, K., Ruoslahti, E. & Chan-Hui, P.Y. (1996) Control of adhesion-dependent cell survival by focal adhesion kinase. *J. Cell. Biol.* **134,** 793-799.

Fulop, V. & Jones, D.T. (1999) β-propellers: structural rigidity and functional diversity. *Curr., Op. Struct. Biol.* **9,** 715-721.

Garcia-Higuera, I., Fenoglio, J., Li, Y., Panchenko, M.P., Reiner, O., Smith, T.F. & Neer, E.J. (1996) Folding of proteins with WD-repeats: comparison of six members of the WD-repeat superfamily to the G protein β subunit. *Biochemistry* **35,** 13985-13994.

Goodman, T.G. & Bajt, M.L. (1996) Identifying the putative metal ion-dependent adhesion site in the β2 (CD18) subunit required for αLβ2 and αMβ2 ligand interactions. *J. Biol. Chem.* **271,** 23729-23736.

Grzesiak, J.J. & Pierschbacher, M.D. (1995) Shifts in the concentrations of magnesium and calcium in early porcine and rat wound fluids activate the cell migratory response. *J. Clin. Invest.* **95,** 227-233.

Guan, J.-L., & Shalloway, D. (1992) Regulation of focal adhesion-associated protein tyrosine kinase by both cellular adhesion and oncogenic transformation. *Nature* **358,** 690-692.

Gulino, D., Boudignon, C., Zhang, L.Y., Concord, E., Rabiet, M.J. & Marguerie, G. (1992) $Ca^{(2+)}$-binding properties of the platelet glycoprotein IIb ligand-interacting domain. *J. Biol. Chem.* **267,** 1001-1007.

Hangtan, R.R., Paumi, C., Rocco, M. & Weisel, J.W. (1999) Effects of ligand-mimetic peptides Arg-Gly-Asp-X (X=Phe, Trp, Ser) on alphaIIbbeta3 integrin conformation and oligomerisation. *Biochemistry* **38,** 14461-14474.

Hill, C.S. & Treisman, R. (1995) Transcriptional regulation by extracellular signals: mechanisms and specificity. *Cell* **80,** 199-211.

Hogg, N. & Leitinger, B. (2001) Shape and shift changes related to the function of leukocyte integrins LFA-1 and Mac-1. *J. Leukoc. Biol.* **69,** 893-898.

Hogg, N., Stewart, M.P., Scarth, S.L., Newton, R, Shaw, J.M., Law, S.K. & Klein, N. (1999) A novel leukocyte adhesion deficiency caused by expressed but nonfunctional beta2 integrins Mac-1 and LFA-1. *J. Clin. Invest.* **103,** 97-106.

Holly, S.P., Larson, M.K. & Parise, L.V. (2000) Multiple roles of integrins in cell motility. *Exp. Cell Res.* **261,** 69-74.

Howe, A., Aplin, A.E., Alahari, S.K. & Juliano R.L. (1998) Integrin signaling and cell growth control. *Curr. Op. Cell Biol.* **10,** 220-231.

Hu, D.D., Barbas, C.F. & Smih, J.W. (1996) An allosteric Ca^{2+} binding site on the β3 integrins that regulate the dissociation rate for RGD ligands. *J. Biol. Chem.* **271,** 21745-21751.

Huang, C., Lu, C. & Springer, T.A. (1997a) Folding of the conserved domain but not flanking region in the integrin beta2 subunit requires association with the alpha subunit. *Proc. Natl. Acad. Sci. USA* **94,** 3156-3161.

Huang, C. & Springer, T. A. (1995) A binding interface on the I domain of lymphocyte function associated antigen-1 (LFA-1) required for specific interaction with Intercellular Adhesion Molecule-1 (ICAM-1). *J. Biol. Chem.* **270,** 19008-19016.

Huang, C. & Springer, T. A. (1997b) Folding of the β-propeller domain of the integrin αL subunit is independent of the I domain and dependent on the β2 subunit. *Proc. Natl. Acad. Sci. USA* **94,** 3162-3167.

Huang, C., Zang, Q., Takagi, J. & Springer, T.A. (2000) Structural and functional studies with antibodies to the integrin β2 subunit. *J. Biol. Chem.* **275,** 21514-21524.

Hubbard, A.K.& Rothlein, R. (2000) Intercellular adhesion molecule-1 (ICAM-1) expression and cell signaling cascades. *Free Radic. Biol. Med.* **28,** 1379-1386.

Hughes, P.E., O'Toole, T.E., Ylanne, J., Shattil, S.J. & Ginsberg, M.H. (1995) The conserved membrane-proximal region of an integrin cytoplasmic domain specifies ligand binding affinity. *J. Biol. Chem.* **26,** 12411-12417.

Hughes, P.E. & Pfaff, M. (1998) Integrin affinity modulation. *Trends Cell Biol.* **8,** 359-364.

Hughes, P.E., Diaz-Gonzalez, F., Leong, L., Wu, C., McDonald, J.A., Shattil, S. & Ginsberg, M. H. (1996) Breaking the integrin hinge: a defined structural constraint regulates integrin signaling. *J. Biol. Chem.* **271,** 6571-6574.

Hughes, P.E., Renshaw MW, Pfaff M, Forsyth J, Keivens VM, Schwartz MA, Ginsberg MH. (1997) Suppression of integrin activation: a novel function of a Ras/Raf-initiated MAP kinase pathway. *Cell* **88,** 521-530.

Humphries, M.J. (2000) Integrin structure. *Biochem. Soc. Trans.* **28,** 311-339.

Huth, J.R., Olejniczak, E.T., Medoza, R., Liang, H., Harris, E.A.S., Lupher, M.L., Wilson, A.E., Fesik, S.W. & Staunton, D.E. (2000) NMR and mutagenesis evidence for an I domain allosteric site that regulates lymphocyte function-associated antigen-1 ligand binding. *Proc. Natl. Acad. Sci. USA* **97,** 5231-5236.

Hynes, R. O. (1992) Integrins: versatility, modulation and signaling in cell adhesion. *Cell* **69,**11-25.

Ikura, M. (1996) Calcium binding and conformational response in EF-hand proteins.

T.I.B.S. **21,** 14-17.

Irie, A., Kamata, T., Puzon-McLaughlin, W. & Takada, Y. (1995) Critical amino acid residues for ligand binding are clustered in a predicted beta-turn of the third N-terminal repeat in the integrin alpha 4 and alpha 5 subunits. *EMBO J.* **14,** 5550-5556.

Irie, A., Kamata, T. & Takada, Y. (1997) Multiple loop structures critical for ligand binding of the integrin alpha4 subunit in the upper face of the beta-propeller mode 1. *Proc. Natl. Acad. USA* **94,** 7198-7203.

Isobe, M., Yagita, H., Okumura, K. & Ihara, A. (1992) Specific acceptance of cardiac allograft after treatment with anti-ICAM and anti-LFA-1. *Science* **255,** 125-1127.

Ivaska, J., & Heino, J. (2000) Adhesion receptors and cell invasion: mechanisms of integrin-guided degradation of extracellular matrix. *Cell. Mol. Life Sci.* **57,** 16-24.

Jonsson, U., Fagerstam, L., Ivarsson, B., Johnsson, B., Karlsson, R., Lundh, K., Lofas, S., Persson, B., Roos, H., Ronnberg, I. *et al.*. (1991) Real-time bispecific interaction analysis using surface plasmon resonance and a sensor chip technology. *BioTechniques* **193,** 620-627.

Jun, C.-D., Carman, C.V., Redick, S.D., Shimaoka, M., Erickson, H.P. & Springer, T.A. (2001a) Ultrastructure and function of dimeric, soluble intercellular adhesion molecule (ICAM-1) *J. Biol. Chem.* **276,** 29019-29027.

Jun, C.-D., Shimaoka, M., Carman, C.V., Takagi, J. & Springer, T.A. (2001b) Dimerisation and the effectiveness of ICAM-1 in mediating LFA-1 dependent adhesion. *Proc. Natl. Acad. Sci. USA* **98,** 6830-6835.

Kallen, J., Welzenbach, K., Ramage, P., Geyl, D., Kriwacki, R., Legge, G., Cottens, S.,

Wetiz-Schmidt, G. & Hommel, U. (1999) Structural basis for LFA-1 inhibition upon lovastatin inhibition ti the CD11a I-domain. *J. Mol. Biol.* **292,** 1-9.

Kamata, T., Irie, A., Tokuhira, M. & Takada, Y. (1996) Critical residues of integrin alphaIIb subunit for binding of alphaIIbbeta3 (glycoprotein IIb-IIIa) to fibrinogen and ligand-mimetic antibodies (PAC-1, OP-G2, and LJ-CP3). *J. Biol. Chem.* **271,** 18610-18615.

Kamata, T., Liddington, R.C. & Takada, Y. (1999) Interaction between collagen and alpha (2) I-domain of integrin $\alpha 2\beta 1$ – critical role of conserved residues in the metal ion-dependent adhesion site (MIDAS) region. *J. Biol. Chem.* **274,** 32108-32111.

Kamata, T., Wright, R. & Takada, Y. (1995) Critical threonine and aspartic acid residues within the I domain of beta 2 integrins for interactions with intercellular adhesion molecule 1 (ICAM-1). *J. Biol. Chem.* **270,** 12531-12535.

Kavanaugh, A.F., Davis, L.S., Nichols, L.A., Norris, S.H., Rothlein, R., Scharschmidt, L.A. & Lipsky, P.E. (1994) Treatment of refractory rheumatoid arthritis with a monoclonal antibody to intercellular adhesion molecule-1. *Arthritis Rheum.* **37,** 992-999.

Keely, P., Parise. L. & Juliano, R. (1998) Integrins and GTPases in tumour cell growth, motility and invasion. *Trends Cell Biol.* **8,** 101-106.

Kern, A., Briesewitz, R., Bank, I. & Marcantonio, E.E. (1994) The role of the I domain in ligand binding of the human integrin $\alpha 1\beta 1$. *J. Biol. Chem.* **269,** 22811-22816.

Kleywegt, G.J., Zhou, J.Y., Kjeldgaard, M. & Jones, T.A. (2001) Around O. International tables for crystallograghy, volume F. Crystallograpghy of biological macromolecules. (Rosmann & Arnold, eds). Chapter 17.1, 353-356, 366-367.

Knight, C.G., Morton, L.F., Onley, D.J., Peachey, A.R., Messent, A.J., Smethurst, P.A., Tuckwell, D.S., Farndale, R.W. & Barnes, M.J. (1998) Identification in collagen type I of an integrin α2β1-binding site containing an essential GER sequence. *J. Biol. Chem.* **273,** 33287-33294.

Koivunen, E., Ranta, T.-M., Anila, A., Taube, S., Uppala, A., Jokinen, M., van Willigen, G., Ihanus, E. & Gahmberg, C.G. (2001) Inhibition of β2 integrin-mediated leukocyte cell adhesion by leucine-leucine-glycine motif-containing peptides. *J. Cell Biol.* **153,** 905-915.

Kuijpers, T. W., van Lier, R.A.W., Hamann, D., de Boer, M., Thung, L.Y., Weening, R.S., Verhoeven, A.J. & Roos, D. (1997) Leukocyte adhesion deficiency type 1 (LAD-1 variant) *J. Clin. Invest.* **7,** 1725-1733.

Labadia, M.E., Jeanfavre, D.D., Caviness, G.O. & Morelock, M.M. (1998) Molecular recognition of the interaction between lymphocyte function-associated antigen-1 and soluble ICAM-1 by divalent metal cations. *J. Immunol.* **161,** 836-842.

Lambright, D., Sondek, J., Bohm, A., Skiba, N., Hamm, H. & Sigler, P. (1996) The 2.0Å crystal structure of a heterodimeric G-protein. *Nature* **379,** 311-319.

Lamzin, V. & Wilson, K.S. (1997) Automated refinement for protein crystallography. *Methods in Enzym.* **277,** 269-305.

Languino, L.R., Duperray, A., Joganic, K.J., Fornaro, M., Thornton, G.B. & Altieri, D.C. (1995) Regulation of leukocyte-endothelium interaction and leukocyte transendothelial migration by intercellular adhesion molecule 1-fibrinogen recognition. *Proc. Natl. Acad. Sci. USA* **92,** 1505-1509.

Laskowski, R.A., Moss, P.S. & Thornton, J.M. (1993) Main-chain bond lengths and bond angles in protein structures. *J. Mol. Biol.* **231,** 1049-1067.

Leahy, D.J., Aukhil, I. & Erickson, H.P. (1996) 2.0 Å crystal structure of a four-domain segment of human fibronectin encompassing the RGD loop and synergy region.*Cell* **84,** 155-164.

Lee, G.F., Burrows, G.G., Lebert, M.R., Dutton, D.P. & Hazelbauer, G.C. (1994) Deducing the organisation of a transmembrane domain by disulphide cross linking. The bacterial chemoreceptor Trg. *J. Biol. Chem.* **269,** 29920-29927.

Lee, J-O., Bankston, L.A., Arnaout, M.A. & Liddington, R.C. (1995a) Two conformation s of the integrin A domain (I domain): a pathway for activation? *Structure* **3,** 1333-1340.

Lee, J-O., Rieu, P., Arnaout, M.A. & Liddington, R.C. (1995b) Crystal structure of the A domain from the α subunit of integrin CR3 (CD11b/CD18). *Cell* **80,** 631-638.

Legge, G.B., Kriwacki, R.W., Chung, J., Hommel, U., Ramage, P., Case, D.A., Dyson, H.J. & Wright, P.E. (2000) NMR structure of the inserted domain of human leukocyte function associated antigen-1. *J. Mol. Biol.* **295,** 1251-1264.

Leitinger, B. & Hogg, N. (2000) Effects of I domain deletion on the function of the β2 integrin lymphocyte function-associated antigen-1. *Mol. Biol. Cell* **11,** 677-690.

Li, R., Rieu, P., Griffith, D.L., Scott, D. & Arnaout, M.A. (1998) Two functional states of the CD11b A-domain: Correlations with key features of two Mn^{2+}-complexed crystal structures. *J. Cell Biol.* **143,** 1523-1534.

Lin, E.C.K., Ratnikov, B.I., Tsai, P.M., Carron, C.P., Myers, D.M., Barbas, C.F. & Smith, J.W. (1997a) Identification of a region in the integrin β3 subunit that confers ligand binding specificity. *J. Biol. Chem.* **272,** 23912-23920.

Lin, E.C.K., Ratnikov, B.I., Tsai, P.M., Gonzalez, E.R., McDonald, S., Pelletier, A.J. & Smith, J.W. (1997b) Evidence that the integrin β3 and β5 subunits contain a metal ion-

dependent site-like motif but lack an I domain. *J. Biol. Chem.* **272,** 14236-14243.

Liu, S., Calderwood, D.A. & Ginsberg, M.H. (2000) Integrin cytoplasmic domain-binding proteins. *J. Cell Sci.* **113,** 3563-3571.

Lobb, R.R. & Hemler, M.E. (1994) The pathophysiologic role of α4 integrins in vivo. *J. Clin. Invest.* **94,** 1722-1728.

Loftus, J.C., O'Toole, T.E., Plow, E.F., Glass, A., Frelinger III, A.L. & Ginsberg, M.H. (1990) A β3 integrin mutation abolishes ligand binding and alters divalent cation-dependent conformation. *Science* **249,** 915-918.

Loftus, J. C., Halloran, C.E., Ginsberg, M.H., Feigen, L.P., Zablocki, J.A. & Smith, J.W. (1996) The amino terminal third of alpha IIb defines the ligand recognition specificity of integrin alpha IIb beta 3. *J. Biol. Chem.* **271,** 2033-2039.

Loftus, J.C. & Liddington, R.C. (1997) New insights into integrin-ligand recognition. *J. Clin. Invest.* **99,** 2302-2306.

Loftus, J.C., Smith, J.W. & Ginsberg, M.H. (1994) Integrin-mediated cell adhesion: the extracellular face. *J. Biol. Chem.* **269,** 25235-25238.

Lollo, B.A., Chan, K.W., Hanson, E.M., Moy, V.T. & Brian, A.A. (1993) Direct evidence for two affinity states for lymphocyte function-associated antigen 1 on activated T cells. *J. Biol. Chem.* **268,** 21693-21700.

Lu, C., Oxvig, C. & Springer, T.A. (1998) The structure of the β-propeller domain and C-terminal region of the integrin αM subunit. *J. Biol. Chem.* **273,** 15138-15147.

Lu, C., Shimaoka, M., Ferzly, M., Oxvig, C., Takagi, J. & Springer, T.A. (2001a) An isolated, surface-expressed I domain of the integrin αLβ2 is sufficient for strong adhesive function when locked in the open conformation with a disulphide bond. *Proc.*

Natl. Assoc. Sci. USA **98,** 2387-2392.

Lu, C., Shimaoka, M., Zang, Q., Takagi, J. & Springer, T.A. (2001b) Locking in alternate conformations of the integrin αLβ2 I domain with disulphide bonds reveals functional relationships among integrin domains. *Proc. Natl. Assoc. Sci. USA* **98,** 2393-2398.

Lu, C., Takagi, J & Springer T.A. (2001c) Association of the membrane proximal regions of the α nd β subunit cytoplasmic domains constrains an integrin in the inactive state. *J Biol. Chem.* **276,** 14642-14648.

Lub, M., van Kooyk, Y., van Vliet, S.J. & Figdor, C.G. (1997) Dual role of the actin cytoskeleton in regulating cell adhesion mediated by the integrin lymphocyte function-associated molecule-1. *Mol. Biol. Cell* **8,** 341-351.

Matthews, B.W. (1968) Solvent content of protein crystals. *J. Mol. Biol.* **33,** 491-497.

McDowall, A. Letinger, B., Stanley, P., Bates, P.A., Randi, A.M. & Hogg, N. (1998) The I domain of integrin leukocyte function-associated antigen-1 is involved in a conformational change leading to high affinity binding to ligand intercellular adhesion molecule 1 (ICAM-1). *J. Biol. Chem.* **42,** 27396-27403.

McGuire, S.L. & Bajt, M.L. (1995) Distinct ligand binding sites in the I domain of integrin αMβ2 that differentially affect a divalent cation-dependent conformation. *J. Biol. Chem.* **270,** 25866-25871.

Mesri, M., Plescia, J. & Altieri, D. C. (1998) Dual regulation of ligand binding by CD11b I domain. *J. Biol. Chem.* **273,** 744-748.

Michishita, M., Videm, V. & Arnaout, M.A. (1993) A novel divalent cation-binding site in the A-domain of the β2 integrin CR3 (CD11b/CD18) is essential for ligand binding. *Cell* **72,** 857-867.

Miyamoto, S., Teramoto, H., Gutkind, J. & Yamada, K. (1996) Integrins can collaborate with growth factors for phosphorylation of receptor tyrosine kinases and MAP kinase activation: roles of integrin aggregation and occupancy of receptors. *J. Cell Biol.* **135,** 1633-1642.

Mould, A.P., Akiyama, S.K. & Humphries, M.J. (1995) Regulation of integrin alpha 5 beta 1-fibronectin interactions by divalent cations. Evidence for distinct classes of binding sites for Mn2+, Mg2+, and Ca2+. *J. Biol. Chem.* **270,** 26270-26277.

Mould, A.P., Askari, J.A. & Humphries, M.J. (2000) Molecular basis of ligand recognition by integrin α5β1. *J. Biol. Chem.* **275,** 20324-20336.

Mould, A.P., Burrows, L. & Humphries. M.J. (1998a) Identification of amino acid residues that form part of the ligand binding pocket of integrin α5β1. *J. Biol. Chem.* **273,** 25664-25672.

Mould, A.P., Garratt, A.N., Puzon-McLaughlin, W., Takada, Y. & Humphries, M.J. (1998b) Regulation of integrin function: evidence that bivalent-cation-induced conformatioal changes lead to the unmasking of ligand-binding sites within integrin α5β1. *Biochem. J.* **331,** 821-828.

Muñoz, M., Serrador, J., Nieto, M., Luque, A., Sánchez-Madrid, F. & Teixidó, J. (1997) A novel region of the α4 integrin subunit with a modulatory role in VLA-4-mediated cell adhesion to fibronectin. *Biochem. J.* **327,** 727-733.

Navaza, J. (1994) AMoRe: an automated package for molecular replacement. *Acta Crys.* **A50:** 157-163.

Nolte, M., Pepinsky, R.B., Venyaminov, S.Y., Koteliansky, V., Gotwals, P.J. & Karpusas, M. (1999) Crystal structure of the alpha1beta1 integrin I-domain: insights into integrin I-domain function. *FEBS Lett* **452,** 379-385.

Otey C. A., Vasquez G. B., Burridge K. and Erickson B. W. (1993) Mapping of the alpha-actinin binding site within the beta 1 integrin cytoplasmic domain. *J. Biol. Chem.* **268,** 21193–21197.

O'Toole, T.E., Katagiri, Y., Faull, R.J., Peter, K., Tamura, R., Quaranta, V., Loftus, J.C., Shattil, S.J. & Ginsgerg, M.H. (1994) Integrin cytoplasmic domains mediate inside-out signal transduction. *J. Cell. Biol.* **124,** 1047-1059.

O'Toole, T.E., Mandelman, D., Forsyth, J., Shattil, S.J., Plow, E.F. & Ginsberg, M.H. (1991) Modulation of the affinity of integrin alpha IIb beta 3 (GPIIb-IIIa) by the cytoplasmic domain of alpha IIb. *Science* **254,** 845-847.

Otwinowski, A. & Minor, W. (1997) Processing of X-ray diffraction data collected in oscillation mode. *Methods Enzymol.* **276,** 307-326.

Oxvig, C. & Springer, T. A. (1998) Experimental support for a beta-propeller domain in integrin alpha-subunits and a calcium binding site on its lower surface. *Proc. Natl. Acad. USA* **95,** 4870-4875.

Oxvig, C., Lu, C. & Springer T. A. (1999) Conformational changes in tertiary structure near the ligand binding site of an integrin I domain. *Proc. Natl. Acad. Sci. USA* **96,** 2215-2220.

Perczel, A., Hollosi, M., Tusnady, G. & Fasman, G.D. (1991) Convex constraint analysis: A natural deconvolution of circular dichroism curves of proteins. *Protein Eng.* **4,** 669-679.

Perczel, A., Park, K. & Fasman, G.D. (1992a) Analysis of the circular dichroism spectrum of proteins using the convex constraint alogrithm: apractical guide. *Anal. Biochem.* **15,** 83-93.

Perczel, A., Park, K. & Fasman, G.D. (1992b) Deconvolution of the circular dichroism spectra of proteins: the circular dichroism spectra of the antiparallel β-sheet in protein. *Proteins* **13,** 57-69.

Perez, R.L. & Roman, J. (1995) Fibrin enhances the expression of IL-1β by human peripheral blood mononuclear cells. Implications in pulmonary inflammation. *J. Immunol.* **154,** 1879-1887.

Pierschbacher, M.D. & Ruoslahti, E. (1984) Cell attachment activity of fibronectin can be duplicated by small synthetic fragments of the molecule. *Nature* **309,** 30-33.

Plescia, J. & Altieri, D.C. (1996) Activation of Mac-1 (CD11b/CD18)- bound factor X by released cathepsin G defines an alternative pathway of leukocyte initiation of coagulation. *Biochem. J.* **319,** 873-879.

Plescia, J., Conte MS, VanMeter G, Ambrosini G, Altieri DC. (1998) Molecular identifaction of the cross-reacting epitope on αMβ2 integrin I domain recognised by anti-αIIbβ3 monoclonal antibody 7E3 and its involvement in leukocyte adherence. *J. Biol. Chem.* **273,** 20372-20377.

Plow, E.F., Haas, T.A., Zhang, L., Loftus, J. & Smith, J.W. (2000) Ligand binding to integrins. *J. Biol. Chem.* **275,** 21785-21788.

Previtali, S.C., Felrti, M.L., Archelos, J.J., Quattrini, A., Wrabetz, L. & Hartung, H.P. (2001) Role of integrins in the peripheral nervous system. *Prog. Neurobiol.* **64,** 35-49.

Pujades, C., Alon, R., Yauch, R.L., Masumoto, A., Burkly, L.C., Chen, C. Springer, T.A., Lobb, R.R. & Hemler, M.E. (1997) Defining extracellular integrin alpha-chain sites that affect cell adhesion and adhesion strengthening without altering soluble ligand binding. *Mol. Biol. Cell* **8,** 2647-2657.

Pulkkinen, L. & Uitto, J. (1999) Mutational analysis and molecular genetics of epidermolysis bullosa. *Matrix Biol.* **18,** 29-42.

Puzon-McLaughlin, W., Kamata, T. & Takada, Y. (2000) Multiple discontinuous ligand-mimetic antibody binding define a ligand binding pocket in integrin αIIbβ3. *J. Biol. Chem.* **275,** 7795-7802.

Puzon-McLaughlin, W. & Takada, Y. (1996) Critical residues for ligand binding in an I domain-like structure of the integrin β1 subunit. *J. Biol. Chem.* **271,** 20438-20443.

Qu, A. & Leahy, D. J. (1995) Crystal structure of the I domain CD11a/CD18 (LFA-1, αLβ2) integrin. *Proc. Natl.* Acad. *Sci. USA* **92,** 10277-10281.

Qu, A. & Leahy D. J. (1996) The role of the divalent cation in the structure of the I-domain from the CD11a/CD18 integrin. *Structure* **4,** 931-942.

Reilly, P. L., Woska, J.R., Jeanfavre, D.D., McNally, E., Rothlein, R. & Bormann, B.-J. (1995) The native structure of intercellular adhesion molecule-1 (ICAM-1) is a dimer. Correlation with binding to LFA-1. *J. Immunol.* **155,** 529-532.

Rieu, P., Sugimori, T., Griffith, D.L. & Arnaout, M.A. (1996) Solvent accessible residues on the metal ion-dependent adhesion site face of the integrin CR3 mediate its binding to the neutrophil inhibitory factor. *J. Biol. Chem.* **271,** 15858-15861.

Rieu, P., Ueda, T., Haruta, I., Sharma, C.P. & Arnaout, M.A. (1994) The A-domain of β2 integrin CR3 (CD11b/CD18) is a receptor for the hookworm-derived neutrophil adhesion inhibitor NIF. *J. Cell Biol.* **127,** 2081-2091.

Roskelley, C.D., Desprez, P.Y. & Bissell, M.J. (1995) A hierarchy of ECM-mediated signalling regulates tissue-specific gene expression. *Curr. Op. Cell Biol.* **7,** 736-747.

Ross, F.P., Chappel, J., Alvarez, J.I., Sander, D., Butler, W.T., Farach-Carson, M.C.,

Mintz, K.A., Robey, P.G., Teitelbaum, S.L. & Cheresh, D.A. (1993) Interactions between the bone matrix proteins osteopontin and bone sialoprotein and the osteoclast integrin alpha v beta 3 potentiate bone resorption. *J. Biol. Chem.* **268,** 9901-9907.

Ross, G.D. (2000) Regulation of the adhesion versus cytotoxic functions of the Mac-1/CR3/alphaMbeta2-integrin glycoprotein. *Crit. Rev. Immunol.* **20,** 197-222.

Roussel, A. & Cambillau, C. (1992) TURBO-FRODO, Biographics LCCMB, Marseille, France.

Ruoslahti, E. (1996) RDG and other recognition sequences for integrins. *Annu. Rev.Cell Dev. Biol.* **12,** 697-715.

Sastry, S.K. & Burridge, K. (2000) Focal adhesions: a nexus for intracellular signaling and cytoskeletal dynamics. *Exp. Cell. Res.* **261,** 25-36.

Schlaepfer, D.D., Hanks, S.K., Hunter, T. & van der Geer, P. (1994) Integrin-mediated signal transduction linked to ras pathway by GRB-2 binding to focal adhesion kinase. *Nature* **372,** 786-791.

Schlaepfer, D.D. & Hunter, T. (1998) Integrin signalling and tyrosine phosphorylation: just the FAKs? *Trends Cell Biol.* **8,** 151-157.

Schwartz, M. A., Schaller, M. D. & Ginsberg, M. H. (1995) Integrins: emerging paradigms of signal transduction. *Annu. Rev. Cell Dev. Biol.* **11,** 549-599.

Seftor, R.E., Seftor, E.A., Gehlsen, K.R., Stetler-Stevenson, W.G., Brown, P.D., Ruoslahti, E. & Hendrix, M.J. (1992) Role of the αVβ3 integrin in human melanoma cell invasion. *Proc. Natl. Acad. Sci. USA* **89,** 1557-1561.

Seftor, R.E., Seftor, E.A., Gehlsen, K.R., Stetler-Stevenson, W.G. & Hendrix, M.J.

(1993) The 72 kDa type IV collagenase is modulated via differential expression of αVβ3 and α5β1 integrins during human melanoma cell invasion. *Cancer Res.* **53,** 3411-3415.

Shappell, S.B., Toman, C., Anderson, D.C., Tayler, A.A., Entman, M.L. & Smith, C.W. (1990) Mac-1 (CD11b/CD18) mediates adherence-dependent hydrogen peroxide production by human and canine neutrophils. *J. Immunol.* **144,** 2702-2711.

Sheldrick, G. & Schneider, T. (1997) SHELXL: high resolution refinement. *Methods Enzymol.* **277,** 319-343.

Shih, D.T., Edelman, J.M., Horwitz, A.F., Grunwald, G.B. & Buck, C.A. (1993) Structure/function analysis of the integrin beta 1 subunit by epitope mapping. *J. Cell Biol.* **122,** 1361-1371.

Shimaoka, M., Lu, C., Palframan, R.T., von Andrian, U.H., McCormack, A., Takagi, J. & Springer, T.A. (2001) Reversibly locking a protein fold in an active conformation with a disulphide bond: Integrin αL I domains with a high affinity and antagonist activity *in vivo. Proc. Natl. Acad. USA* **98,** 6009-6014.

Shimaoka, M., Shifman, J.M., Jing, H., Takagi, J., Mayo, S.L. & Springer, T.A. (2000) Computational design of an integrin I domain stablilsed in the open high affinity conformation. *Nature Struct. Biol.* **7,** 674-678.

Shimizu, Y., Van Seventer, G.A., Horgan, K.J. & Shaw, S. (1990) Regulated expression and binding of three VLA (β1) integrin receptors on T cells. *Nature* **345,** 250-253.

Simon, D.I., Xu, H., Ortlepp,S., Rogers, C. & Rao, N.K. (1997) 7E3 monoclonal antibody directed against platelet glycoprotein Iib/Iia cross-reaxts with the leukocyte integrin Mac-1 and blocks adhesion to fibrinogen and ICAM-1. *Arterioscler. Thromb.*

Vasc. Biol. **17,** 528-535.

Si-Tahar, M., Pidard, D., Balloy, V., Moniatte, M., Kieffer, N., Van Dorsselaer, A. & Chignard, M. (1997) Human neutrophil elastase proteolytically activates the platelet integrin alphaIIbbeta3 through cleavage of the carboxyl terminus of the alphaIIb subunit heavy chain. Involvement in the potentiation of platelet aggregation. *J Biol Chem* **272,** 11636-47.

Sitrin, R.G., Pan, P.M., Srikanth, S. & Todd, R.F. (1998) Fibrinogen activates NF-κB transcription factors in mononuclear phagocytes. *J. Immunol.* **161,** 1462-1470.

Smith, C.W. (2000) Possible steps involved in the transition to stationary adhesion of rolling neutrophils: a brief review. *Microcirculation* **7,** 385-394.

Smith, C.W., Marlin, S.D., Rothlein, R., Toman, C. & Anderson, D.C. (1989) Cooperative interactions of LFA-1 and Mac-1 with the intercellular adhesion molecule-1 in facilitating adherence and transendothelial migrationof human neutrophils in vitro. *J. Clin. Invest.* **83,** 2008-2017.

Schoenwaelder, S.M. & Burridge, K. (1999) Bidirectional signaling between the cytoskeleton and integrins. *Curr. Op. Cell Biol.* **11,** 274-286.

Springer, T.A. (1994) Traffic signals for lymphocyte recirculation and leukocyte emigration: the multistep paradigm. *Cell* **76,** 301-314.

Springer, T.A. (1997) Folding of the N terminal, ligand binding region of the integrin α-subunits into a β-propeller domain. *Proc. Natl. Acad. USA* **94,** 65-72.

Springer, T.A. (2000) A novel Ca^{2+} binding β hairpin loop better resembles integrin sequence motifs than the EF hand. *Cell* **102,** 275-277.

Sriramarao, P., Languino, L.R. & Altieri, D.C. (1996) Fibrinogen mediates leukocyte-

endothelium binding in vivo at low shear forces. *Blood* **88,** 3416-3423.

Stanley, P., Bates, P.A., Harvey, J., Bennett, R.I. & Hogg, N. (1994) Integrin LFA-1 α subunit contains an ICAM-1 binding site in domains V and VI. *EMBO J.* **13,** 1790-1798.

Stanley, P. & Hogg, N. (1998) The I domain of integrin LFA-1 interacts with ICAM-1 domain 1 at residue Glu-34 but not Gln-73. *J. Biol. Chem.* **273,** 3358-3362.

Stanley, P., McDowall, A., Bates, P.A., Brashaw, J. & Hogg, N. (2000) The second domain of intercellular adhesionn molecule-1 (ICAM-1) maintains the structural integrity of the leukocyte function-associated antigen-1 (LFA-1) ligand-binding site in the first domain. *Biochem. J.* **351,** 79-86.

Staunton, D.E., Dustin, M.L., Erickson, H.P. & Springer, T.A. (1990) The arrangement of the immunoglobulin-like domains of ICAM-1 and the binding sites for LFA-1 and rhinovirus. *Cell* **61,** 243-254.

Strynadka, N. & James, M. (1989) Crystal structures of the helix-loop-helix calcium-binding proteins. *Annu. Rev. Biochem.* **58,** 951-998.

Stura, E.A. & Wilson, I.A. (1990) Analytical and production seeding techniques.*Methods* **1,** 38-49.

Sugimori, T., Griffith, D.L. & Arnaout, M.A. (1997) Emerging paradigms of integrin ligand binding and activation. *Kidney Int.* **51,** 1454-1462.

Tailor, A. & Granger, D.N. (2000) Role of the adhesion molecules in vascular regulation and damage. *Curr. Hypertens. Rep.* **2,** 78-83.

Takada, Y. & Puzon, W. (1993) Identification of a regulatory region of integrin beta 1 subunit using activating and inhibiting antibodies. *J. Biol. Chem.* **268,** 17597-17601.

Takagi, J., Erickson, H.P & Springer, T.A. (2001) C-terminal opening mimics 'inside-out' activation of α5β1. *Nature Struct. Biol.* **8,** 412-416.

Tanaka, Y. (2000) Integrin activation by chemokines: relevance to inflammatory adhesion cascade during T cell migration. *Histol. Histopathol.* **15,** 1169-1176.

Tozer, E.C., Baker, E.K., Ginsberg, M.H. & Loftus, J.C. (1999) A mutation in the α subunit of the platelet integrin αIIbβ3 identifies a novel region important for ligand binding *Blood* **93,** 918-924.

Tozer, E.C., Liddington, R.C., Sutcliffe, M.J., Smeeton, A.H. & Loftus, J.C. (1996) Ligand binding to integrin αIIbβ3 is dependent on a MIDAS-like domain in the β3 subunit. *J. Biol. Chem.* **271,** 21978-21984.

Tuckwell, D.S., Brass, A.M. & Humphries, M.J. (1992) Homology modelling of integrin EF hands. Evidence for widespread use of a conserved cation-binding site *Biochem. J.* **285,** 325-331.

Tuckwell, D.S., Calderwood, D.A., Green, L.J. & Humphries, M.J. (1995) Intgerin α2 I-domain is a binding site for collagens. *J. Cell Sci.* **108,** 1629-1637.

Tuckwell, D.S. & Humphries, M.J. (1997) A structure prediction for the ligand-binding region of the integrin beta subunit: evidence for the presence of a von Willebrand factor A domain. *FEBS Lett.* **400,** 297-303.

Ueda, T., Rieu, P., Brayer, J. & Arnaout, M.A. (1994) Identification of the complement iC3b binding site in the β2 integrin CR3 (CD11b/CD18). *Proc. Natl. Acad. Sci.* **91,** 10680-10684.

Ugarova, T.P., Solovjov, D.A., Zhang, L., Loukinov, D.I., Yee, V.C., Medved, L.V. & Plow, E.F. (1998) Identification of a novel recognition sequence for integrin αMβ2 within the γ-chain of fibrinogen. *J. Biol. Chem.* **273,** 22519-22527.

Van Kooyk, Y. & Figdor, C.G. (2000) Avidity regulation of integrins: the driving force in leukocyte adhesion. *Curr. Op. Cell Biol.* **12,** 542-547.

Velling, T., Kusche-Gullberg, M., Sejerson, T. & Gullberg, D. (1999) cDNA cloning and chromosomal localization of human alpha(11) integrin. A collagen-binding, I domain-containing, beta(1)-associated integrin alpha-chain present in muscle tissues. *J. Biol. Chem.* **274,** 25735-25742.

Von Asmuth, E.J., Van der Linden, C.J., Leeuwenberg, J.F. & Buurman, W.A. (1991) Involvement of the CD11b/CD18 integrin, but not of the endothelial cell adhesion molecules ELAM-1 and ICAM-1 in tumour necrosis factor-alpha induced neutrophil toxicity. *J. Immunol.* **147,** 3869-3875.

Wall, A.M., Coleman, D.E., Lee, E., Iniguez-Lluki, J.A., Posner, B.A., Gilman, A.G. & Sprang, S.R. (1995) The structure of the protein heterotrimer Gi 2. *Cell* **83.** 1047-1058.

Wary, K.K., Mainiero, F., Isakoff, S.J., Marcantonio, E.E. & Giancotti, F.G. (1996) The adaptor protein Shc couples a class of integrins to the control of cell cycle progression. *Cell* **87,** 733-743.

Wei, J., Shaw, L.M. & Mercurio, A.M. (1998) Regulation of mitogen-activated protein kinase activation by the cytoplasmic domain of the α6 subunit. *J. Biol. Chem.* **273,** 5903-5907.

Weisel, J.W., Nagaswami, C., Vilaire, G. & Bennett, J.S. (1992) Examination of the platelet membrane glycoprotein IIb-IIIa complex and its interaction with fibrinogen and other ligands by electron microscopy. *J. Biol. Chem.* **267,** 16637-16643.

Wilson, A.J.C. (1950) Largest likely values for the reliability index. *Acta. Cryst.* **3,** 397-398.

Woods, M.L. & Shimizu, Y. (2001) Signaling networks regulating beta1 integrin-

mediated adhesion of T lymphocytes to extracellular matrix. *J. Leukoc. Biol.* **69,** 874-880.

Wright, S.D., Weitz, J.I., Huang, A.J., Levin, S.M., Silverstein, S.C. & Loike, J.D. (1988) Complement receptor type three (CD11b/CD18) of human polymorphonuclear leukocyte recognises fibrinogen. *Proc. Natl. Acad. Sci. USA* **85,** 7734-7738.

Wu, X., Helfrich, M.H., Horton, M.A., Feigen, L.P. & Lefkowith, J.B. (1994) Fibrinogen mediates platelet-polymorphonuclear leukocyte cooperation during immune-complex glomerulonephritis in rats. *J. Clin. Invest.* **94,** 928-936.

Xiong, J.-P., Li, R., Essafi, M., Stehle, T. & Arnaout, M.A. (2000) An isoleucine-based allosteric switch controls affinity and shape shifting in integrin CD11b A-domain. *J. Biol. Chem.* **265,** 38762-38767.

Xiong, J.-P., Stehle, T., Diefenbach, B., Zhang, R., Dunker, R., Scott, D.L., Joachimiak, A., Goodman, S.L. & Arnaout, M.A. (2001) Crystal structure of the extracellular segment of integrin αVβ3. *Science* **294,** 339-345.

Yakubenko, V.P., Solovjov, D.A., Zhang, L., Yee, V.C., Plow, E.F. & Ugarov, T.P. (2001) Identification of the binding site for fibrinogen recognition peptide γ383-395 within the αM I-domain of integrin αMβ2. *J. Biol. Chem.* **276,** 13995-4003.

Yalamanchili, P., Lu, C., Oxvig, C. & Springer, T.A. (2000) Folding and function of I domain-deleted Mac-1 and lymphocyte finction-associated antigen-1. *J. Biol. Chem.* **275,** 21877-21882.

Yan, B. & Smith, J.W. (2000) A redox site involved in integrin activation. *J. Biol. Chem.* **275,** 39964-39972.

Yang, J.T. & Hynes R.O. (1996) Fibronectin receptor functions in embryonic cells deficient in alpha 5 beta 1 integrin can be replaced by αV integrins. *Mol. Biol. Cell* **7,** 1737-1748.

Yauch, R.L., Berditchevski, F., Harler, M.B., Reichner, J. & Hemler, M.E. (1998) Highly stoichiometric, stable, and specific association of integrin α3β1 with CD151 provides a major link to phosphatidylinositol 4-kinase, and may regulate cell migration. *Mol. Biol. Cell* **9,** 2751-2765.

Yauch, R.L., Felsenfeldt, D.P., Fraeft, S.-K., Chen, L.B., Sheetz, M.P. & Hemler, M.E. (1997) Mutational evidence for control of cell adhesion through integrin diffusion/clustering, independent of ligand binding. *J. Exp. Med.* **186,** 1347-1355.

Yee, V.C., Pratt, K.P., Côté, H.C.F., Le Trong, I., Chung, D.W., Davie, E.W., Stenkamp, R.E. & Teller, D.C. (1996) Crystal structure of a 30kDa C-terminal fragment from the γ chain of human fibrinogen. *Structure* **5,** 125-138.

Yu, H., Kono, M. & Oprian, D.D. (1999) State-dependent disulphide cross-linking in rhodopsin. *Biochem.* **38,** 12028-12032.

Zage, P.E. & Marcantonio E.E. (1998) The membrane proximal region of the integrin beta cytoplasmic domain can mediate oligomerisation. *Cell Adhes. Commun.* **5,** 335-347.

Zhang, L. & Plow, E. F. (1996) Overlapping, but not identical, sites are involved in the recognition of C3bi, neutrophil inhibitory factor, and adhesive ligands by the αMβ2 integrin. *J. Biol. Chem.* **271,** 18211-18216.

Zhang, L. & Plow, E. F. (1997) Identification and reconstruction of the binding site within αMβ2 for a specific and high affinity ligand, NIF. *J. Biol. Chem.* **272,** 17558-17564.

Zhang, L. & Plow, E. F. (1999) Amino acid sequences within the alpha subunit of integrin alphaMbeta2 (Mac-1) critical for specific recognition of C3bi. *Biochemistry* **38,** 8064-8071.

Zhang, X.-P., Puzon-McLaughlin, W., Irie, A., Kovach, N., Prokopishyn, N.L., Laferté, S., Takeuchi, K., Tsuji, T. & Takada, Y. (1999) α3β1 adhesion to laminin-5 and invasin: critical and differential role of integrin residues clustered at the boundary between α3 N-terminal repeats 2 and 3. *Biochem.* **38,** 14424-14431.

Zhang, Z., Vuori, K., Wang, H.-G., Reed, J.C. & Ruoslahti, E. (1996) Integrin activation by R-ras. *Cell* **85,** 61-69.

Zhou, L., Lee, D.H.S., Plescia, J., Lau, C.Y. & Altierei, D.C. (1994) Differential ligand binding specifities of recombinant CD11b/CD18 integrin I-domain. *J. Biol. Chem.* **269,** 17075-17079.